

**Technische Universiteit Delft
Faculteit Elektrotechniek, Wiskunde en Informatica
Delft Institute of Applied Mathematics**

**Omtrent Covariante Emergente Zwaartekracht
(Engelse titel: On Covariant Emergent Gravity)**

Verslag ten behoeve van het
Delft Institute of Applied Mathematics
als onderdeel ter verkrijging

van de graad van

**BACHELOR OF SCIENCE
in
TECHNISCHE WISKUNDE & TECHNISCHE NATUURKUNDE**

door

Arthur Carel Platschorre

**Delft, Nederland
12 juli 2019**

BSc verslag TECHNISCHE WISKUNDE & TECHNISCHE NATUURKUNDE

“Omtrent Covariante Emergente Zwaartekracht ”
(Engelse titel: “On Covariant Emergent Gravity ”)

Arthur Carel Platschorre

Technische Universiteit Delft

Begeleiders

Dr. Paul M. Visser
Dr. Jos M. Thijssen

Overige commissieleden

Prof. Dr. ir. C. Vuik
Dr. Stephan W. H. Eijt
Dr. Jeroen G. Spandaw

12 juli, 2019

Delft

Bachelor Thesis

On Covariant Emergent Gravity

Arthur Platschorre

DELFT UNIVERSITY OF TECHNOLOGY

BACHELOR THESIS

On Covariant Emergent Gravity

Author:

Arthur C. PLATSCHORRE

Supervisors:

Dr. Paul M. VISSER

Dr. Jos M. THIJSEN

Committee members:

Dr. Paul M. VISSER

Dr. Jos M. THIJSEN

Prof. Dr. ir. C. VUIK

Dr. Stephan W. H. EIJT

Dr. Jeroen G. SPANDAW



*A thesis submitted in fulfillment of the requirements
for the degree of Bachelor of Science in
Applied Physics & Applied Mathematics*

at

Mathematical Physics

Faculty of Electrical Engineering, Mathematics & Computer Science

July 12, 2019

Cover image copyright © ESA/Hubble

Declaration of Authorship

I, Arthur C. PLATSCHORRE, declare that this thesis titled, “On Covariant Emergent Gravity ” and the work presented in it are my own. I confirm that:

- This work was done wholly or mainly while in candidature for a research degree at this University.
- Where any part of this thesis has previously been submitted for a degree or any other qualification at this University or any other institution, this has been clearly stated.
- Where I have consulted the published work of others, this is always clearly attributed.
- Where I have quoted from the work of others, the source is always given. With the exception of such quotations, this thesis is entirely my own work.
- I have acknowledged all main sources of help.
- Where the thesis is based on work done by myself jointly with others, I have made clear exactly what was done by others and what I have contributed myself.

Signed: *Arthur Carel Platschorre*

Date: *12 July 2019*

*“Oh leave the Wise our measures to collate
One thing at least is certain, light has weight
One thing is certain, and the rest debate—
Light rays, when near the Sun, do not go straight.”*

Sir Arthur Eddington

DELFT UNIVERSITY OF TECHNOLOGY

Abstract

On Covariant Emergent Gravity

by Arthur C. PLATSCHORRE

This report focuses on covariant emergent gravity (CEG), a coordinate-free formulation by Sabine Hossenfelder of Erik Verlinde's emergent gravity (EG). In (C)EG, gravity is considered an emergent, entropic force arising from shifts in the entropy content of the universe due to matter.

The main goal of this report is to identify experimentally verifiable results for CEG through a theoretical analysis of the covariant field equations. The initial goal of this report was to understand both EG and CEG. We have expanded upon this goal both theoretically and numerically.

Our theoretical expansion consists of two parts: a gravitational lensing formalism for CEG and an attempt at a cosmological model. The lensing formalism includes a lensing potential that can be applied to general lensing systems. We show that current assumptions in CEG on the imposter field result in a lensing equation that predicts that the amount of baryonic matter in a galaxy as measured by strong lensing should differ from the amount of baryonic matter as measured from the rotation curves. We have also included an attempt at a cosmological model in which we solve for a vacuum dominated and a matter dominated universe in CEG.

Our numerical expansion also consists of two parts. In our first numerical expansion, we propose and test an iterative algorithm to solve for CEG and MOND in cases of cylindrical symmetric baryonic densities. This is done using an iterative algorithm based on Fourier-Bessel transforms. The algorithm can also be applied to arbitrary baryonic densities using just Fourier methods.

In our second numerical expansion, we fitted both CEG and MOND to 131 galaxies from the SPARC database. The fittings were done by employing a Markov Chain Monte Carlo (MCMC) fitting algorithm using three fit parameters. Both MOND and CEG provide good fits to the rotation curves. Out of the 131 fits, 9 fits (7%) were poor fits ($R^2 < 0$) and 62 galaxies (47%) were excellent fits ($R^2 > 0.9$) and 94 galaxies (72%) good fits ($R^2 > 0.7$). We also provide fits to galaxies that are traditionally considered hard to fit with dark matter maximum-disk models. Such good fits for CEG are in contrast to EG, which was found to be a bad fit to the rotation curves by the SPARC team.

However, scatter plots show a clear correlation between the MOND and CEG fit parameters, making it hard to distinguish between the two experimentally on the basis of rotation curves or other Newtonian features. Another experimentally verifiable result is the proposed lensing formalism, which could be tested by comparing rotation curves of galaxies to strong lensing. We recommend further research into covariant features of both theories in order to arrive at experimentally verifiable differences. Other interesting topics of follow-up research include using the numerical method to solve for the evolution of the galactic disk or in cases that the magnetic term in CEG or MOND becomes non-negligible. The connection to both dark matter and dark energy also make CEG an interesting theory to further research in cosmology.

Acknowledgements

Even-though the rest of this report contains general relativity, curved space-times and tensors, this might be the hardest part of all. I would like to express my sincere and utmost gratitude to my supervisor Dr. Paul Visser for the countless meetings we had, the countless hours he has put into checking and correcting this report, but most of all for the work he has put in me and my development as a physicist. During the span of this project, I have been free to explore general relativity, classic field theory, cosmology etc. and experiment and discuss my own ideas with mister Visser. Such a mentor and guide is priceless and has allowed me to grow into the physicist I am today. Thank you for the time you have put into this report! Thank you for the time you have put in me! And most of all, thank you for your faith in me!

We would also like to thank Dr. Jos Thijssen for his opinions and guidance on the numerical implementation of the presented algorithm and the other committee members for their willingness to review this report.

Contents

Declaration of Authorship	iii
Abstract	vii
Acknowledgements	ix
1 Introduction	1
1.1 Introduction	1
1.2 Structure of the report	1
1.3 Reading routes	2
1.3.1 Bachelor route	2
1.3.2 Astrophysical route	2
1.3.3 Theoretical route	3
2 Astrophysics and galaxies	5
2.1 Rotation curves	5
2.2 Observed velocities and dark matter	7
2.3 Modified gravity	7
2.4 The structure of galaxies	9
2.5 Galactic velocities	11
2.6 The SPARC database	11
2.6.1 Gas profile	12
2.6.2 Stellar disk	13
2.6.3 Mass-to-light ratio	13
2.7 Dark matter in galaxies	14
2.8 Covariant Emergent Gravity	14
2.8.1 Quantum gravity	14
2.8.2 Covariant Emergent Gravity	14
3 From Newtonian to Einsteinian gravity	17
3.1 Classical Gravity	17
3.2 Particles and Field, What's the difference?	18
3.3 Particles and Fields: The field equations	19
3.4 Curved space-time	21
3.5 Covariant Derivatives	22
3.6 Other uses of the metric	24
3.7 General relativity	24
3.8 Cosmology	25
4 Emergent Gravity	27
4.1 Entropic Gravity	27
4.1.1 Emergent properties	27
4.1.2 Entropy and emergent forces	28

4.1.3	Bekenstein's entropy	29
4.1.4	Entropic gravity: Verlinde's first paper	30
4.2	Emergent Gravity; Verlinde's first paper	31
4.2.1	Newton's law of gravity	32
4.2.2	General matter distributions	33
4.2.3	Critique	33
4.3	Apparant dark matter; Erik Verlinde's second paper	34
4.3.1	Entropy and the cosmological constant	34
4.3.2	Introducing mass	36
4.3.3	Mass and entropy	36
4.3.4	Entropy difference	37
4.3.5	Interpretation of results	38
4.4	Stresses and Strains	38
4.4.1	Theory of Strain and Stress	39
4.4.2	Strain in the entropic medium	40
5	Covariant Emergent Gravity	43
5.1	Deriving a Lagrangian	43
5.1.1	The form of the Lagrangian	43
5.1.2	Effective metric	45
5.1.3	The interaction term	45
5.2	Understanding the action	46
5.3	Imposter field equations	49
5.3.1	The Newtonian Limit	49
5.3.2	Newtonian Lagrangian	51
5.4	The Modified Einstein Equations	52
5.5	The Equations of Motion	52
5.6	Perturbation theory	54
5.6.1	Summary of the interactions from the imposter field	55
6	Theoretical applications CEG	57
6.1	Gravitational lensing	57
6.1.1	Newtonian Gravitational lensing	57
6.1.2	Microlensing in CEG	58
6.1.3	Deflection due to the Sun	61
6.1.4	The lens equation	62
6.1.5	General lensing systems	64
6.2	Cosmological model	65
6.2.1	Vacuum dominated universe	66
6.2.2	Matter dominated universe	67
6.2.3	Effective metric	68
7	Fourier-Bessel methods & results	69
7.1	Theoretical Summary	69
7.2	Numerical baryonic potential	70
7.2.1	Fourier-Bessel transform for scalars	70
7.2.2	Bessel-Fourier transform of vectors	72
7.3	Numerical dark potential	73
7.3.1	The Fourier-Bessel method for the dark potential	74
7.3.2	Altered Fourier-Bessel method for the dark potential	77
7.3.3	Software and Implementation	78

7.4	Testing the numerical algorithm; Spherical symmetric case	78
7.4.1	Numerical bright potential	78
7.4.2	Dark potential	80
7.4.3	Alteration to Fourier-Bessel method	81
7.5	Spiral galaxy NGC6503	83
7.5.1	Mass-to-light ratio	83
7.5.2	Results NGC6503	83
8	Testing MOND and CEG to observed rotation curves	87
8.1	MOND and CEG fits	87
8.1.1	Fitting parameters	88
8.1.2	Fitting procedure	89
8.2	Fitting CEG and MOND	90
8.2.1	Fit results	92
9	Discussion & Conclusion	97
9.1	Theoretical discussion & conclusions	97
9.2	Experimental discussion & conclusions	98
	References	99
A	Derivation of the field equations	101
A.1	Geodesic Equation	101
A.2	The imposter field equations	103
A.3	The modified Einstein field equations	104
A.4	Energy momentum tensor	108
B	Constraints on coefficients imposter field scalar	109
B.1	Constraints in De Sitter space	109
C	General lensing systems	111
D	Fits CEG and MOND	113
D.0.1	Fits CEG to SPARC	113
D.0.2	Fits MOND to SPARC	116

Physical Constants

Name	Symbol	Value	Units	Source
Speed of light	c	299792458 (exact)	km s^{-1}	-
Parsec	pc	$3.08567758 \cdot 10^{16}$ (exact)	m	-
Hubble constant	H_0	(74.03 ± 1.42)	$\text{km s}^{-1} \text{Mpc}^{-1}$	1
Solar mass	M_\odot	$(1.98847 \pm 0.00007) \cdot 10^{30}$	kg	2
Solar radius	R_\odot	$(696342 \pm 65) \cdot 10^3$	m	3
Gravitational constant	G	$(6.67408 \pm 0.000046) \cdot 10^{-11}$	$\text{m}^3 \text{kg}^{-1} \text{s}^{-2}$	4
Milgrom's constant	a_m	$1.2 \cdot 10^{-10}$ (exact)	m s^{-2}	5

1. Riess, Adam G., et al. "Large Magellanic Cloud Cepheid Standards Provide a 1% Foundation for the Determination of the Hubble Constant and Stronger Evidence for Physics Beyond LambdaCDM." arXiv preprint arXiv:1903.07603 (2019).
2. Williams, David R. "Sun fact sheet (NASA). 2004.
3. Emilio, Marcelo, et al. "Measuring the solar radius from space during the 2003 and 2006 Mercury transits." *The Astrophysical Journal* 750.2 (2012): 135.
4. Mohr, Peter J., Barry N. Taylor, and David B. Newell. *J. Phys. Chem. Ref. Data* 45 (2016)
5. Bekenstein, Jacob, and Mordehai Milgrom. "Does the missing mass problem signal the breakdown of Newtonian gravity?" *The Astrophysical Journal* 286 (1984)

Dedicated to my parents,

Thank you for your unwavering support and guidance.

Chapter 1 ●■▲

Introduction

1.1 Introduction

In 1933, Swiss astronomer Fritz Zwicky noticed that the visible mass in galaxies was insufficient to explain the dynamics of these galaxies (the observed velocities). He calculated that there had to be at least 400 times the amount of matter present in those galaxies as was predicted from their luminosity. He called this unseen matter 'dunkle materie', which we now refer to as dark matter. Next to explaining the dynamics of galaxies, dark matter has also proven rather successful in explaining a wide-range of other phenomena from the evolution of the universe to the gravitational lensing of galaxies. Nowadays, dark matter has become the dominant theory for explaining the dynamics of the universe.

Instead of proposing extra matter (dark matter), one could of course also alter the gravitational force matter exerts. Such a gravitational theory, in which the gravitational force is altered to fit the measured dynamics of galaxies, is called a modified gravity theory. In this report, we will consider such an alternative to dark matter called covariant emergent gravity (CEG). This theory is a coordinate-free formulation by Sabine Hossenfelder of Erik Verlinde's theory of emergent gravity (EG). Another modified gravity theory that we will focus on is MOND (modified Newtonian dynamics). This theory makes very similar predictions to CEG and we will consider both the similarities and differences of MOND and CEG.

The main goal of this report is to identify experimentally verifiable results for CEG through a theoretical analysis of the covariant field equations. The initial goal of this report was to understand both EG and CEG. We have expanded upon this goal both theoretically and numerically. Our theoretical expansion consists of a gravitational lensing formalism for CEG and an attempt at a cosmological model. Our numerical expansion consists of an algorithm to solve for CEG in cylindrical symmetric densities. We have also tested the prediction of CEG and MOND by fitting fitted CEG and MOND to 131 galaxies using the SPARC database. This was done by employing a Markov Chain Monte Carlo (MCMC) fitting algorithm using three fit parameters.

1.2 Structure of the report

This report can be divided in three parts: introductory chapters, theoretical chapters and numerical chapters. The introductory chapters have been included to introduce readers who are unfamiliar with topics such as galaxies and general relativity to these concepts in a concise and self-contained manner. These chapters are *Astrophysics and galaxies* and *From Newtonian to Einsteinian gravity*.

The theoretical chapters introduce EG and CEG alongside the field equations of CEG and its Newtonian approximation that we will use in the numerical sections. These chapters also include our theoretical contributions, which are a lensing equation for CEG valid for the current assumptions in CEG and an attempt at a cosmological model for a vacuum/matter-dominated universe. These chapters include *Emergent Gravity*, *Covariant Emergent Gravity* and *Theoretical applications of CEG*.

The final part of this report consists of the numerical chapters. In these chapters we provide the numerical algorithm we have developed for solving for CEG and MOND for cylindrical symmetric matter densities. We test this method by applying it to both a spherical symmetric density and SPARC galaxy NGC6503 using assumed density profiles. In order to also test MOND and CEG, we have also fitted MOND and CEG velocity predictions in galaxies to the observed velocities in these galaxies using the SPARC data set. This is done using a Markov Chain Monte Carlo (MCMC) fitting algorithm using three fit parameters. The numerical chapters include *Fourier-Bessel method & results* and *Testing MOND and CEG to observed rotation curves*.

The report concludes with a chapter discussion & conclusions which summarizes the entire report and lists our theoretical and numerical results and discussion on these results. We purposefully chose to separate the theoretical and numerical part of this report to accommodate readers unfamiliar with general relativity. The numerical sections are written in such a way to be readable by an audience familiar with Newtonian gravity.

1.3 Reading routes

In order to accommodate readers of different disciplines and level of expertise, we have included different routes to navigate this report based on the time available, the level of expertise and the primary interest of the reader. These routes also attempt to make the size of this report manageable. There are three distinct routes, the bachelor route, the astrophysical route and the theoretical route. Each route has a distinct symbol. The bachelor route is indicated by a green circle ●, the astrophysical route by a blue square ■ and the theoretical route by a red triangle ▲. At the beginning of each chapter, we indicate whether the chapter is included in the route by a coloured symbol (included) ● or grayed-out symbol ● (not included). Each route is self-contained. Additionally the routes are marked by thumb marks, such as the magenta '1st' thumb mark on the top of this page. The white text indicates the chapter number, whilst a blue thumb marker indicates it as part of the astrophysical route, a red marker as part of the theoretical route and a magenta marker (red + blue) as part of both routes. This is done in order to make the various routes easier to identify whilst reading.

1.3.1 Bachelor route

● The bachelor route consists of the introductory chapters, theoretical chapters and the numerical chapters. This is a time consuming route and only applicable to bachelor students that are also prepared to learn the basics of general relativity and field theory. A less time consuming route at third year bachelor level is the astrophysical route, which does not require the reader to learn general relativity or know astrophysics.

1.3.2 Astrophysical route

■ The astrophysical route focuses on the dynamics of galaxies and the predictions MOND and CEG make for these dynamics. This route includes the introductory chapter on astrophysics

and galaxies and the numerical chapters and is meant to be at third year bachelor level. The reader is not required to know astrophysics nor general relativity. The route is designed for readers that are interested in the testable predictions MOND and CEG make without going over the relativistic aspects of both theories. Readers already familiar with the dynamics of galaxies and the SPARC data set can skip directly to the numerical chapters. A reader interested in cosmology can also read the relevant section in the chapter on theoretical applications of CEG. This route covers the chapters: *Astrophysics and galaxies*, *Fourier-Bessel methods & results*, *Testing MOND and CEG to observed rotation curves* and *Discussion & Conclusion*.

1.3.3 Theoretical route

▲ The theoretical route consists of the introductory chapters and the theoretical chapters. This route is intended for readers that are primarily interested in general relativity, the covariant version CEG of emergent gravity and theoretical applications. Readers already familiar with general relativity can skip the chapter on from Newtonian to Einsteinian gravity. This route covers the chapters *Astrophysics and galaxies*, *From Newtonian to Einsteinian gravity*, *Emergent Gravity*, *Covariant Emergent Gravity*, *Theoretical applications CEG* and *Discussion & Conclusion*.

Amends to all routes can of course be made based on the preference of the reader. Whichever route the reader embarks on, have fun!

Chapter 2 ●■▲

Astrophysics and galaxies

“Far out in the uncharted backwaters of the unfashionable end of the western spiral arm of the Galaxy lies a small unregarded yellow sun. Orbiting this at a distance of roughly ninety-two million miles is an utterly insignificant little blue green planet whose ape-descended life forms are so amazingly primitive that they still think digital watches are a pretty neat idea.”

Douglas Adams, *The Hitchhiker’s Guide to the Galaxy*

In order to make the reader familiar with the various physical objects we will study, we have included this chapter on astrophysics of galaxies. This chapter introduces the following relevant subjects:

1. Galaxies, their compositions and defining parameters
2. Rotation Curves and the SPARC data

We introduce these subjects here to make the subsequent chapters more accessible to the reader. The section on galaxies also introduces the data set and the various parameters we will use throughout the report. Thus readers already familiar with the mentioned subjects can skip this chapter except for the section on the SPARC database.

2.1 Rotation curves

The main subject of this report is the rotational velocity of galaxies. In fact, the greater part of this report concentrates on just one question: *How fast do galaxies rotate?* For planets like the earth orbiting a star like the sun in a circular orbit such a question is rather trivial. Calculate the gravitational force the sun exerts on the earth using Newton’s laws and you will find that the earth should rotate at nearly 30 kilometers per second.

What makes the fact that we are dealing with a galaxy so hard to justify the length of this report? A galaxy is not fundamentally different from the solar system. We calculate the gravitational force in the galaxy based on the matter we observe and from that we are perfectly able to calculate how hard it should rotate. Yes, it is admittedly harder because a galaxy is made up of various components from which we only receive a shimmer of light here on earth. But still, it is doable and will be done in this report. No, it is not the computational complexity that hinders us. It is the simple fact that we would get the wrong answer for the velocities inside the galaxies. Even invoking the advanced machinery of general relativity would not get us much further.

In figure 2.1, we have plotted the baryonic velocity versus the observed velocity for the spiral galaxy aptly named NGC6503. For now, baryonic velocity simply means the velocity as you would calculate with (Newtonian) physics based on the matter you directly observe in the

galaxy. On the horizontal axis is the radius with respect to the center of the galaxy and on the vertical axis the velocity measured at that radius. A plot of the rotation speed of a galaxy versus radial distance is called a rotation curve. This is a word to remember, as we will keep returning to these plots throughout the report. Moreover, spiral galaxy NGC6503 is also on the cover of this report, as it will serve as a testing ground for all our ideas and theories.

It is clear that we are not even off by a simple scaling factor, the two curves look differently. We will fix this problem in due time, but let it be clear that we need a whole new theory beyond Newton to explain these results. Or not? An observant reader might note that we calculated the velocity based on the visible matter. What if there is matter that we cannot see?

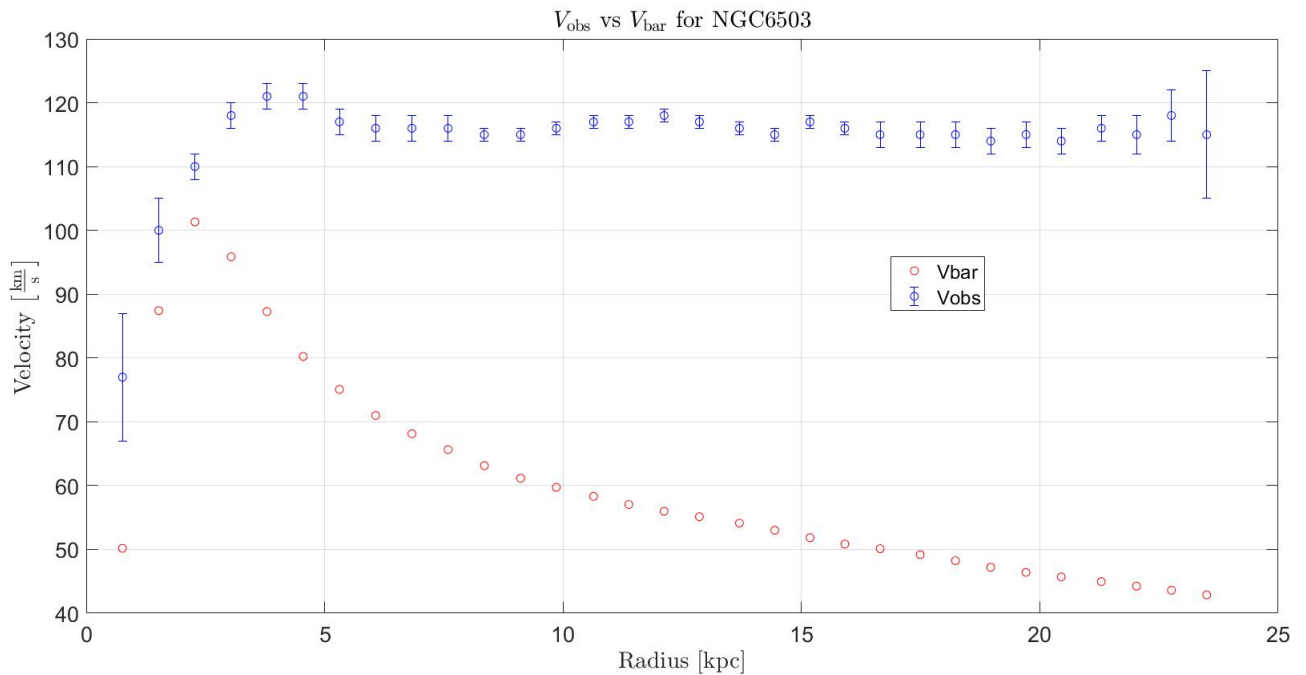


FIGURE 2.1: The observed velocity (blue) and the Newtonian/baryonic velocity (red) versus radial distance for NGC6503 from the SPARC [15] database. The baryonic velocity was plotted for a mass-to-light ratio of $0.5 \frac{M_{\odot}}{L_{\odot}}$.

In 1933, Swiss astronomer Fritz Zwicky noticed that the visible mass in galaxies was insufficient to explain the dynamics of these galaxies (the observed velocities). He calculated that there had to be at least 400 times the amount of matter present as was predicted from their luminosity. He called this unseen matter 'dunkle materie', which we know refer to as dark matter.

Subsequently, Vera Rubin, an American astronomer, found that stars at the edges of galaxies had a much larger speeds than predicted by either Einstein or Newton. This is called the galaxy rotation problem and one way to reconcile these results with the theory is to propose the existence of extra mass (dark matter) in the galaxy. She calculated that there had to be at least 5 to 10 times as much dark matter as ordinary matter. Images of gravitational lensing around these galaxies also seemed to require this much dark matter.

Furthermore, she recorded the rotation curves of galaxies: the rotation speeds of its stars and the gas. She found that the rotation curves tended to flatten at large radial distances as shown

in figure 2.1. This implies that after a certain distance from the galaxies center, stars have a uniform rotational velocity, independent of the distance from the center.

2.2 Observed velocities and dark matter

It appears that in order to save Newtonian/Einsteinian gravity, we will have to introduce a form of invisible matter aptly named dark matter. There are several reasons why one would want to save at least general relativity. For one, the small number of assumptions that are needed to arrive at the theory of general relativity make it a compelling and powerful theory. Secondly, general relativity has made a number of successful predictions beyond Newtonian physics. These were the bending of light in gravitational fields, which was measured by Sir Arthur Eddington, the redshift of light, which was confirmed by the Pound–Rebka experiment and the deviation of Mercury’s orbit from a perfect stationary ellipse by 43 arc-seconds per century, which was a known effect since the 18th century. Its prediction of black holes, which were finally captured on photo in 2019, were disputed until the 70’s. Other phenomena, such as the predicted expansion of the universe have made it an exciting field to study and experiment in. Recently, Kip Thorne and his team at LIGO have confirmed another prediction made by general relativity: gravitational waves. Nonetheless, we have seen that the recent observations of galaxies and also the Cosmic Microwave Background suggest that modifications to either the theory or our understanding of the universe have to be made.

We appear to have no choice but to introduce extra mass in order to make our rotation curves fit the observed rotation curves. However, as we will see later on, on cosmological scales, there is also a need for an additional force, called dark energy to explain the measured acceleration of the expansion of the universe. Dark energy is different from dark matter in that it is not just present in galaxies, but fills the entirety of space as a vacuum energy. We thus see that in order to save Einsteinian gravity, we need to introduce both dark matter and dark energy.

The current measurements indicate that 68% of our universe consists of dark energy, 27% of dark matter and 5% of ordinary matter, called baryonic matter. We would like to add that dark energy has much stronger theoretical grounds than dark matter. Introducing dark energy to general relativity is mathematically similar to adding a constant to the energy in Newtonian physics. The new energy remains conserved, but as adding energy in general relativity is the same as adding mass ($E = mc^2$), introducing dark energy does impact the curvature of space-time. In fact, Einstein introduced it in order to try to make the universe static/non-changing. When observations later indicated that the universe was in fact expanding, the term was reintroduced to explain the acceleration of the expansion.

2.3 Modified gravity

In order to save Einsteinian gravity, we thus need to introduce both dark matter and dark energy. But there is also another option. We can also modify the laws of gravity. We know that gravity works extremely well for problems concerning our solar system, but it is also clear from figure 2.1 that it does not work at all on much larger scales, such as our own Milky Way galaxy. A theory in which we alter the laws of gravity is called a modified gravity theory. We will concern us with two of them: covariant emergent gravity (CEG) and modified Newtonian gravity (MOND).

Modified gravity theories have existed for a long time. It is clear from our rotation curve (2.1), that the first few data points could be made to fit the observed velocity by scaling them

slightly. However, in order to explain the velocity after the initial peak in the velocity, we need to modify our theory. This is because the peak in the baryonic velocity is not present in the observed velocity. Such a modification would need to explain why the rotation curves flatten. Early attempts at fixing the rotation curve problem focused mainly on altering gravity after a certain radius in order to explain the behaviour of the rotation curves.

However, as the location of the baryonic peak depends on the size of the galaxy (mainly the distribution of the stars), such attempts proved futile. More successful was MOND as invented by Mordehai Milgrom [2]. Instead of considering a certain important radius, his idea was to change gravity after a certain threshold acceleration was reached. Milgrom noticed that the the rotational curves flattened when the stars experience an acceleration of less than $a_m \approx 1.2 \cdot 10^{-10} \frac{\text{m}}{\text{s}^2}$. In fact, the peak in figure 2.1 occurs at an acceleration of $1.3a_m$, with the next data point feeling an acceleration of $0.89a_m$.

His modification of Newton's theory was that when the acceleration a is larger than a_m that the gravitational force behaved similar to the Newtonian gravitational force: $\mathbf{g} \sim \frac{1}{r^2}$. However, when $a \leq a_m$ he proposed a modification to gravity. So what forces yield flat velocities? Well the centripetal law states that in nearly circular orbits, the force on a star of mass m with velocity v in a circular orbit of radius r is given by:

$$F_{\text{cent}} = m \frac{v^2}{r} \quad (2.1)$$

For stars in the flat part of the rotation curve ($a \leq a_m$), we see that when we have a force that also goes as $\frac{1}{r}$ the radius in the formulae of the centripetal force cancel and we are left with a constant velocity. It is also clear that a force that goes as $\frac{1}{r^2}$ will always result in a declining velocity profile. The only way to overcome this problem without modifying gravity is to have a lot of mass at larger radii such that the gravitational force does not decrease: dark matter.

Instead of adding more matter at larger radii (dark matter), Milgrom altered the force to be of the form $\frac{1}{r}$ when the acceleration drops below a_m . This would make the velocity of stars that feel an acceleration less than a_m flat. Instead of using a discrete transition $a \geq a_m$ and $a \leq a_m$, one usually uses a interpolation function $\mu(x)$ with $x = \frac{a}{a_0}$. The acceleration a on a mass m in MOND is then given by the Newtonian force F_N via the relation:

$$F_N = m\mu\left(\frac{a}{a_0}\right)a \quad (2.2)$$

When $x \gg 1$, we want Newtonian behaviour, thus $\mu(x) \approx 1$. When $x \ll 1$, we want to alter the force to be of the form $\frac{1}{r}$. As $F_N \sim \frac{1}{r}$, this requires $\mu(x) \approx x$, such that $a^2 \sim F_N$. The standard choice for the interpolating function is the standard interpolating function:

$$\mu(x) = \frac{x}{\sqrt{1+x^2}} \quad (2.3)$$

Using this interpolation function, the velocity of the flat part of the rotation curves can be calculated in the Deep MOND regime $\frac{a}{a_0} \ll 1$. For a spherical mass distribution in the galaxy of total mass M , we know that $F_N = \frac{GM}{r^2}$. Using equation 2.2, the centripetal law 2.1 and our interpolation function, the flat velocity becomes:

$$v_{\text{flat}} = (GMa_m)^{\frac{1}{4}} \quad (2.4)$$

In fact, it is known from observations that there exists a direct relation between the galaxies total mass and the rotational velocity of its stars, which is known as the Tully-Fisher ($v^4 \sim M$)

relation and conforms with experiments closely, such as a recent study of 175 galaxies by Lelli et al [13].

The predictions of MOND are best summarized in the form of a gravitational potential as in the Newtonian case. We will call the Newtonian gravitational potential ϕ_B from baryonic matter. The baryonic potential satisfies Poisson's equation:

$$\nabla^2 \phi_B = 4\pi G \rho \quad (2.5)$$

In MOND there is also just one potential, which we will call ϕ_m . This potential satisfies the equation:

$$\nabla \cdot \left(\mu \left(\frac{|\nabla \phi_m|}{a_m} \right) \nabla \phi_m \right) = 4\pi G \rho \quad (2.6)$$

For accelerations much larger than a_m , $\mu(x) \rightarrow 1$, such that $\phi_m \approx \phi_B$ to recover Newtonian behaviour at high accelerations. At accelerations much smaller than a_m , the function is chosen such that $\mu(x) \rightarrow x$, to arrive at the flat velocity profile. In figure 2.2, we have again plotted the observed velocity, this time against the velocity as predicted by MOND using the standard interpolation function. We see that MOND provides a much better description of the rotational velocities of galaxies than our earlier Newtonian attempts.

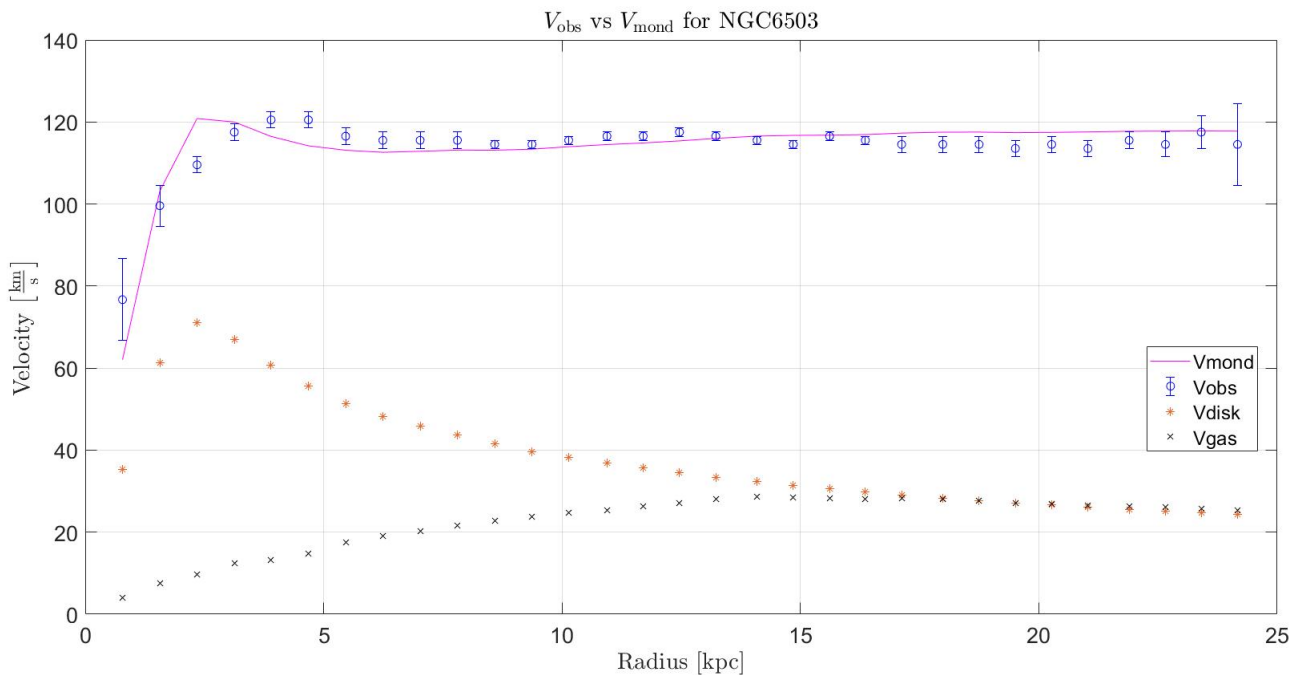


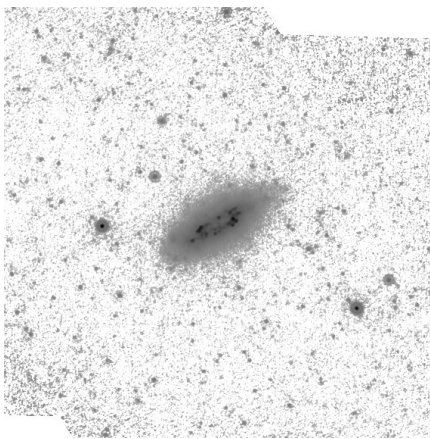
FIGURE 2.2: The observed velocity (blue) and the MOND velocity (magenta) versus the radial distance for NGC6503 from the SPARC [15] database. The disk velocity was plotted for a mass-to-light ratio of $0.5 \frac{M_{\odot}}{L_{\odot}}$. The MOND velocity was calculated as indicated in the chapter on Testing MOND and CEG to observed rotation curves.

2.4 The structure of galaxies

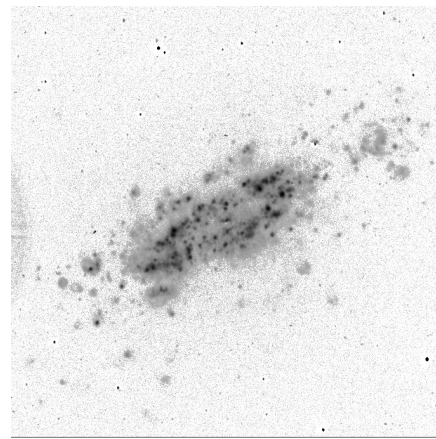
It is now time to explore the stars and beyond. A picture of our favorite galaxy NGC6503 is included in figure 2.3. Of course, this is not what we see through our telescopes, but rather the result of many fine-tunings and coloring schemes. A galaxy, such as our own Milky Way, consists of two main components: stars and gasses. Both components produce light at



FIGURE 2.3: Hubble Space Telescope image of galaxy NGC6503. Copyright © ESA/Hubble.



(A) photometric profile of NGC6503 at $24 \mu\text{m}$ from the Spitzer archive [30].



(B) The H_α photometric profiles of NGC6503 from the Spitzer archive [30].

FIGURE 2.4: Images of NGC6503 from the Spitzer mission [30].

different wavelengths. In figure 2.4a we have shown the photometric profile of NGC6503 at $24 \mu\text{m}$ as obtained by the Spitzer telescope missions [30]. These infra-red wavelengths are mainly produced by the stars of the galaxy. The right image (2.4b) shows the H_α hydrogen lines, one of the major gasses of the galaxy. The left profile thus shows the distributions of stars in NGC6503, whilst the right profile shows the distribution of gas.

Galaxies are characterized by their Hubble type. This scheme divides galaxies into three major classes. Elliptical galaxies, lenticular galaxies and spiral galaxies. Both lenticular and spiral galaxies are disk galaxies, but lenticular galaxies are disk galaxies that do not appear to have spiral arms. Most of the galaxies we are interested in will be disk spiral galaxies. For instance, NGC6503 has Hubble type Scd (or 7) indicating that it is a spiral galaxy (S) with diffuse arms (d). Some galaxies also contain a third component: bright spherical centers, called bulges. However, we will ignore these throughout the report.

Two other important parameters of a galaxy include the galactic distance D from us to the galaxy and the inclination i of the normal of the disk with respect to us. The distance of the galaxy is usually based on the intensity of the light we receive on earth from objects

such as supernovae near the galaxy. As we know very well what the initial intensity of such supernovae is, we can estimate the distance the light traveled from the received intensity.

The disk inclination i is based on numerically fitting an inclined disk on the observed photometric profiles. As the galaxy is a flat circular disk, it is always observed under an angle such that its circular shape appears as an ellipse to us. We can thus fit such an elliptical shape to a galaxy to recover its inclination i with respect to us.

2.5 Galactic velocities

Both the stellar disk and the gas add to the total gravitational pull of the galaxy on its disk. Let us indicate the baryonic gravitational pull of the stellar disk at a radius R from the galaxies center by g_{disk} and of the gas g_{gas} . The total baryonic gravitational pull is then $g_{\text{tot}} = g_{\text{disk}} + g_{\text{gas}}$. According to the centripetal law, this yields a total baryonic velocity of V_{bar} :

$$V_{\text{bar}}^2 = R \cdot g_{\text{tot}} = R \cdot g_{\text{disk}} + R \cdot g_{\text{gas}} \quad (2.7)$$

Thus, when we keep the velocities squared, we can linearly add the contributions of the disk and the gas. We therefore decompose the velocity into two components, namely:

$$\frac{V_{\text{disk}}^2}{R} = g_{\text{disk}} \quad , \quad \frac{V_{\text{gas}}}{R} |V_{\text{gas}}| = g_{\text{gas}} \quad (2.8)$$

We thus decompose the velocity into a velocity V_{disk} as caused by the stellar disk and a velocity V_{gas} as caused by the gas. The absolute value in V_{gas} is needed to account for the fact that the gas is sometimes more widespread than the disk, making it possible that the disk and gas contributions are in different directions.

The database we will use later on does not list the acceleration of the individual components. It lists the velocities such as we have defined them above together with the radius R . Whilst V_{disk} will always be positive, V_{gas} might be negative, indicating that the gas pulls outward at that radius, instead of towards the galactic center. We will discuss the data set next.

2.6 The SPARC database

We will use the SPARC database [15]: a set of observations of 175 nearby galaxies. The SPARC data set encompass a large variety of galaxies with both high surface brightness (HSB) spirals and low surface brightness disks (LSB). The LSB galaxies often show slowly rising rotation curves, whilst the HSB galaxies have fast rising rotations curves that flatten at small radii. The SPARC sample of 175 nearby galaxies consists of both surface photometric profiles at $3.6 \mu\text{m}$ (the stars) and high quality H_I/H_α (the gas) rotation curves. The $3.6 \mu\text{m}$ profile is similar to figure 2.4a, whilst the H_I/H_α are similar to figure 2.4b.

Don't worry. We don't actually have to calculate V_{disk} and V_{gas} based on the photometric profiles. This was already done by the SPARC team. They also calculated the galactic distance D and inclination of the disk i and provided errors for these parameters. Since H_I gas is dynamically cold (low thermal motion), it directly traces the gravitational potential. Since we know the emission lines of H_α exactly, we can calculate the observed velocities in the galaxy by studying the Doppler shifts of these lines. Thus the data also contains V_{obs} , the observed velocity in the galaxy. The H_I gas is also diffuse and extends further than the stellar mass as can also be seen in our favorite galaxy NGC6503 from figure 2.4a and 2.4b. This

means that the rotation curves of the gas probe the gravitational potential out to large radii, making it an excellent data set to test the predictions of MOND and CEG.

We will make a couple of assumptions about the SPARC galaxies. For instance, we ignore pressures in the gas as they only become significant in very low mass galaxies with velocities of $\approx 20 \text{ km s}^{-1}$ [14]. We also ignore the hot gas component, as it only has a significant impact for radii larger than 1000 kpc [4]. Thirdly, we also neglect the contribution of the molecular gas as this does not provide a major contribution to the total baryonic mass of nearby galaxies [21].

A quick summary of this database is thus that we have both the observed velocities V_{obs} and the velocities V_{gas} and V_{disk} that the gas and disk respectively contribute based on Newtonian gravity. For most of the report V_{disk} and V_{gas} will be sufficient in order to test the predictions of MOND and CEG. However, there will be times in which we also need to know the matter density profiles of the stellar disk and gas components. These can be extracted from the photometric profiles such as figure 2.4a and 2.4b. From these photometric profiles one can estimate the surface brightness at each radius R . A profile with the surface brightness at each radius R is called a luminosity profile. We will use these profiles to solve for the matter densities ρ of the stellar disk. This will be necessary to solve differential equations such as 2.6 in the remainder of the report. We will now discuss how one would estimate the density profiles from the luminosity profiles.

2.6.1 Gas profile

The decomposition of galaxies into mass profiles for the various components is not an easy task. We will start with the diffuse cold gas. At the time of writing this report, no luminosity profiles for the gas components were available in the SPARC data set. This is because V_{gas} was easier to collect/extract from the literature by the SPARC team than the original H_I surface photometric profiles.

This implies that we need to estimate the gas profile from the available data. For the gas components, the available data in the SPARC database is the contribution of the gas to the rotation curve called V_{gas} . But we also have access to defining parameters of the gas in the galaxy such as the total measured gas mass in the galaxy M_{HI} and the radius R_{HI} where the H_I surface density reaches a value of 1 solar mass per pc^2 . The last radius is simply a characteristic radius of the gas profile. Both these quantities were extracted from the photometric profiles of the galaxies by the SPARC team. The gas mass can be exactly calculated from the photometric profile, as the conversion from light to mass is exactly known for gas from the spin-flip transition [15].

A Gaussian profile surface density for the H_I gas components of late type spiral galaxies was found to be a good fit by a recent paper by Thomas P. K. Martinsson [19], but the fit may break down for low-mass dwarf galaxies. Such a fit is described by a surface density of the form:

$$\Sigma(R) = \Sigma_{\text{max}} e^{-\frac{(R-R_{\text{max}})^2}{2\sigma^2}} \quad (2.9)$$

They found that $R_{\text{max}} = 0.40R_{HI}$ and $\sigma = 0.36R_{HI}$. The prefactor Σ_{max} will be fixed such that the total gas mass is $M_{\text{gas}} = 1.33M_{HI}$ when we integrate over the entire galaxy. The factor of 1.33 accounts for the Helium contribution to the total gas in the disk [15] that is not visible in the photometric profiles.

2.6.2 Stellar disk

The next component of a galaxy are the stars confined to the stellar disk. The stellar disk follows a well established exponential density profile of the form $\Sigma \propto e^{-\frac{R}{R_d}}$ in which R_d is the disk scale length. For the stellar disk, the 3.6 μm photometric profiles are available in contrast to the gas. Thus for the gas, we need to estimate the density profile, but for the stars, we can simply use the luminosity profiles.

A major assumption we now make is that we assume that the matter density at radius R is proportional to the amount of light we observe at radius R . This is similar to assuming that the entire stellar disk is made up of the same material. We can thus use the luminosity profiles (the light surface density at each point) as calculated by SPARC and scale them appropriately such that the total mass of the disk will be the total stellar mass.

2.6.3 Mass-to-light ratio

Thus we see that we need a scaling factor γ_{disk} called the mass-to-light ratio to convert the amount of light we observe from the stars in a galaxy into their mass. If L_* is the total luminosity in units of solar luminosity of the disk and M_* the total mass in units of solar mass, then we thus assume the relation $M_* = \gamma_{\text{disk}} L_*$. The value of γ_{disk} can be estimated from population synthesis models and is found to be $\gamma_{\text{disk}} = 0.5 \frac{M_\odot}{L_\odot}$ [20] in which M_\odot is one solar mass and L_\odot one solar luminosity.

You might now wonder how we knew the velocity contribution of the disk V_{disk} , when we did not know the matter density, just the luminosity density. Well, take a second look at the caption of figure 2.1 and figure 2.2. The baryonic velocity and disk velocity in the SPARC data are in units of luminosity, thus based on the luminosity profiles, such that we can use our own mass-to-light ratio if necessary. This implies that for the SPARC data, we have:

$$V_{\text{bar}}^2 = \gamma_{\text{disk}} V_{\text{disk}}^2 + V_{\text{gas}} |V_{\text{gas}}| \quad (2.10)$$

In fact, we plotted figure 2.1 for a mass-to-light ratio of $\gamma_{\text{disk}} = 0.5 \frac{M_\odot}{L_\odot}$. Note that V_{gas} does not need a conversion factor, as this factor is exactly known from spin-flip transitions, as said before.

We would also like to add that estimates for γ_{disk} do not necessarily work for MOND/CEG models. Another reason to not use this $\gamma_{\text{disk}} = 0.5 \frac{M_\odot}{L_\odot}$ is because the values of γ_{disk} as calculated by Nathaniel Starkman [25] using a maximum-disk model (dark matter) for the SPARC galaxies sometimes differ significantly from the population synthesis model. The way we do calculate this mass-to-light ratio will be discussed later.

In order to also be able to describe the density profiles at radii further than measured by SPARC, we also fit an exponential density distribution to the tail of the luminosity profile to describe the density profile beyond measured radii. This does not affect our results as the observed velocities were measured at the same radii as the luminosity profiles. However, this allows us to determine the rotation curves further out.

In summary, throughout most of the report we will only use the contribution the disk provides to the rotation curves called V_{disk} and the contribution the cold gas provides called V_{gas} as in equation 2.8. If we want to estimate the true contribution of the stars in the disk, we have to provide a mass-to-light ratio γ_{disk} . Sometimes, we will need to refer back to the actual density profiles of the components of the galaxy. For the gas component, we use an assumed

Gaussian density profile based on defining parameters from SPARC. For the stellar disk, we use the luminosity profiles and a conversion ratio γ_{disk} to convert these to matter profiles.

2.7 Dark matter in galaxies

If we were not to modify Newton's law of gravity, we could also ask how much dark matter there should be in our galaxy NGC6503. Such a procedure is similar to our previous procedure. In such a procedure, one usually uses estimated density profiles for the different components of the galaxies. The amount of dark matter is usually fitted such that the observed velocity coincides with the calculated velocity from the baryonic profiles plus the dark matter density.

The dark matter density profile is usually taken to be a Navarro–Frenk–White profile of the form:

$$\rho(r) = \frac{\rho_0}{\frac{r}{R_s} \left(1 + \frac{r}{R_s}\right)^2} \quad (2.11)$$

The density ρ_0 and the scale radius R_s are fitted as is the mass to light ratio for the disk γ_{disk} . Such a fitting procedure is called a maximum-disk model. Note that the dark matter profile does not have a maximum at the center of the disk, but rather forms a sort of halo with radius R_s .

We have now said all that we need to know about galaxies. It is clear from our discussion that we need to alter Newtonian/Einsteinian gravity. Three possible candidates are dark matter, MOND and the theory we will introduce next: (covariant) emergent gravity.

2.8 Covariant Emergent Gravity

2.8.1 Quantum gravity

Recently, physicists have been trying to reconcile general relativity with quantum mechanics. Many physicist believe that quantum mechanics is the true representation of the world and that general relativity thus has to be described in a quantum mechanical framework and be 'quantized'. The general rules for quantizing a theory have successfully quantized the theory of electromagnetism and the strong and weak nuclear force, but have failed at quantizing general relativity. It is thus believed that general relativity is more deeply connected with quantum mechanics than is now known. One reason for this are the infamous black holes. Black holes have been shown to carry a finite entropy by Jacob Bekenstein. This is odd for a classic field theory. Classical theories often lead to an infinite amount of entropy, as is known from the ultra-violet catastrophe. These infinities are resolved by quantizing phase-space, like in the case of the ideal gas.

Recent progress by Susskind and other in the field shows that the finite entropy derived by Jacob Bekenstein comes from the entanglement present between the inside of the black holes and the outside of the black hole horizon. Thus it seems that black holes are the key to combining concepts of gravity and quantum mechanics.

2.8.2 Covariant Emergent Gravity

A modified theory of gravity that incorporates the ideas of entanglement in a black hole is the theory of Erik Verlinde. He claims that the laws of gravitation can be derived from applying

the same principles that Bekenstein applied to black holes to derive the entropy of the black hole.

However, such a procedure could only recover the usual law of gravity. But we have seen that these are simply not enough to explain the observations. Therefore, Erik Verlinde proposed in 2016 that there is another source of entropy associated with the dark energy content of the universe. This paper will explore the effects of the model of Verlinde on the rotation speeds of stars in galaxies and the bending of light in these galaxies. However, we are not at that point yet, as we still want to cover the basics of field theory and general relativity.

Chapter 3 ● ■ ▲

From Newtonian to Einsteinian gravity

3rd

“When I was in high school, my physics teacher—whose name was Mr. Bader—called me down one day after physics class and said, “You look bored; I want to tell you something interesting.” Then he told me something which I found absolutely fascinating, and have, since then, always found fascinating. . . . the principle of least action.”

Richard P. Feynman

This chapter is a concise introduction to general relativity (GR) and classic field theory for readers that are already familiar with Newtonian gravity and Lagrangian mechanics. If you are already familiar with general relativity, you may skip this chapter.

The aim of this chapter is to introduce all the concepts of general relativity and classic field theory that are used in the subsequent chapters on emergent gravity (EG) and covariant emergent gravity (CEG). We introduce the concepts: Lagrangians, metrics, geodesics, covariant derivatives and the Einstein equations. The last section is also an introduction to the physics of the expanding universe.

3.1 Classical Gravity

Our story starts where most modern physical theories begin: with a loud bang. Not the sound of an universe forming, but of an apple falling on Newton’s head, and the subsequent explosion of scientific discoveries that followed. The age of a non-violent revolution had begun, when Newton formulated his laws for fruits and non-fruits alike that would determine physics forever.

According to Newton’s theory of Gravity, a particle with mass m obtains an acceleration \mathbf{a} in a gravitational field ϕ_B as:

$$\mathbf{F} = m\mathbf{a} = -m\nabla\phi_B \quad (3.1)$$

However, these vector equations can prove to be rather pesky to solve. This is why physicist have invented conservation laws, such as the conservation of energy, momentum and angular momentum. In fact, in his book *Mechaniques Analytiques*, Joseph Lagrange found that these vector equations could equivalently be derived from a single scalar formalism, called Lagrangian mechanics. The Lagrangian L and action S of a particle in a gravitational field is:

$$L = \frac{1}{2}v^2 - \phi_B \quad \text{with} \quad S = \int_0^T L dt \quad (3.2)$$

Note that I have conveniently left out the mass m of the body. The crux here is that a particle's acceleration in a gravitational field does not depend on its mass m . According to Einstein, this is because the gravitational force is not a force between two particles as Newton formulated it, it is a property of space-time.

Joseph Lagrange showed that solving Newton's equations was similar to choosing the path through space between two fixed endpoints that minimized/maximized the action S . This is equivalent to finding a path $x(t)$ that satisfies the Euler-Lagrange equations:

$$\boxed{\frac{d}{dt} \frac{\partial L}{\partial \mathbf{v}} = \nabla L} \quad (3.3)$$

Plugging in our Lagrangian 3.2 indeed yields Newton's equation 3.1. The Euler-Lagrange equations also be derived from Hamilton's principle, stating that the particles path $\mathbf{x}(t)$ that maximizes/minimizes the action S , is the physical taken path. This is equivalent to making the variation in the action δS vanish up to first order in $\delta \mathbf{x}(t)$.

You might now wonder: *Did you not just write Newton's equations differently?* and you would be correct. No information is contained in Lagrange formalism for gravity that cannot be obtained from Newton's formulation. However, it is much easier to recover conserved quantities from Lagrangian's using Noether's theorem than it is to recover them from Newton's equations. In Newton's equations conservation of angular momentum is something you stumble upon, whilst in Lagrange's theorem it is a matter of choosing the right coordinates. Secondly, Lagrangians will also prove to be useful not only in solving for the motion of particles, but also for solving for the dynamics of a field ϕ_B as we will see next.

3.2 Particles and Field, What's the difference?

A valid concern you might have at this point is how do we know what ϕ_B is in Lagrange's formalism. Well, let's touch upon that next. In order to prevent using the same example over and over again, let us use the Lagrangian from the prototypical field of electromagnetism instead.

For a system of particles x_i with charge q_i and velocity \mathbf{v}_i , the Lagrangian in a EM field given by a magnetic vector potential \mathbf{A} and electric scalar potential ϕ is:

$$L = \sum_i \frac{1}{2} m \mathbf{v}_i^2 + q_i \mathbf{A} \cdot \mathbf{v}_i - q_i \phi \quad (3.4)$$

From this Lagrangian it is easy to make the translation to the Lagrangian of a continuous body. For a continuous body with charge density ρ and a current \mathbf{J} , the Lagrangian becomes:

$$L = \iiint \{ \mathbf{A} \cdot \mathbf{J} - \phi \rho_c \} dV \quad (3.5)$$

How can we distill from this Lagrangian how the fields \mathbf{A} and ϕ behave? This is in fact quite simple and the keyword here is to insert the word field everywhere in our single particle formalism.

Like in the single particle case, the ideas are similar. In the single particle case, one can derive the Euler-Lagrange equations from varying the particles path $\mathbf{x}(t) \rightarrow \mathbf{x}(t) + \delta \mathbf{x}$. Similarly, we can derive the Euler-Lagrange field equations by varying the field $\phi(\mathbf{x}, t) \rightarrow \phi(\mathbf{x}, t) + \delta \phi$. Note that in the single particle case, the particle position only depends on the time t . The field

however, is a three dimensional quantity that also depends on the space point \mathbf{x} you evaluate the field at.

Now, we assume our fields do not depend on time t . The translation from particle to field equations then become:

$$\mathbf{x} \rightarrow \phi \quad (3.6)$$

$$\mathbf{v} \rightarrow \nabla\phi \quad (3.7)$$

$$\frac{d}{dt} \rightarrow \nabla \quad (3.8)$$

The Euler-Lagrange equations for a field ϕ , then become:

$$\frac{d}{dt} \frac{\partial L}{\partial \mathbf{v}} = \nabla L \rightarrow \nabla \cdot \frac{\partial L}{\partial \nabla \phi} = \frac{\partial L}{\partial \phi} \quad (3.9)$$

As in the single particle case, we could have derived these field equations from varying the field and searching for a maximum/minimum of the corresponding action, but this is not a report on deriving the Lagrange equations. For a more in-depth treatment of Lagrangians and field, see Goldstein's classic [7].

Applying our Euler-Lagrange field equations 3.9 to the electromagnetic Lagrangian, the equations for the electric scalar potential ϕ become:

$$0 = \rho_c \quad (3.10)$$

This not quite yet the first of Maxwell's equations, but we are close nonetheless. What we need is a source term for the field ϕ , such that the left hand side of the Euler-Lagrange field equations 3.9 becomes non-zero. From Maxwell's equations, we know that the correct alteration is:

$$L = \iiint \left\{ \mathbf{A} \cdot \mathbf{J} - \phi \rho_c + \frac{1}{2} \epsilon_0 \nabla \phi \cdot \nabla \phi \right\} dV \quad (3.11)$$

The additional term $\frac{1}{2} \epsilon_0 \nabla \phi \cdot \nabla \phi$ is called the source term of the field ϕ . Note that the source term is similar to the kinetic energy term in our single particle Lagrangian. Using the Euler-Lagrange field equations 3.9 on this new Lagrange would yield the correct result for the scalar potential ϕ . The term $\phi \rho_c$ is called the interaction term between the field and the particles. Can you see how to make the action S correct for the remaining vector potential \mathbf{A} by including a similar source term such that we recover the other Maxwell equations for a static current and charge density?

3.3 Particles and Fields: The field equations

We will now combine our Lagrangian formalism for particles with our formalism for fields. In both instances, one want to maximize/minimize an action S . This is done by varying either the particles position $\mathbf{x}(t)$ or the fields value ϕ . As we assume that these variations are independent, our total action will simply be the sum of the single particle formalism and the field formalism. If one wants to obtain the equation of motion for the single particle, this total action is varied with respect to the particles position $\mathbf{x}(t)$. For the field one varies the total action with respect to the field.

The total action S for the electromagnetic field (equation 3.11) plus the action of a single particle becomes:

$$S = \iiint \left\{ \frac{1}{2} \epsilon_0 \nabla \phi \cdot \nabla \phi - \phi \rho_c \right\} dV dt + \int \left\{ \frac{1}{2} m \mathbf{v}^2 - q \phi \right\} dt \quad (3.12)$$

Here we set the magnetic vector potential $\mathbf{A} = 0$ for educational purposes. q is the charge of the single particle. Before we move on to derive the field equations for the field ϕ and particles position $\mathbf{x}(t)$, let us first make comparisons between the field and particle parts of the action. We see that the kinetic part of the field Lagrangian $\frac{1}{2} \epsilon_0 \nabla \phi \cdot \nabla \phi$ is very similar to the kinetic part of the particle Lagrangian $\frac{1}{2} m \mathbf{v}^2$ with the substitutions $m \rightarrow \epsilon_0$ and $\mathbf{v} \rightarrow \nabla \phi$. The term $\frac{1}{2} \epsilon_0 \nabla \phi \cdot \nabla \phi$ is often called the kinetic or source part of the Lagrangian.

Another prominent term in the Lagrangian is the interaction term $\phi \rho_c$, which is similar to the interaction term for one particle ($q\phi$). The interaction term determines the interaction between the field and the particles, whilst the source term determines how the field responds to these interactions. Viewed in this way, Maxwell's equation $\epsilon_0 \nabla^2 \phi = \rho_c$ are very similar to Newton's equations in one-dimension $m \frac{d^2 x}{dt^2} = F$ with $m \rightarrow \epsilon_0$, $\frac{d^2 x(t)}{dt^2} \rightarrow \nabla^2 \phi$ and $F \rightarrow \rho_c$.

From the action 3.12 we can determine both the equations of motion for a single particle in a field ϕ and the value of the electric field for a charge density of ρ_c . In fact, we already know how to do this. Apply the Euler-Lagrange equations 3.3 to all the terms involving to the particle part yields the single particles motion and applying to Euler-Lagrange field equations (3.9) yields the fields dependence on the charge ρ_c .

This procedure is however not satisfactory for two reasons. Firstly, if we were to give the reader a general action, how would he be able to tell which part belongs to the single particle's motion and which part to the field's. Secondly, how would one approach an action involving higher derivatives in ϕ , which our Euler Lagrange field equations 3.9 do not account for.

A more general approach is already known from classical mechanics. Instead of applying it to the single particle case, we will apply the procedure to the field ϕ . For our field ϕ to be a maximum/minimum of the action S , it has to be a stationary point, thus $\delta S = 0$ up to first order in $\delta \phi$. Thus let us calculate δS when we vary the field from $\phi \rightarrow \phi + \delta \phi$:

$$\delta S = \iiint \{-\delta \phi \rho_c + \epsilon_0 \nabla \delta \phi \cdot \nabla \phi\} dV dt - \int q \delta \phi dt + O(\delta \phi^2) \quad (3.13)$$

In which we make use of the variational rules:

$$\delta(AB) = B\delta A + A\delta B + O(\delta A \delta B^2) \quad \text{and} \quad \delta \nabla A = \nabla \delta A \quad (3.14)$$

We will make use of integration by parts to get rid of the term $\nabla \phi$ as is done in classical mechanics. As in classical mechanics, the variation $\delta \phi$ on the boundary vanishes or put more simply:

$$\iiint \nabla \delta \phi \cdot \nabla \phi dV = \iint_{\partial \Omega} \delta \phi \nabla \phi \cdot d\mathbf{S} - \iiint \delta \phi \cdot \nabla^2 \phi dV = 0 - \iiint \delta \phi \cdot \nabla^2 \phi dV \quad (3.15)$$

In which $\delta \Omega$ indicates the boundary of our space. We thus see that the variation in our action is simply:

$$\delta S = \iiint [-(\rho_c + q\delta(\mathbf{r} - \mathbf{r}')) + \epsilon_0 \nabla^2 \phi] \delta \phi dV dt + O(\delta \phi^2) \quad (3.16)$$

Here $\delta(\mathbf{r} - \mathbf{r}')$ is a Dirac delta function at the particles current position for the sake of completeness. We thus see that if we want the action δS to be stationary (first order in $\delta\phi$), we need that:

$$\epsilon_0 \nabla^2 \phi = (\rho_c + q\delta(\mathbf{r} - \mathbf{r}')) \quad (3.17)$$

Thus we recover the same equation as we recovered from the field Euler-Lagrange equations 3.9 applied to the electromagnetic field Lagrangian 3.11. The approach we followed is of course more general and will be used many times throughout this report. As a way of checking your understanding, see if you can derive the Euler-Lagrange field equations from the general action:

$$S = \iiint \mathcal{L}(\phi, \nabla\phi) dV dt \quad (3.18)$$

3.4 Curved space-time

Now that we have all the required equations from classical field theory, let's translate them into general relativity and curved space-times. It is actually not that hard to figure out how particles will move in curved space-time as we will see next. The real problem is finding out how particles curve space-time, which took Einstein more than 5 years.

Like in classical physics, at every point in space-time, we can define a vector space. This vector space has as origin the specific point in question and vectors pointing from this specific point. However, this time the point in question is indicated with four coordinates (t, x, y, z) in which the time coordinate is called the zeroth coordinate. The vectors therefore necessarily also carry four components. The phrase this space is curved, simply means that the distances between two points in this vector space are no longer given by the Euclidean distance $\Delta x^2 + \Delta y^2 + \Delta z^2$. This is no problem however, as we know we can simply calculate distances in vector spaces by using the inner product or metric on the vector space.

Let us denote the inner product, henceforth called metric, on our vector space by g such that the length of a four-dimensional vector \mathbf{v} is given by $g(\mathbf{v}, \mathbf{v})$. A common example of an inner product is the inner product on Minkowski space in special relativity: $ds^2 = -\Delta t^2 + \Delta x^2 + \Delta y^2 + \Delta z^2$. For a four-vector with components $\mathbf{v} = (v^0, v^1, v^2, v^3)$ this implies $g(\mathbf{v}, \mathbf{v}) = (v^0)^2 + (v^1)^2 + (v^2)^2 + (v^3)^2$. This metric deserves a special name and is called the Minkowskian metric $\eta_{\mu\nu}$.

Before we start confusion four-vector with three-dimensional vectors, let us introduce some shorthand notation. Let the variable μ range from 0, 1, 2, 3 such that the μ th-component of a vector is given by v^μ . We will no longer refer to vectors by \mathbf{v} but rather by their components v^μ for simplicity.

Let us also choose basis vectors e_μ on our vector space. Note that we write basis vectors with downstairs indices and components of vectors with upstairs indices. This has a true mathematical meaning, but for our purposes, it is simply such that we can use Einstein notation. In Einstein notation, indices that appear both upstairs and downstairs are summed over, such that:

$$\mathbf{v} = \sum_{\mu} v^\mu e_\mu \rightarrow v^\mu e_\mu \quad (3.19)$$

This will save us a lot of writing pesky sums.

The inner product on our space is then completely determined by the way it acts on our basis vectors e_μ and e_ν . By linearity of the inner product, we find that:

$$\mathbf{v}^2 = g(\mathbf{v}, \mathbf{v}) = g(v^\mu e_\mu, v^\nu e_\nu) = v^\mu v^\nu g(e_\mu, e_\nu) := v^\mu v^\nu g_{\mu\nu} \quad (3.20)$$

In which we have defined the shorthand notation $g(e_\mu, e_\nu) = g_{\mu\nu}$. An important point to keep in mind is that the inner product will generally depend on the position in space-time.

Thus far, all we have done is applied the formalism of vector spaces equipped with inner products to our space-time and introduced some short-hand notation. So where is the physics? Well, remember Einstein's idea. According to Einstein, particles do not move due to forces but due to the curvature of space-time. His formalism is in principle much simpler than Newton's. We have no need for the a force, as there are no forces. It is all in the inner product $g_{\mu\nu}$. The Lagrangian of single particle thus simply becomes:

$$L = \mathbf{v}^2 = v^\mu v^\nu g_{\mu\nu} \quad (3.21)$$

Thus we have replaced the potential ϕ (the force) by the dependence of $g_{\mu\nu}$ of the position of the particle in space-time.

This is actually all there is to it. In terms of physics we are done now. There is however still a mathematical trick we can pull in order to make our lives simpler. Let our particle follow a path $x^\mu(\tau)$ in space-time parametrized by some parameter τ . From Analysis, we know that there is one special parameter τ , namely the arc length parametrization such that $\mathbf{v}^2 = 1$. Let us therefore choose this parameter throughout this report.

Applying the Euler-Lagrange equations to the Lagrangian 3.21 to the particles position $x^\mu(\tau)$ and velocity $v^\mu(\tau)$ yields the equation of motion:

$$\ddot{x}^\mu g_{\mu\alpha} - \dot{x}^\mu \dot{x}^\lambda \partial_\lambda g_{\mu\alpha} = -\frac{1}{2}(-\dot{x}^\mu \dot{x}^\nu \partial_\alpha g_{\mu\nu}) \quad (3.22)$$

In which the dots indicate derivatives with respect to τ and Einstein summation is assumed. We also introduce the shorthand notation $\frac{\partial}{\partial x^\mu} = \partial_\mu$.

These equations completely determine the motion of a particle in GR. Nonetheless, they are not very pretty. Let us change this by introducing the inverse metric $g^{\mu\nu}$. This is simply the inverse of the matrix with components $g_{\mu\nu}$. Thus $g^{\mu\alpha} g_{\alpha\nu} = \delta_\nu^\mu$ in which δ_ν^μ is the Kronecker delta.

Multiplying equation 3.22 by the inverse metric $g^{\alpha\beta}$, using properties of the inverse metric and rearranging terms, we arrive at the geodesic equations or acceleration equation of the particle:

$$\ddot{x}^\mu = -\dot{x}^\alpha \dot{x}^\beta \Gamma_{\alpha\beta}^\mu \quad (3.23)$$

In which we defined Christoffel symbols to be:

$$\Gamma_{\alpha\beta}^\mu = \frac{1}{2} g^{\mu\delta} (\partial_\alpha g_{\delta\beta} + \partial_\beta g_{\delta\alpha} - \partial_\delta g_{\alpha\beta}) \quad (3.24)$$

3.5 Covariant Derivatives

We thus see from equation 3.23 that the equations in general relativity are very similar to the Newtonian equations. The left hand side contains the acceleration \ddot{x}^μ and the right hand

side contains the "force" $\dot{x}^\alpha \dot{x}^\beta \Gamma_{\alpha\beta}^\mu$. Note that the equations do not depend on the mass of the particle and that the force is due to the difference between inner products at different points (curvature) in space-time.

However, the whole point of general relativity was that particles do not accelerate in space-time as they feel no force. This might feel like a weird notion. Didn't we just show that particles do experience an acceleration? Yes, they do in our coordinate systems in which straight lines are straight lines by Euclidean standards. The geodesic equation 3.23 tells us that particles deviate from these straight lines. But they do not accelerate in the sense that they follow straight lines through space-time. Stated differently, we observe particles following non-straight lines as space is curved.

To make this argument more qualitative. Consider an ant walking on a globe with the globe being our curved space. As the ant walks from the North Pole to the South Pole it will follow a straight line on the globe. But this is not a straight line for someone that observes the ant from a three-dimensional world. He will see that the ant followed a curved path. So who is right?

Well, they are both correct. Even in Newtonian physics, the acceleration you ascribe to an object depends on your coordinate system. But the whole point of relativity is that physics should not depend on your coordinate system but only on the geometry of space-time itself. So is there a way to mathematically capture the idea that particles that obey the geodesic equation 3.23 travel in straight lines on the curved space-time?

Well, one interpretation of non-accelerated particles are the fact that they follow straight lines. For an observer on such a straight line, this statement is equivalent to the fact that the velocity vector v^μ of the line does not change as he moves along the line. Mathematically, this implies $\partial_\alpha v^\mu = 0$.

This is however not true for true for vectors obeying the geodesic equation 3.23. This can easily be seen. Suppose we would formulate the geodesic equation 3.23 in terms of velocities v^μ :

$$\dot{v}^\mu + v^\alpha v^\beta \Gamma_{\alpha\beta}^\mu = 0 \quad (3.25)$$

These equations can be written more cleanly by removing the need for a derivative with respect to the parameter τ by:

$$\frac{d}{d\tau} = \frac{dx^\alpha}{d\tau} \frac{\partial}{\partial x^\alpha} = v^\alpha \partial_\alpha \quad (3.26)$$

Inserting this expression into our velocity geodesic equation 3.25 and cancelling the v^α , we obtain:

$$\partial_\alpha v^\mu + v^\beta \Gamma_{\alpha\beta}^\mu = 0 \quad (3.27)$$

This is the equation we were after. We see that $\partial_\alpha v^\mu \neq 0$ except for spaces in which $\Gamma_{\alpha\beta}^\mu = 0$ or equivalently, flat spaces. Thus our Euclidean notion of non-accelerated ($\partial_\alpha v^\mu = 0$) does not carry over.

Yet, all is not lost. Let us thus introduce an extension of the known derivative ∂_α , called the covariant derivative ∇_α . The definition is:

$$\nabla_\alpha v^\mu = \partial_\alpha v^\mu + v^\beta \Gamma_{\alpha\beta}^\mu \quad (3.28)$$

By the geodesic equation 3.27, particles that obey the geodesic equation obey:

$$\nabla_{\alpha} v^{\mu} = 0 \quad (3.29)$$

We thus see that the notion that particles follow straight lines on space-time is equivalent to $\nabla_{\alpha} v^{\mu} = 0$. This is different from particles following straight lines in Euclidean coordinate systems, which was $\partial_{\alpha} v^{\mu} = 0$.

And with a single sweep (equation 3.29), we have united all. Particles follow straight lines on the curved space-time. If you want to calculate what lines this would be in your coordinate system, you use equation 3.29 to solve for the velocity v^{μ} of the particle. But always remember, the particles actually follow (unaccelerated) straight lines. There is no physics in the choice of your coordinate system.

This covariant derivative will be our replacement of the normal derivative in general relativity. If you will, the covariant derivative is a sort of derivative that also account for the flaws in your coordinate system. Of course, there are a lot of mathematical reasons to choose the covariant derivative, such as the fact that it transforms correctly from one coordinate system into the next etc, but that will be our little secret.

The Euler-Lagrange field equations for a field ϕ for a Lagrangian density \mathcal{L} in our new formalism become:

$$\nabla_{\alpha} \left(\frac{\partial \mathcal{L}}{\partial (\nabla_{\alpha} \phi)} \right) = \frac{\partial \mathcal{L}}{\partial \phi} \quad (3.30)$$

3.6 Other uses of the metric

Apart from its role in the geodesic equations, the metric can also be used to raise and lower components. For instance, we can lower the components of a vector v^{μ} as $v_{\mu} := g_{\mu\nu} v^{\nu}$, in which we assume Einstein summation. Vectors with lower components are called dual vectors. We will not need them in this report, but they are of paramount importance in general relativity and differential geometry.

In order to also make sure that integrals are independent of the coordinates used, we also need to slightly alter volume integrals by the following replacement:

$$\iiint f(\mathbf{x}, t) dV dt \rightarrow \iiint f(x^{\alpha}) \sqrt{-g} dx^{\gamma} \quad (3.31)$$

The $\sqrt{-g}$ is the Jacobian for a general coordinate system. The coordinates x^{α} and dx^{β} are just dummy coordinates. The indices do not indicate vectors but rather volume elements with $dV dt \rightarrow dx^{\gamma}$.

3.7 General relativity

As stated earlier, the hard part is not to solve for the motion of particles, but to solve for the curvature of space-time, a.k.a. the metric $g_{\mu\nu}$. In GR, the metric $g_{\mu\nu}$ is the solution to the Einstein equations:

$$R_{\mu\nu} - \frac{1}{2} g_{\mu\nu} R + \Lambda g_{\mu\nu} = \frac{8\pi G}{c^4} T_{\mu\nu} \quad (3.32)$$

The left hand side contains $R_{\mu\nu}$ and R (which are both function of $g_{\mu\nu}$ and its 1st and 2nd order partial derivatives) are the mathematical expressions for the curvature of space-time.

The right hand side is the energy-momentum tensor $T_{\mu\nu}$, a indication of the amount of energy and mass in the space-time. The definition of this tensor is such that the component $T_{\mu\nu}$ is the flow of energy/momentum density p^μ in the direction x^ν . The constant Λ is simply a constant. We thus see that the left hand side describe the curvature and the right hand side the energy in space-time. Thus energy is a source of curvature and curvature implies energy. Not just matter curves space-time, all sorts of energies such as electrical energy etc. In these equations the metric is dynamic variable and represents the field associated with gravity and space-time curvature.

What form can the energy-momentum tensor $T_{\mu\nu}$ take? From fluid dynamics, the flow of momentum density $\rho\mathbf{v}$ in the x-direction is $\rho\mathbf{v}v_x$. Thus a general relativistic formulation for a fluid with density ρ and four-velocity v^μ would be $T_{\mu\nu} = \rho v_\mu v_\nu$. Note that we have lowered the components of the velocity in order to make sure that the indices match.

The left hand side of these equations have to do with the curvature of space-time, whilst the right hand side have to do with the density and flow of mass and energy. Thus mass curves space-time and a curved space-time implies movement of masses/energies. For a derivation of the Einstein equations and a discussion on their consequences, see Sean Carroll's excellent book [5].

For our purposes, the reader will not need to know how to solve these equations. It is however handy to know that these equations can be derived from varying an action of the following form with respect to the metric $g^{\mu\nu}$:

$$S = S_H + S_m = \frac{1}{16\pi G} \int R\sqrt{-g} dx^\nu + S_m \quad \text{with} \quad \frac{\delta S_m}{\delta g^{\mu\nu}} = -\frac{1}{2}T_{\mu\nu} \quad (3.33)$$

3.8 Cosmology

For a model of the universe, we will only need one simple solution to the Einstein equations. This is the solution of an expanding universe. In this section, we will only be concerned with a spatially flat universe ($\kappa = 0$), to make the equations more feasible.

Suppose that in our universe, the distance between two objects ℓ grows by a scaling factor $f(t)$ such that after a time t , the distance goes from $\ell \rightarrow f(t)\ell$. A metric that incorporates this idea is easy to come up with and is the Friedman-Robertson-Walker metric:

$$ds^2 = g_{\mu\nu}dx^\mu dx^\nu = -dt^2 + f(t)^2 [dx^2 + dy^2 + dz^2] \quad (3.34)$$

This is just shorthand notation in which the components $g_{\mu\nu}$ are indicated in front of the terms $dx^\mu dx^\nu$. For instance, the g_{00} component of the metric is $g_{00} = -1$.

Note that the fact that this is the correct metric actually depends on several assumptions about space, such as homogeneity (space is the same in all locations) and isotropy (space looks the same in every direction). However, we skip these assumptions in order to provide a feasible discussion of an actual solution to Einstein's equations. For convenience, we also use units such that $c = 1$.

We can solve for the scalar factor $f(t)$ by plugging the metric (equation 3.34) into the Einstein equations 3.32. But in order to solve the resulting equations, we also need to evaluate the right hand side of Einstein's equations. We suppose that the entire universe is filled with

matter with density ρ and pressure p . We then obtain the Friedman equations:

$$H^2 = \left(\frac{\dot{f}}{f}\right)^2 = \frac{8\pi G\rho}{3} + \frac{\Lambda}{3} \quad (3.35)$$

$$\dot{H} + H^2 = \frac{\ddot{f}}{f} = -\frac{4\pi G}{3}(\rho + 3p) + \frac{\Lambda}{3} \quad (3.36)$$

Here we have defined the Hubble parameter as $H = \frac{\dot{f}}{f}$.

The easiest non-trivial solution to these equations is of course provided by $\rho = p = 0$. We then find that the Hubble parameter H becomes the Hubble constant $H_0 = \sqrt{\frac{\Lambda}{3}}$. This is the famous dark energy solution hinted at earlier. Note that it is on a completely different footing than dark matter, as it is simply a solution to the Einstein equations.

Another solution we will need is the solution for a pressure-less fluid $p = 0$ and zero dark energy $\Lambda = 0$. Without plugging this into the Friedman-equations, we can already guess what the effect of the scale factor on the density $\rho(t)$ will be. As the lengths scale by $f(t)$, the density decreases as $\rho(t) = \rho_0 f(t)^{-3}$. Plugging this into the Friedman-equations, we find that $f(t) \sim \sqrt{t}$ and $H = \frac{1}{t}$. Thus if we know the current value of the Hubble parameter and the universe were solely made up of this pressure-less fluid, we find that the age of the universe $T = \frac{1}{H_0}$ with H_0 the current Hubble constant. From our table of constants, we find that the age of the universe is $T = 13 \cdot 10^9$ years old. Isn't that amazing? Just 21 pages ago you might not have known anything about galaxies and now you are able to calculate the age of the universe.

One more question we should address is: *How do you find the current value of the Hubble parameter?* This is not done by studying the matter density in the universe, but rather by studying photons. The energy density of photons also decays due to the expanding universe. From our matter density, we know that it should at least decrease as $f(t)^{-3}$. For photons, there is however the added effect that their wavelengths also get stretched, further reducing their energy by a factor of $f(t)^{-1}$. Thus the photon energy decreases because the photons drift apart ($f(t)^{-3}$) and because their wavelengths increase ($f(t)^{-1}$) both due to the expansion of the universe. Thus the photon density $\rho(t) = \rho_0 f(t)^{-4}$ is also a way to recover the scale factor. Luckily for us, there are a lot of sources for which we exactly know the initial photon density, such as supernovae (exploding stars) or Cepheid (stars that pulsate radiation radially with well-defined period and amplitude). In fact, the value of H that we used is based on photon measurements from the Cepheids in the Large Magellanic Cloud (LMC), a satellite galaxy of the Milky Way.

Chapter 4 ●■▲

Emergent Gravity

4th

This theoretical chapter will mainly be concerned with the theory proposed by Erik Verlinde in an attempt to explain gravity and dark matter. The papers by Erik Verlinde include the paper from 2010 [27], in which gravity is explained as an emergent force. The main focus will however be on the paper from 2016 [26] in which the force normally attributed to dark matter is explained by Erik Verlinde by associating an entropy to the dark energy content of our universe. As these papers both contain highly abstract results, we will first explain his ideas in a condensed form starting with the paper from 2010. We will then explain the ideas of the paper from 2016.

It is assumed throughout this chapter that the reader is familiar with the laws of GR as formulated in the chapter on From Newtonian to Einsteinian gravity. The sections on the first paper by Erik Verlinde are primarily focused on explaining the concept of emergent forces and gravity. The sections on the second paper in contrast focus on explaining the extra force Erik Verlinde associates with the entropy of the dark energy content of our universe. In the next chapter, we will convert these ideas into a general relativistic formulation of Erik Verlinde's formulation of emergent gravity as was done by Sabine Hossenfelder [11].

4.1 Entropic Gravity

4.1.1 Emergent properties

In 2010, Erik Verlinde released a paper titled: *On the Origin of Gravity and the Laws of Newton* [27], in which he argued that gravity has an entropic origin. In order to understand these ideas, we will first have to understand several key concepts, namely the concept of emergence and the concept of entropic forces.

We will first focus on the meaning of emergent properties and entropy. Consider a box filled with a certain gas. The molecules jiggle about due to their interactions with one another. From the perspective of a single molecule these motions appear quite random, but when one considers a large number of these molecules one finds that the average of their energies e.g. the square of their velocities are related to the quantity we call temperature. Temperature is an example of an emergent property. It has no meaning when one considers but one molecule, only when one considers a large number of molecules, can one ascribe a temperature to the gas. This is of course because temperature is related to the average energy, thus by definition a large number of molecules is needed to define the concept of temperature.

The beauty of the concept of temperature is that it is not concerned with the motion of individual molecules. All one needs to know to define the temperature is the average motion of these molecules. We do not need to know the underlying theory that causes these random motions of the molecules, but only its average effect on a molecule. This idea, that we do not need to know the underlying forces but simply its average effects, is the driving principle

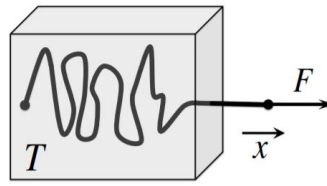


FIGURE 4.1: A polymer suspended in a heat bath with temperature T . A force of size F is applied on the polymer. Credits to Erik Verlinde [27].

behind what is called the entropy of the gas. The entropy S is a number that indicates the total number of possible configurations the molecules of the gas can have that are compatible with the total energy of the gas. Namely, let Ω be the total number of possible configurations, then $S := \ln \Omega$. The $\ln(\cdot)$ is chosen such that the entropy of different gasses are additive. A more in depth discussion of entropy can be found in any book on statistical mechanics, for instance Thermal Physics by Daniel Schroeder [24].

Let us calculate the entropy associated with a number of coins. Each coin can either be heads or tails. The total number of states is then $\Omega = 2^N$, thus $S = N \ln 2$. In more modern language, the entropy S is proportional to the number of bits N . Entropy is therefore the natural quantity associated with information.

4.1.2 Entropy and emergent forces

As we have now covered the concept of entropy, let us look at the meaning of an entropic force. Consider a gas with a fixed temperature T . Let us change the energy E of this gas slightly by an amount dE . This extra average energy allows the molecules to follow a larger amount of random motions, thus increasing the entropy S by dS . In fact, for a reversible process, a standard relation from thermodynamics is $dE = T dS$. This change in energy could have been caused by a certain force F working over a distance dx , such that we obtain $F dx = T dS$ or in higher dimensions, this is written as:

$$\mathbf{F} = T \nabla S \quad (4.1)$$

This is the defining formula for an entropic force. As this remains a rather vague concept, let us consider an example. Suppose we model a chain of polymers by a chain of rods connected at the ends that can all move freely with respect to one-another. A pictorial interpretation can be found in figure 4.1. Since all chains can move independently, we never expect the chain to be fully stretched, but rather in a random messy configuration. When we stretch the chain and let it rest, it will return to such a random messy configuration over time. Thus, on average, there seems to be an overall force keeping it from being stretched. In fact, calculating the entropy of this system and the entropic force, it is found that the force is similar to that of a spring. Thus an entropic force can be viewed as a force that tries to restore the system to a state with maximum entropy (randomness). Alternatively, the formula suggests that a system always behaves in such a way as to maximize its entropy. Erik Verlinde claims that gravity is such an entropic force. He claims that gravitational forces arise when a particle tries to lower the total entropy of the system, in exactly the same vein as above. The gravitational forces then attempt to restore the system to a state with maximum entropy. As we have now covered entropic forces and emergent properties, let us calculate the entropy associated with a certain matter distribution.

4.1.3 Bekenstein's entropy

In order to arrive at the entropy of a matter distribution, let us consider a totally different object: a black hole. Every black hole has an event horizon at a distance R_s from the center. This distance is determined by the mass M of the black hole given by:

$$R_s = \frac{2GM}{c^2} \implies M = \frac{R_s c^2}{2G} \quad (4.2)$$

From the relation $E = Mc^2$, we find that the energy of a black hole can be written as:

$$E = \frac{R_s c^4}{2G} \quad (4.3)$$

The fact that a black hole has a certain energy is of course not new, but the fact that it has an entropy might be. Objects in classical theories often have an infinite amount of entropy, as they can take any position and momentum between some predetermined bounds. Boltzmann solved this problem by quantizing phase-space, which was later also done by Planck in order to solve the Ultra-Violet catastrophe. The reason why a black hole should have a certain entropy is straightforward. When a gas with a certain entropy passes the horizon, all information about the gas is gone except for its mass, charge and angular momentum. The black hole does not allow for information to be transmitted from inside its horizon to the outside world. But this would violate the second law of thermodynamics that says that entropy has to always increase. Therefore, a black hole should have a certain amount of entropy that is bounded below by the entropy of the substances it was made of. This was first proposed by Jacob Bekenstein and is still a topic of heated debate.

We will now derive the main result of Bekenstein for the entropy of a black hole through a non-rigorous method. Let us build the black hole bit by bit by dropping in bits of entropy in order to recover its total entropy. What could function as a physical bit? It must be something that is either in the black hole or not. But it cannot be something that is either in one half of the black hole or outside the black hole, as this would contain more information than just being in the black hole. Therefore let us consider a photon with the smallest possible wavelength to fit in the black hole of length $2R_s$, thus $\lambda = 4R_s$. We will build our black hole photon by photon, bit by bit, until we have reached the required entropy.

The energy associated with one such photon is $\Delta E = h \frac{c}{\lambda} = h \frac{c}{4R_s}$ with h Planck's constant. If our black hole consist of N bits with a total energy of E , then the total number of bits $N = \frac{E}{\Delta E}$. We know from our example with coins that the entropy S is related to the number of bits as $S = N \ln 2 = \frac{E}{\Delta E} \ln 2$. Inserting our expression for the energy associated with one bit ΔE and the total energy E of a black hole (equation 4.3) yields:

$$S = \frac{4R_s^2 c^3}{4\pi G \hbar} = \frac{1}{\pi^2} \frac{A(R_s) c^3}{4G \hbar} \quad (4.4)$$

In formula 4.4, $A(R_s)$ is the area of the horizon and \hbar the reduced Planck's constant. Note that we have used formulae from both quantum mechanics and general relativity to arrive at this result. The true Bekenstein entropy coming from a more delicate quantum theoretical derivation is:

$$S_{BH} = \frac{A(R_s) c^3}{4G \hbar} \quad (4.5)$$

The original derivation by Stephen Hawking is not suited for such a small section, but this non-rigorous method yields the same results up to a factor of $\frac{1}{\pi^2}$. The main take-away is that the entropy of a black hole is proportional to the area of the horizon instead of the volume of

the black hole. We will generalize this result as the entropy across any surface with area A . This is an important formula and it will return many times throughout this report.

4.1.4 Entropic gravity: Verlinde's first paper

Now that we know what emergent properties and forces are, we can add gravity. In his first paper, Erik Verlinde proposed that gravity is such an emergent force. If gravity is emergent and gravity is simply the curvature space-time, then space-time must also be emergent. The idea that gravitational forces are emergent and that what we perceive as space and time is simply a result of averaging over microscopic processes that we do not yet understand is called coarse-graining.

The content of the next section is not in Erik Verlinde's paper, but uses several of the concepts introduced in the paper to show how gravity could arise as an entropic force. It also serves to lay down several key ideas we will use later in Erik Verlinde's explanation of gravity.

In this section we will try to reformulate gravity as an entropic force. We will show that we can arrive at the laws of gravity using only thermodynamic principles. In order to find the gravitational or entropic force \mathbf{F} on one particle, we need to know the change of entropy S the particle causes by formula 4.1 and the temperature T . Let us first calculate this temperature at the horizon of the black hole. In thermodynamic equilibrium, the energy associated with N bits or N degrees of freedom is $E = \frac{1}{2}NT$. Since we already have an expression for the number of bits N from formula 4.4, we find that:

$$T = \frac{E}{\frac{1}{2}N} = \frac{E8\pi^2\hbar G}{Ac^3} = \frac{2\pi MG\hbar}{R_s^2 c} \quad (4.6)$$

In formula 4.6 we have again used that $E = Mc^2$. The temperature of a black hole is thus inversely proportional to the total mass of the black hole (using equation 4.2).

Now that we have the temperature, we need the change in entropy due to one particle to calculate the entropic force. This entropic force will be exerted on the particle because it changes the entropy of the black hole. We will now calculate the difference in entropy caused by adding one particle of mass m to the event horizon of a black hole. A pictorial interpretation of this can be found in figure 4.2. If our particle would arrive at the horizon, the entropy would increase by the amount of bits contained in the particle. Thus adding a particle to the black hole is equivalent to adding an equivalent number of photons in terms of energy. If we consider a particle of mass m , this implies we need to adding an equivalent number of bits $N = \frac{mc^2}{\Delta E}$ from the photons to our black hole. Using that our photons have wavelength λ , we find that $N = \frac{mc\lambda}{h}$. Thus the total entropy associated with this mass m is:

$$S_m = N = \frac{mc^2}{\Delta E} = \frac{mc\lambda}{h} = \frac{mc4R_s}{2\pi\hbar} \quad (4.7)$$

Thus when the particle reaches the horizon, it will increase the entropy by S_m . We will now make an assumption on how much entropy the particle adds to the black hole when it is a distance x away from the black hole horizon. Since we are talking about small changes, we can assume the change of entropy is approximately linear in x . We will also assume that the particle adds zero entropy when its $4R_s$ away from the horizon of the black hole, as this implies it is exactly one wavelength away. This assumption is made in order to arrive at the correct constants in the laws of gravitation.

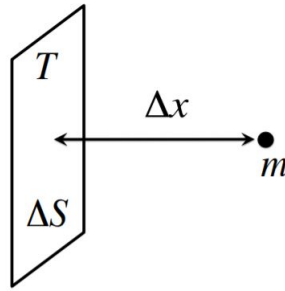


FIGURE 4.2: A particle of mass m approaching the boundary of a black hole. At a distance Δx , the particle changes the entropy of the black hole by an amount ΔS . Credits to Erik Verlinde [27].

Thus when $x = 4R_s$ the mass contributes no entropy to the horizon. The contribution to the entropy of the black hole by the particle is a distance x away is then::

$$\delta S = S_m \left(\frac{4R_s - x}{4R_s} \right) \quad (4.8)$$

Now that we have the change in entropy from equation 4.8 and the temperature from equation 4.6, we can finally calculate the entropic force by equation 4.1 as:

$$F = T \frac{\partial S}{\partial x} = -\frac{2\pi MG\hbar}{R_s^2 c} \frac{mc}{2\pi\hbar} = -\frac{GmM}{R_s^2} \quad (4.9)$$

Thus we recover Newton's law of gravitation. This derivation was not meant to be a rigorous one, but merely to show how gravity can arise as an entropic force. We would like to remark that it is not at all odd that we arrive at a theory of gravity as we used formula from general relativity. We will now look at Erik Verlinde's interpretation of this phenomenon.

4.2 Emergent Gravity; Verlinde's first paper

We have just witnessed that we can obtain Newton's laws of gravity from a thermodynamic model. This suggest that gravity has a thermodynamic origin, emerging from the microscopic laws that govern our universe. Erik Verlinde uses these same principles but in a slightly different manner.

One key point is that the entropy of our black hole is proportional to the area of the black hole and not its volume, as is the case for ideal gases and a whole other range of systems. This has led Gerard van 't Hooft and later Susskind to the idea that the information of a black hole is stored on its horizon. This is called the holographic principle. The basic idea is that the information of the interior of the black hole can be mapped onto the horizon like a projection. This, together with the temperature and entropy law, leads to the new theory of Erik Verlinde.

Erik Verlinde splits our universe in a part that is accessible and thus exists and a part that has not yet emerged. One can think of the emerged part as a sphere surrounded by nothing. The boundary of this sphere is called the holographic screen. As with the black hole, he identifies this holographic screen with a horizon. He proposes that all the information of the emerged space is located on the boundary or horizon just as in the holographic principle. This boundary carries the Bekenstein entropy (equation 4.5) that we associated with a black hole, but now distributed over to a holographic screen (the boundary of space-time).

When a particle approaches this boundary from the emergent side of space, it then slowly changes the information stored on the boundary. This is the same picture as in figure 4.2, but with the boundary being the holographic screen, the boundary of the emerged space. The particle again changes the entropy of the space by approaching the boundary and this causes a force on the particle. Bekenstein showed that when the particle is a Compton wavelength away from the boundary, thus $x = \frac{\hbar}{mc}$, the entropy changes by one bit. Erik Verlinde therefore proposes that the change in entropy when the particle is a certain displacement Δx away from the horizon is:

$$\Delta S = 2\pi \frac{mc}{\hbar} \Delta x \quad (4.10)$$

Thus he also proposes that the entropy changes linearly, as we have done (compare with equation 4.8), and ensures that the entropy changes by exactly 2π when $\Delta x = \frac{\hbar}{mc}$. This was chosen such that we arrive at the right value of the gravitational force later. The fact that the entropy grows linear with mass is not surprising, as the number of bits associated with a particle is proportional to its energy.

The temperature associated with the horizon is the same as the one we derived, which is called the Hawking temperature. A different interpretation of this temperature was given by Unruh. He calculated that an observer in an accelerated frame with acceleration a experiences a temperature:

$$T = \frac{1}{2\pi} \frac{\hbar a}{c} \quad (4.11)$$

This is, up to a factor of $\frac{1}{4\pi^2}$, exactly the temperature we calculated with $a = \frac{GM}{R_s^2}$ in equation 4.6. If we now insert the expression for the change in entropy (equation 4.10) and the Unruh temperature (equation 4.11) into formula 4.1 for the entropic force, we obtain Newton's second law of motion:

$$F = T\nabla S = ma \quad (4.12)$$

Thus when the particle approaches the holographic screen, the force it feels is proportional to its acceleration. We thus recover Newton's second law from thermodynamic considerations.

4.2.1 Newton's law of gravity

We have seen that Newton's second law is actually an entropic principle. Let us now derive gravity from the same principles. We already know the value of the change in entropy, but we would also like the temperature in terms of properties of the horizon such as mass and area. From the equipartition theorem, we know that the total energy associated with N number of bits is:

$$E = \frac{1}{2}NT \quad (4.13)$$

Since we suppose the the information is stored on the boundary, let us assume that we are again dealing with an entropy/number of bits of the form 4.5. We then propose that the number of bits N in terms of the size of the area of the boundary is given up to a constant of 4 by formula 4.5 :

$$N = \frac{Ac^3}{G\hbar} \quad (4.14)$$

This is up to a constant multiplication by 4 also the number of bits associated with the horizon that we recovered earlier. Using that the total energy in our emerged space is $E = Mc^2$ and combining this with the formula for the total number of bits on the boundary 4.14 and the

temperature formula 4.13, we arrive at a formula for the temperature at the horizon:

$$T = \frac{2Mc^2G\hbar}{Ac^3} \quad (4.15)$$

Now that we have the temperature in terms of properties of the horizon, we may ask what force the horizon exerts on the particle. Using the change in entropy proposed by Erik Verlinde 4.10 and this temperature and plugging it into formula the formula for the entropic force 4.1, we arrive at:

$$F = T\nabla S = -G\frac{Mm}{R^2} \quad (4.16)$$

Thus we arrive at Newton's law of universal gravitation from purely thermodynamical arguments and the holographic principle. In the next section we will repeat this calculation for general matter distributions.

4.2.2 General matter distributions

For non-spherical distributions of matter, it is postulated by Erik Verlinde that the holographic screens (the boundary of the emergent space) corresponds to the level surfaces of the gravitational potential Φ . Particles at such a horizon feel an acceleration of $\mathbf{a} = \nabla\Phi$. This results in a local Unruh temperature of:

$$T = \frac{1}{2\pi} \frac{\hbar|\nabla\Phi|}{c} \quad (4.17)$$

The number of bits associated with an area on the horizon of size dA is again:

$$dN = \frac{c^3}{G\hbar} dA \quad (4.18)$$

The energy is again given by the equipartition theory as:

$$E = \frac{1}{2} \int_{\partial\Omega} T dN \quad (4.19)$$

In which $\partial\Omega$ indicates the surface area of the boundary. Using that $E = Mc^2$, we arrive at:

$$M = \frac{1}{4\pi G} \int_{\partial\Omega} \nabla\Phi \cdot d\vec{A} \quad (4.20)$$

We thus find that the total mass in our space M is related to the gravitational potential. We would like to invert this relationship. When we write M as an integration of the mass density ρ over the volume in the emerged space, we find that:

$$\int_{\Omega} \rho dV = \frac{1}{4\pi G} \int_{\partial\Omega} \nabla\Phi \cdot d\vec{A} \implies \nabla^2\Phi = 4\pi G\rho \quad (4.21)$$

The last implication can be seen by requiring that this holds for all level surfaces. Thus we have arrived at the general law of gravitation. This concludes our section on Erik Verlinde's first paper. He has shown that one can arrive at the laws of gravitation purely from thermodynamical principles.

4.2.3 Critique

There are theoretical difficulties with making gravity an entropic force. As was shown by Tower Wang [29], models of entropic gravity are severely restricted by the requirement that the energy-momentum tensor be conserved and the universe should be isotropic and

homogeneous. It was also shown by Matt Visser [28], that entropic forces that are used to explain conservative forces place significant constraints on the form of the entropy and temperature functions.

4.3 Apparant dark matter; Erik Verlinde's second paper

We now move from the known gravitational forces, to the effects attributed to dark matter. We will lay down the main ideas of Erik Verlinde in his second paper in a more condensed form. It will be clearly stated when we deviate from the methods used by Erik Verlinde. Later on, we will cast this theory on dark matter into a Lagrange formalism and derive the exact field equation following Hossenfelder's paper [11].

Recent progress in the field has shown that the quantum information associated with the Bekenstein-Hawking entropy is not just stored on the horizon of the black hole, but can also be associated with information carriers inside the black hole, called tensor networks. These tensor networks are similar to the bits of information we had on the boundary earlier, but this time inside the volume of our space. These tensor networks can describe several quantum states, in particular states near the ground state. In condensed matter physics, the entropy of an ensemble of quantum states often scales with the area of the boundary if all the quantum states are near the ground state. A tensor network with all tensors near the ground state could account for the area law (equation 4.5) for the entropy we found earlier. Erik Verlinde argues that the excited state of these tensors yield an additional entropy effect. He argues that the dark energy present in our universe could excite these tensors to excited states. Systems with particles in excited states often result in an entropy that scales with the volume, like an ideal gas. These extra contributions to the entropy due to the excitations of these tensors due to dark energy would then account for dark matter.

The tensor network states yield both an area law for the entropy when the states are near the ground state, but also a volume law due to the excitations by dark energy. Erik Verlinde therefore argues that the area law yields exactly the Einstein equations (as we saw in the previous section) and the volume law becomes apparent precisely when we observe effects commonly attributed to dark matter. However, entropy itself does not give rise to a force, that is done by changes in entropy. The change in the area law entropy due to the addition of matter gives rise to gravity as we saw before when matter changed the information on the boundary. Similarly, the addition of mass causes a disruption in the volume law entropy, which gives rise to the forces commonly attributed to dark matter. We will now derive the effect of these extra forces by borrowing ideas from both Verlinde and Hossenfelder. Since we have already covered the area law entropy in the previous section on Erik Verlinde's first paper, we will now mainly be concerned with the volume law entropy, thus the entropy associated with the excitations due to dark energy. A pictorial interpretation of this discussion is given in figure 4.3. We will see in the next sections that masses remove the information of these tensor networks, causing a shift in the volume entropy, which is why a mass feels an additional force.

4.3.1 Entropy and the cosmological constant

For now, we will not consider these tensors networks, as they are rather abstract objects which are still researched heavily. We will instead focus on the effects dark energy has on our universe. Dark energy causes the accelerated expansion of our universe, which is characterized by the Hubble constant H . Due to this expansion, there exists a sphere called

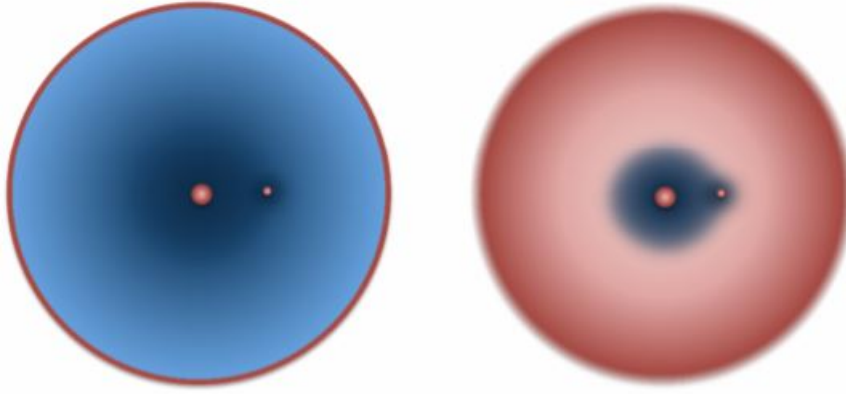


FIGURE 4.3: On the left a space is shown in which all information is stored on the boundary and thus the particles feel a normal gravitational force. On the right a space is shown in which information is also stored in the volume, which causes an additional force. Credits to Erik Verlinde[26].

the Hubble sphere, which has a radius $L = \frac{c}{H}$. We cannot receive information from galaxies that lie beyond our Hubble sphere as this information would have to travel faster than the speed of light to reach us. It is thus only natural to associate dark energy with this Hubble sphere. In turn this sphere acts as an apparent horizon. We will therefore associated dark energy with a horizon, namely the Hubble sphere horizon. Let us therefore propose that dark energy adds a total entropy to our universe of the form:

$$S_{DE} := \frac{A(L)c^3}{4G\hbar} \quad \text{with} \quad A(L) = 4\pi L^2 \quad (4.22)$$

Which is simply the Bekenstein entropy of the Hubble horizon. This is different from the area law entropy that we associate with the ground state of the tensor networks. The area law accounts for the usual gravitational laws and the volume law accounts for the dark matter contribution to the gravitational effects.

Erik Verlinde then proposes that this entropy (equation 4.22) is divided equally over the tensors in the volume, which are spread evenly throughout the volume. Thus the total dark energy entropy 4.22 is spread evenly over the volume in the Hubble sphere, whereas the Hawking-Bekenstein entropy (equation 4.5) was spread over the area of the horizon. Suppose we have a ball with volume $V(r)$ inside this sphere, what will its entropy content be? Well the entropy contained in this ball of radius r is proportional to its volume as:

$$S_{DE}(r) = \frac{V(r)}{V_0} \quad (4.23)$$

With V_0 a constant. Since we know the entropy at the horizon of the sphere $r = L$, we can thus calculate V_0 by equating formula 4.23 at $r = L$ with formula 4.22. This yields:

$$S_{DE}(r) = \frac{r}{L} \frac{A(r)}{4G\hbar} \quad , \quad V_0 = \frac{4G\hbar L}{3c^3} \quad (4.24)$$

We have obtained a volume law expression for the entropy associated with dark energy in a certain volume. Note that if we let one tensor represent one bit of information, then these tensors occupy a volume of V_0 .

4.3.2 Introducing mass

As with in our previous section an important question is: How does this entropy change when we introduce matter into our Hubble sphere? Specifically, we will introduce this matter at the center of the Hubble sphere, as this makes our lives much easier. The metric associated with the Hubble sphere is the De Sitter metric. This metric has the following form:

$$ds^2 = \left(1 - \frac{r^2}{L^2}\right) c^2 dt^2 + \frac{1}{\left(1 - \frac{r^2}{L^2}\right)} dr^2 + r^2 d\Omega^2 \quad (4.25)$$

In formula 4.25, L is the radius of the Hubble sphere and $d\Omega^2$ the metric of a 2-dimensional unit sphere. Note that our horizon L is a horizon induced by the metric, as setting $r = L$ yields an infinite distance $ds = \infty$ to cross. We thus identify the horizon of our space with the point our distances become infinitely large to cross.

When we introduce matter to our space, the metric becomes the De Sitter-Schwarzschild metric, which is:

$$ds^2 = \left(1 - \frac{r^2}{L^2} - \frac{2Gm}{rc^2}\right) c^2 dt^2 + \frac{1}{\left(1 - \frac{r^2}{L^2} - \frac{2Gm}{rc^2}\right)} dr^2 + r^2 d\Omega^2 \quad (4.26)$$

This introduction of matter shifts the horizon (the value of r at which our metric diverges). Note that we could have made the same observation in the case of the particle changing the entropy in our section on the first paper. The particle changes the entropy of the horizon, which implies that it changes the horizon area (equation 4.5) and thereby the position of the horizon.

If the mass is sufficiently small, this shift will also be small. Let us call this displacement $u(L)$ such that the horizon shifts from $L \rightarrow L + u(L)$. Using the fact that $-\frac{Gm}{r} = \phi(r)$ is the Newtonian potential $\phi(r)$ associated with mass m , the new horizon is at:

$$1 - \frac{r^2}{L^2} - 2\frac{\phi(r)}{c^2} = 0 \implies r = L\sqrt{1 + 2\frac{\phi(r)}{c^2}} \approx L + L\frac{\phi(L)}{c^2} \quad (4.27)$$

We have assumed that the shift is small, such that we can approximate $\phi(r) \approx \phi(L)$ with $\frac{\phi(L)}{c^2} \ll 1$, in order to apply a Taylor series around $r = L$. Thus we find that the displacement of the horizon is $u(L) = L\frac{\phi(L)}{c^2}$. Note that the horizon shrinks as the Newtonian potential is negative. Thus introducing mass into our space shrinks the horizon of our space. This is an important fact that we will come back to later.

This fact can also be seen intuitively. Consider a space that is contained in a sphere with a radius L . When we place a mass in this sphere, the space around this mass has to become more curved by Einsteins equations. But the only way to make a ball more curved is to shrink the ball. In this way the horizon has larger curvature. Hence; the volume of space shrinks when we introduce a small mass into the space.

4.3.3 Mass and entropy

Upon introducing a mass m to our space, our horizon shift by $u(L) = L\frac{\phi(L)}{c^2}$. We would now like to calculate the amount of force exerted upon the mass m during this process. However, our operation was not a continuous process, therefore we cannot use 4.1. Nonetheless, we will

show that our change in entropy causes a stress in space-time, that exerts a force on particles. We will do this step by step, starting with the change in the total entropy due to the shift:

$$\Delta S_{DE}(L) = \frac{dS}{dL} u(L) = u(L) \frac{d}{dL} \left(\frac{A(L)c^3}{4G\hbar} \right) = -\frac{2\pi mLc}{\hbar} \quad (4.28)$$

The total entropy changes by the amount given in formula 4.28. We would now also like to know how much entropy is taken away from a spherical ball $B(r)$ with radius r inside our Hubble horizon. This will allow us to calculate the stress inside this ball. However, as we change from one metric to another, the way in which we measure distances changes as well. Thus the question at hand is: How do we know what happened to our ball of radius r ?

At this point we will deviate from the results of Erik Verlinde to allow for our own interpretation. One way to identify a ball, is to identify its effect in the metric. In our original De Sitter metric our ball of radius r yields a temporal component in our metric of $s = 1 - \frac{r^2}{L^2}$. Thus we identify the horizon of our ball in this metric as that r which yields a certain value of s . We do the same in our new metric, and then the new radius r of our horizon has become that new r that yields the same value for $s = 1 - \frac{r^2}{L^2} - \frac{2\phi(r)}{c^2}$. This implies that the horizon of the ball has shifted by an amount $u(r) = L \frac{\phi(r)}{c^2}$ as the calculation is identical to the one we performed at the horizon $r = L$.

We can think of our balls with radius r as being displaced by an amount $u(r) = L \frac{\phi(r)}{c^2}$ when we introduce mass into our system. Note that our treatment is different than that of Erik Verlinde but it yields the same result.

4.3.4 Entropy difference

Since our entropy is related to the volume of our ball, a change in the position of the horizon of our ball causes a change in the volume entropy of the ball. Note that as our horizon shifts, the volume occupied by one tensor does not necessarily have to be V_0 anymore. With this in mind let us calculate the lost entropy due to the introduction of mass m . We assume that the entropy loss at radius r is proportional to the loss in volume $u(r)A(r)$, such that the loss in entropy $S_m(r)$ is equal to:

$$S_m(r) = \frac{u(r)A(r)}{V_0^*} \quad (4.29)$$

Here V_0^* is yet another constant. Since we know the entropy loss at the Hubble radius $r = L$ from 4.28, we can calculate V_0^* . From our discussion on balls, we also know that the shift in the balls radius was $u(r) = L \frac{\phi(r)}{c^2}$. Plugging this into equation 4.29 and our newly found value for V_0^* yields:

$$S_m(r) = -\frac{2\pi mrc}{\hbar} \quad \text{with} \quad V_0^* = \frac{2G\hbar L}{c^3} \quad (4.30)$$

The amount of entropy lost by this interaction between mass and space-time had to be stored in a certain volume beforehand. Let us indicate this volume by $V_m(r)$. From the volume law 4.23, we know how to calculate this volume:

$$S_m(r) = -\frac{V_m(r)}{V_0} \implies V_m(r) = \frac{8\pi GmrL}{3c^2} \quad (4.31)$$

Let us quickly recap what we have found. Due to the introduction of mass, our space shrinks. This implies that we lose part of our entropy S_{DE} as entropy is related to volume. The

amount of entropy we have lost inside a ball of radius r is $S_m(r)$. This amount of entropy was originally contained in a volume $V_m(r)$ inside this ball.

4.3.5 Interpretation of results

At a radius r , we can calculate the amount of volume that has been lost which is $u(r)A(r) = \frac{3}{2}V_m(r)$. Thus it appears that we have lost more volume than was needed. Let us explain this discrepancy, which is not done by Verlinde. It lies in our identification of the different balls in our different metrics. If we assume that the radius of a ball of radius r shrinks by $u(r)$ and the horizon L also shrinks by $u(L)$, we obtain a change in entropy of:

$$\Delta S_{DE}(r) = u(r)\frac{dS_{DE}}{dr} + u(L)\frac{dS_{DE}}{dL} = -\frac{3\pi mrc}{\hbar} + \frac{1}{L^2}\frac{mc\pi r^3}{\hbar} \quad (4.32)$$

Notice that the results still agree at $r = L$, but not for $r \ll L$. For $r \ll L$ we obtain exactly the factor $\frac{3}{2}$ with respect to $S_m(r)$ in equation 4.31. The fact that we lose more volume than necessary thus lies in the way in which we identify different balls in our metric. The amount of volume lost in the original metric is not equal to the amount of volume lost in the remaining metric, due to the introduction of matter. It is thus very dangerous to equate different balls from different metrics.

Two things are however certain. A volume of $u(r)A(r) = V_m^*(r) = \frac{3}{2}V_m(r)$ has been removed and the lost entropy was originally contained in a volume of $V_m(r)$. Erik Verlinde proposes the following interpretation:

If $V_m(r) \gg V(r)$, then all entropy has been removed from our ball of radius r . Since the medium that carried the volume law entropy has totally been removed, only the area law remains and thus a particle would only experience the normal gravitational force. This is similar to the requirement that $a \geq a_m$ in MOND. Why? Well, when:

$$V_m(r) \gg V(r) \implies \frac{8\pi GmrL}{3c^2} \gg \frac{4}{3}\pi r^3 \implies \frac{Gm}{r^2} \gg \frac{1}{2}\frac{c^2}{L} \approx a_m \quad (4.33)$$

If $V_m(r) \ll V(r)$, only part of the entropic medium of the ball has been removed. This is similar to the requirement that $a \leq a_m$ in MOND. Since only part of the entropic medium has been removed, we would obtain both an area law and volume law and we would notice additional effects normally attributed to dark matter.

Since $V_m^*(r) \geq V_m(r)$, a part of the medium has to have been removed outside of $V_m(r)$ (the volume that originally contained the removed entropy). However, Erik Verlinde proposes that this removal of additional entropy is still done from inside a ball of volume $V_m(r)$. Pictorially, this implies that the entirety of the volume of the ball inside $V_m(r)$ is removed plus a part of the surrounding volume that has flowed inside volume $V_m(r)$ from the outside during the process. The total removed volume is $\frac{3}{2}V_m(r)$.

4.4 Stresses and Strains

So far, we have established that a certain amount of entropy $S_m(r)$ is removed from a ball of volume $V(r)$. This volume is removed inside a region of size $V_m(r)$ and the total amount of volume lost is $V_m^*(r) = \frac{3}{2}V_m(r)$. Just as in the case of the polymer chain, Erik Verlinde proposes that the entropic force due to this change in entropy can be calculated by considering the medium as a linear incompressible elastic medium. The additional force would then be

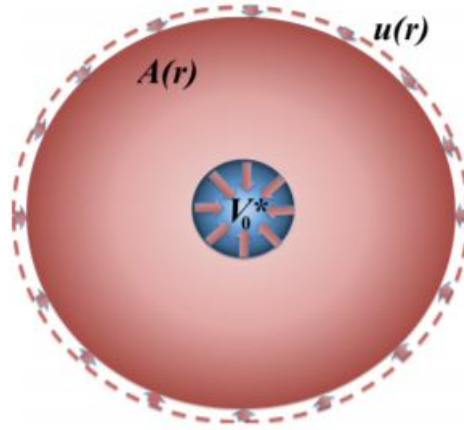


FIGURE 4.4: A volume of V_0^* is removed from a ball with volume $V(r)$. Credits to Erik Verlinde [26].

related to the strain in the medium. We therefore need to calculate the displacement $u(r)$ and strain $\epsilon(r)$ in the entropic medium, caused by removing a part of this medium. Thus we need to take a quick detour into the theory of stresses and strains.

We will now calculate the displacement $u(r)$ and strain $\epsilon(r)$ caused by removing a volume of $V_m^*(r) = \frac{3}{2}V_m(r)$ from a region of $V_m(r)$ inside our ball of volume $V(r)$. We assume that $V(r) \geq V_m(r)$ as this is where the effects of dark matter come into play. A pictorial interpretation of this can be found in figure 4.4.

4.4.1 Theory of Strain and Stress

A difficulty that we now face is the fact that the removed volume $V_m^*(r)$ grows with the radius. Thus it is not at all clear what form or topology this volume takes. Let us therefore consider a much simpler problem. Suppose we remove from a ball with radius R_a , a volume of V_0^* . The displacement of a point on the medium is denoted by $u(r)$ and is assumed to be spherically symmetric. Since we know that the total volume changes by V_0^* , the shift at the boundary R_a should be:

$$u(R_a) = \frac{-V_0^*}{A(R_a)} \quad (4.34)$$

Let us calculate the shift of a particle of the medium at a radius r inside the volume, called the displacement $u(r)$. Since the medium is incompressible, we have the following continuity equation due to the incompressibility condition:

$$\frac{\partial \rho}{\partial t} = 0 \implies \nabla \cdot \vec{u} = 0 \quad (4.35)$$

In spherical coordinates, this implies that $u(r)$ is of the form $\frac{1}{r^2}$. Thus using our boundary condition (4.34) and the incompressibility condition, we arrive at a formula valid at all radii outside the removed volume V_0^* as:

$$u(r) = \frac{-V_0^*}{A(r)} \quad (4.36)$$

For incompressible media, we know the displacement within the medium when we consider the removal of a volume from a spherical ball. This is actually all we need to know, since our entropic medium is assumed to be linear and elastic. We can always decompose our entropic

medium into tiny spherical balls from which a tiny volume is removed, such that the total removed volume is the sum of these tiny removed volumes. Since the equations are linear, the strain due to the total removed volume is then the same as the sum of the strains due to the tiny removed volumes.

4.4.2 Strain in the entropic medium

Let us those decompose our volume of size $V(r)$ into tiny balls of size $N_i V_0$. From these balls, a volume of $N_i V_0^*$ will be removed. Note that the removed volume is greater than the volume of the tiny ball. Therefore, we will mainly focus on the displacement outside the balls of volume $N_i V_0$. The main focus in this section is to identify the square of the stress, as we will need this later to formulate a Lagrangian.

Since a volume of $N_i V_0^*$ is removed, the displacement outside these balls will of course again be given by equation 4.36 as:

$$u(r) = -\frac{N_i V_0^*}{A(r)} \quad (4.37)$$

The strain $\epsilon(r)$ is related to the displacement $u(r)$ as $\epsilon(r) = \frac{du(r)}{dr}$, which yields:

$$\epsilon_i(r) = \frac{2 N_i V_0^*}{3 V(r)} = \frac{N_i V_0}{V(r)} \quad (4.38)$$

The energy of such a displacement is related to the square of the strain of the remaining volume by an integral:

$$E \propto \int_{N_i V_0}^{\infty} \epsilon_i^2(r) A(r) dr = \int_{N_i V_0}^{\infty} \left(\frac{N_i V_0}{V(r)} \right)^2 dr = N_i V_0 \quad (4.39)$$

The energy is related to the removed volume, which is a well known result. We would have obtained the same result if the tiny ball would not be at the center of our ball. We would now like to sum over all the tiny balls to obtain the total strain. However, since we are dealing with the square of the strain, we can no longer sum over the individual strains as $\epsilon = \sum_i \epsilon_i$. We therefore assume that all strains are very localized, such that $\epsilon_i(r) \epsilon_j(r) \approx 0$. This allows us to simply sum over all contributions to obtain:

$$\int \epsilon^2(r) dV \approx \sum_i \int \epsilon_i^2 dV = \sum_i N_i V_0 = V_m(r) \quad (4.40)$$

For our entire ball of radius r , the result is thus:

$$\int_0^r \epsilon^2(r') A(r') dr' = V_m(r) \quad (4.41)$$

Differentiating this yields:

$$\epsilon^2(r) = \frac{1}{A(r)} \frac{dV_m(r)}{dr} = \frac{m}{A(r)} \frac{8\pi G c^2}{3L} \quad (4.42)$$

We have found that the square of the strain is related to the normal gravitational force exerted by the mass m .

Erik Verlinde then moves on to calculate the force this would exert on a particle by using analogies with the theory of stresses and strains in linear incompressible media. We will

however stop here, as the strain is all we need to formulate our covariant formalism, which was already done by Hossenfelder, whose approach we follow now.

Chapter 5 ● ■ ▲

Covariant Emergent Gravity

In this chapter, we convert the statements and concepts of Erik Verlinde's first [27] and second paper [26] into a fully general relativistic or covariant formulation. In this endeavor, we follow the approach taken by Hossenfelder [11] along with small deviations to her equations as proposed by Yen-Kheng Lim and Qing-hai Wang [18]. We will use these covariant formulations in the subsequent chapter on theoretical applications of CEG.

The reader is required to know GR as formulated in the section on From Newtonian to Einsteinian gravity.

5.1 Deriving a Lagrangian

We will now follow the approach taken by Hossenfelder [11] to arrive at a covariant theory involving a Lagrangian of Emergent Gravity. This is done by converting concepts such as the shift in the horizon of the De Sitter space $u(r)$ and the strain into covariant formulations.

5.1.1 The form of the Lagrangian

The important quantity in Erik Verlinde's view is the shift in the Hubble horizon, denoted by $u(r)$. In a non-spherical symmetric view, this becomes a vector field $\mathbf{u}(\vec{r})$. Hossenfelder refers to this field as the imposter field. All other quantities, such as the strain ϵ , follow from this imposter field.

In a covariant theory, the imposter field becomes a four-dimensional vector u^μ . From equation 4.42, we observe that strain is related to the gravitational force as $\epsilon^2 \sim F_g = \nabla\phi_B$ in which ϕ_B is the normal gravitational potential. The strain is related to the imposter field by the usual Hooke's law $\epsilon \sim \nabla u$. These two yield $(\nabla u)^2 \sim \nabla\phi_B$. Thus our covariant formulation for the imposter field should lead to field equations that have as solution $(\nabla u)^2 \sim \nabla\phi_B$.

Since a Lagrangian involves second derivatives, we differentiate $(\nabla u)^2 \sim \nabla\phi_B$, which yields $\nabla(\nabla u)^2 \sim \nabla^2\phi_B \sim \rho$ by Poisson's equation.

Thus we propose that our covariant Lagrangian must lead to a field equation of the form $\nabla(\nabla u)^2 \sim T$ with T the energy-momentum tensor. We start with the usual gravitational action in which S_H is the Einstein-Hilbert action for the space-time metric and S_m the action of matter:

$$S = S_H + S_m = \frac{1}{16\pi G} \int R\sqrt{-g} dx^\gamma + S_m \quad \text{with} \quad \frac{\delta S_m}{\delta g^{\mu\nu}} = -\frac{1}{2}T_{\mu\nu} \quad (5.1)$$

In order to arrive at a relation of the form $\nabla(\nabla u)^2 \sim T$, we have to add a source term for the imposter field. It is not immediately obvious how this should be done, as this is a non-linear

differential equation. Hossenfelder proposed a scalar of the form $\chi \sim (\nabla u)^2$, which is a function of the imposter field u^μ . This scalar would enter the Lagrangian in the form of a source term as $\chi^{\frac{3}{2}}$ such that $\chi^{\frac{3}{2}} \sim \left((\nabla u)^2\right)^{\frac{3}{2}}$. Upon using the Euler-Lagrange equations (differentiating with respect to ∇u) we then correctly recover $\nabla(\nabla u)^2$.

A true covariant description for such a scalar $\chi \sim (\nabla u)^2$ is of the general form:

$$\boxed{\chi(u^\mu) = \bar{a}(\nabla_\mu u^\mu)^2 + \bar{b}(\nabla_\mu u_\nu)(\nabla^\mu u^\nu) + \bar{d}(\nabla_\mu u_\nu)(\nabla^\nu u^\mu)} \quad (5.2)$$

Einstein summation is implied and $\bar{a}, \bar{b}, \bar{d}$ are constants, which we will determine later on. We will also introduce the strain and stress tensors as:

$$\epsilon_{\mu\nu} = \nabla_\mu u_\nu + \nabla_\nu u_\mu, \quad F_{\mu\nu} = \nabla_\mu u_\nu - \nabla_\nu u_\mu \quad (5.3)$$

The strain tensor is simply the generalization of the strain ϵ in Erik Verlinde's formulation. Using these tensors, we find that we can write the scalar of equation 5.2 as:

$$\chi(u^\mu) = \frac{a}{2}(\epsilon_\mu^\mu)^2 + \frac{b}{2}\epsilon^{\mu\nu}\epsilon_{\mu\nu} + \frac{d}{2}F^{\mu\nu}F_{\mu\nu} \quad (5.4)$$

Here we have made the substitution:

$$a = \frac{\bar{a}}{2}, \quad b = \frac{\bar{b} + \bar{d}}{2}, \quad \text{and} \quad d = \frac{\bar{b} - \bar{d}}{2} \quad (5.5)$$

The constants a, b and d thus determine the importance of the stress and strain in our covariant description. From Erik Verlinde's formulation (equation 4.39), we know that ϵ^2 is related to the energy that it costs to introduce mass into our space or equivalently shift the Hubble horizon. Thus we find that our scalar χ is related to the energy density in the entropic medium.

If we want to recover the equation $\nabla(\nabla u)^2 \sim T$, we have to add the source term to the Lagrangian:

$$S = S_H + S_{\text{source}} + S_m = \frac{1}{16\pi G} \iiint\!\!\!\int R\sqrt{-g} dx^\gamma + \frac{\alpha}{16\pi G} \iiint\!\!\!\int \chi^{\frac{3}{2}}\sqrt{-g} dx^\gamma + S_m \quad (5.6)$$

In this equation α is an arbitrary constant to be fixed later. The exponent of $\frac{3}{2}$ for χ has been discussed before and ensures that $\nabla(\nabla u)^2 \sim T$. It is however unusual and leads to complex equations as its derivative becomes a square root. Note that χ is not the only possible combination for a scalar as something like $\chi \sim \nabla u \nabla u \nabla u$ would also have worked, but would have resulted in more difficult equations involving more indices.

We thus have a source term for the Lagrangian of the imposter field u_μ . When we apply the Euler-Lagrange equations, such a source term yields $\nabla(\nabla u)^2$. We would like to have an equation of the form $\nabla(\nabla u)^2 \sim T$, which implies that we need to add an extra interaction of the imposter field with matter. This will also ensure that matter feels the additional force. We will now try to identify such an additional force through an effective metric and interaction terms.

5.1.2 Effective metric

When we introduced a mass m , to our metric, we found that the temporal component of the metric changed by:

$$\left(1 - \frac{r^2}{L^2}\right) \rightarrow \left(1 - \frac{r^2}{L^2} - 2\frac{u(r)}{L}\right) \quad (5.7)$$

Introducing a mass m to our space is equivalent to stating that the imposter field changes our metric. This idea is captured in Hossenfelder's model by an effective metric:

$$\widetilde{g}_{\mu\nu} = g_{\mu\nu} - \beta \frac{u^\mu u^\nu}{u} \quad (5.8)$$

From comparison with Erik Verlinde's equation 5.7, we find that $\beta = \frac{2}{L}$. Notice that this metric is simply the covariant version of a shift by $u(r)$. In Erik Verlinde's paper, he also hinted at this effective metric to explain the effects of dark matter. This was done by studying the analogies between stress in our entropic medium and the gravitational forces, but we will not repeat his arguments here as that would require several pages, whereas Hossenfelder's motivations are quite clear.

5.1.3 The interaction term

Note that the fact that there is an effective metric implies a certain interaction between our imposter field and the curvature of our space. Thus our Lagrangian should include an interaction term. We will derive this interaction term by considering the interaction a single test particle has with the imposter field. This test particle has coordinates x^μ and a mass m . The following derivation is based on the derivation done by Yen-Kheng Lim and Qing-hai Wang [18] in their paper on the field equations of CEG.

The energy-momentum tensor of a single particle is given by the usual formula:

$$T_{\mu\nu} = \rho v_\mu v_\nu \rightarrow T^{\mu\nu} = -\frac{m}{\sqrt{-g}} \int \delta(x^\alpha - x^\alpha(\tau)) \dot{x}^\mu \dot{x}^\nu d\tau \quad (5.9)$$

Here $\sqrt{-g}$ is evaluated at $x^\alpha(\tau)$. The 4-dimensional Dirac delta function simply picks out the position the particle is currently at. The $\frac{1}{\sqrt{-g}}$ is introduced to make sure that when we integrate over the entire volume it cancels with the $\sqrt{-g}$ in the volume integral. For the remainder of this derivation we will use an action contribution of the single particle of $S_m = \frac{m}{2} \int g_{\mu\nu} \dot{x}^\mu \dot{x}^\nu d\tau$.

To ensure that our particle feels a total effective metric of $\widetilde{g}_{\mu\nu}$, we must add an interaction term S_{int} . This interaction term S_{int} would make sure that the total action of the single particle is not dependent on $g_{\mu\nu}$ but on the effective metric $\widetilde{g}_{\mu\nu}$:

$$S_{\text{tot}} = \frac{m}{2} \int \widetilde{g}_{\mu\nu} \dot{x}^\mu \dot{x}^\nu d\tau = \frac{m}{2} \int \left(g_{\mu\nu} - \beta \frac{u^\mu u^\nu}{u} \right) \dot{x}^\mu \dot{x}^\nu d\tau \quad (5.10)$$

As we postulated, this is due to an extra interaction term with:

$$S_{\text{tot}} = S_m + S_{\text{int}} \quad \text{with} \quad S_m = \frac{m}{2} \int g_{\mu\nu} \dot{x}^\mu \dot{x}^\nu d\tau \quad (5.11)$$

Comparing equation 5.10 with equation 5.11, we find that:

$$S_{\text{int}} = -\frac{m}{2} \int \beta \frac{u^\mu u^\nu}{u} \dot{x}^\mu \dot{x}^\nu d\tau \quad (5.12)$$

Our actions for the fields (equation 5.6) involve integrals over all of space-time, whereas the interaction action for a single particle is over the proper time and still depends on the path of the particle. Of course, we want our interaction term to apply to any energy-momentum distribution. This can be fixed however, by introducing a delta peak. This allows us to be able to integrate over the entire 4d volume and arrive at our interaction term:

$$S_{\text{int}} = -\frac{m}{2} \int \iiint \frac{1}{\sqrt{-g}} \delta(x^\alpha - x^\alpha(\tau)) \beta \frac{u^\mu u^\nu}{u} \dot{x}^\mu \dot{x}^\nu \sqrt{-g} dx^\gamma d\tau \quad (5.13)$$

Note that this is almost the energy-momentum tensor of the single particle (equation 5.9). We can substitute the energy-momentum tensor of the single particle to arrive at a formulation independent of the particles properties. We use the matter energy-momentum tensor for a single particle to obtain an interaction term for the Lagrangian:

$$S_{\text{int}} = \frac{\beta}{2} \iiint \frac{u^\mu u^\nu}{u} T_{\mu\nu} \sqrt{-g} dx^\gamma \implies L_{\text{int}} = \frac{\beta}{2} \frac{u^\mu u^\nu}{u} T_{\mu\nu} \sqrt{-g} \quad (5.14)$$

We now simply postulate that action 5.14 is valid for any form of energy with energy-momentum tensor. Inserting this interaction term (equation 5.14) in our action with source term (equation 5.6), we find a total action for the theory of the form:

$$S = \iiint \sqrt{-g} \left[\frac{1}{16\pi G} R + \frac{\alpha}{16\pi G} \chi^{\frac{3}{2}} + \frac{\beta}{2} \frac{u_\mu u_\nu}{u} T^{\mu\nu} \right] dx^\gamma + S_m \quad (5.15)$$

The first term is the Einstein-Hilbert action S_H . The second term is called the kinetic term of the field and determines the energy of the field. The third term is the interaction term between the imposter field and matter. The last term is the matter action.

5.2 Understanding the action

Before we move on to the equations determining the motions of matter and the imposter field, let us shed some light on the individual terms in the action and make correspondences with the electromagnetic Lagrangian.

In the Electromagnetic Lagrangian, we had a source term for the field ϕ of the form $\frac{1}{2} \epsilon_0 \nabla \phi \cdot \nabla \phi$. Similar source terms are present in the action 5.15. The term $\frac{\alpha}{16\pi G} \chi^{\frac{3}{2}}$ is the source term of the imposter field u^μ with equation 5.2 given the scalar χ in terms of u^μ . This source term responds to the interaction the imposter field has with the baryonic matter. This interaction is present in $\frac{\beta}{2} \frac{u_\mu u_\nu}{u} T^{\mu\nu}$.

In figure 5.1, we show the different components of the action and the way they interact. These interactions will be the focus of the next section and this figure should accommodate the reader alongside the following discussion on all the interaction terms. From the figure we see that we have three important quantities, matter, the imposter field and the effective metric. Matter influences the imposter field via the interaction term in the action. The imposter field then determines the effective metric and in turn the effective metric dictates how matter moves. Additionally, matter also dictates the behaviour of the metric through the modified Einstein equations. We will calculate these different interactions in the coming sections.

As this is a rather complicated construction, we will discuss all the interactions in detail next. The derivation of all the interaction terms between the various component of the action 5.15 is done in appendix A. As such a derivation is rather heavy on the algebra, we have not included

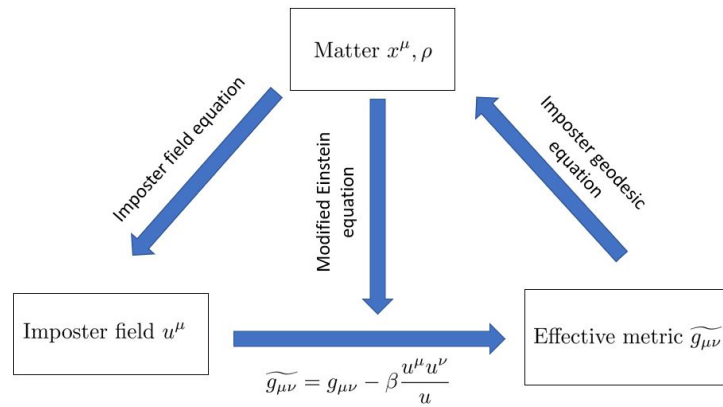


FIGURE 5.1: This figure shows the interactions between the different components involved in the action 5.15.

it here. However it can also be insightful for readers who are unfamiliar with varying actions in curved space-time. We therefore invite the reader to at least gloss over the appendix, as the true machinery behind the next sections are all happening there.

We have provided a summary of the coming results on the next page.

Action

$$S = \iiint \sqrt{-g} \left[\frac{1}{16\pi G} R + \frac{\alpha}{16\pi G} \chi^{\frac{3}{2}} + \frac{\beta}{2} \frac{u_\mu u_\nu}{u} T^{\mu\nu} \right] dx^\nu + S_m$$

Important quantities

Imposter field u^μ

Space-time metric $g_{\mu\nu}$

Effective metric $\widetilde{g}_{\mu\nu} = g_{\mu\nu} - \beta \frac{u^\mu u^\nu}{u}$

Energy-momentum tensor baryonic matter/energy $T_{\mu\nu}$

Derived tensors

Imposter scalar $\chi(u^\mu) = \bar{a}(\nabla_\mu u^\mu)^2 + \bar{b}(\nabla_\mu u_\nu)(\nabla^\mu u^\nu) + \bar{d}(\nabla_\mu u_\nu)(\nabla^\nu u^\mu)$

Strain tensor $\epsilon_{\mu\nu} = \nabla_\mu u_\nu + \nabla_\nu u_\mu$

Stress tensor $F_{\mu\nu} = \nabla_\mu u_\nu - \nabla_\nu u_\mu$

Imposter Christoffel symbols $C_{\mu\nu}^\delta = \frac{1}{2} g^{\delta\alpha} \left[\partial_\mu \left(\frac{u_\alpha u_\nu}{u} \right) + \partial_\nu \left(\frac{u_\alpha u_\mu}{u} \right) - \partial_\alpha \left(\frac{u_\mu u_\nu}{u} \right) \right]$

Auxiliary tensors

$A_{\mu\nu} = a\epsilon_\lambda^\lambda \epsilon_{\mu\nu} + b\epsilon_{\mu\lambda} \epsilon_\nu^\lambda + d F_{\mu\lambda} F_\nu^\lambda$

$B^{\mu\nu} = a\epsilon_\lambda^\lambda g^{\mu\nu} + b\epsilon^{\mu\nu} + d F^{\mu\nu}$

Field equations

Imposter field equations (determine evolution of imposter field u^μ in terms of $T_{\mu\nu}$)

$$\frac{3\alpha}{16\pi G} \nabla_\mu \left(\chi^{\frac{1}{2}} B^{\mu\nu} \right) = \frac{\beta}{2} \left[2 T^{\mu\nu} \frac{u_\mu}{u} + \frac{T^{\mu\lambda} u_\mu u_\lambda u^\nu}{u^3} \right]$$

Imposter geodesic equations (determine motion single particle with path $x^\delta(\tau)$)

$$\ddot{x}^\delta - \beta \frac{u^\delta u_\nu}{u} \dot{x}^\nu = \dot{x}^\mu \dot{x}^\nu \left(\beta C_{\mu\nu}^\delta - \Gamma_{\mu\nu}^\delta \right)$$

Modified Einstein equations (determine evolution $g_{\mu\nu}$ in terms of u^μ and $T_{\mu\nu}$)

$$R_{\mu\nu} - \frac{1}{2} g_{\mu\nu} R = 8\pi G T_{\mu\nu} - \frac{1}{2} g_{\mu\nu} \left[\alpha \chi^{\frac{3}{2}} + 8\pi G \beta \frac{u_\alpha u_\beta}{u} T^{\alpha\beta} \right] + \frac{3\alpha}{2} \chi^{\frac{1}{2}} A_{\mu\nu} - \frac{3\alpha}{2} \nabla_\alpha \left[\chi^{\frac{1}{2}} \left(B^\alpha_{(\mu} u_{\nu)} + u_{(\nu} B_{\mu)}^\alpha - B_{(\mu\nu)} u^\alpha \right) \right] - 8\pi G \beta \left[\frac{u_\alpha u_\beta}{2u^3} u_\mu u_\nu T^{\alpha\beta} + \frac{2u_\beta}{u} u_{(\mu} T_{\nu)}^\beta \right]$$

5.3 Imposter field equations

The next step is to derive the field equations from the newly obtained total action 5.15. From these equations we will derive the Newtonian limit and the weak-field limit. This action was based on the assumptions made in the previous sections on Erik Verlinde's theory. However, one can also take this action at face value and in the next sections we will check whether it yields any interesting results.

From this action 5.15, one can derive the field equations by varying the action with respect to $g_{\mu\nu}$ and u_μ . The derivation of this was not done in by Yen-Kheng Lim and Qing-hai Wang [18] and we have included our derivations in the appendix as they are rather long and don't provide any new insights.

From our action 5.15, we know that the imposter field has a Lagrangian with a source term and an interaction term coupled to baryonic matter. This implies that the field equations for the imposter field u_μ can be found by varying this Lagrangian with respect to u_μ .

When we vary the action with respect to u_μ , we obtain the differential equations for the vector field u_μ . In order to understand these equations, let us first introduce two simplifying tensors:

$$A_{\mu\nu} = a\epsilon_\lambda^\lambda \epsilon_{\mu\nu} + b\epsilon_{\mu\lambda} \epsilon_\nu^\lambda + d F_{\mu\lambda} F_\nu^\lambda \quad , \quad (5.16)$$

and the second simplifying tensor:

$$B^{\mu\nu} = a\epsilon_\lambda^\lambda g^{\mu\nu} + b\epsilon^{\mu\nu} + d F^{\mu\nu} \quad . \quad (5.17)$$

From the action 5.15, one can recover the field equations for u_μ by varying the action with respect to u_μ . This is done in the appendix A. The results are the field equations for the imposter field:

$$\boxed{\frac{3\alpha}{16\pi G} \nabla_\mu \left(\chi^{\frac{1}{2}} B^{\mu\nu} \right) = \frac{\beta}{2} \left[2 T^{\mu\nu} \frac{u_\mu}{u} + \frac{T^{\mu\lambda} u_\mu u_\lambda u^\nu}{u^3} \right]} \quad (5.18)$$

This equation provide the left arrow in figure 5.1, it describes the way in which matter determines the evolution of the imposter field. Note that the term $\chi^{\frac{1}{2}}$ makes sense, as this is the derivative of $\chi^{\frac{3}{2}}$. Since $\chi^{\frac{1}{2}} \sim \nabla u$ and $B_{\mu\nu} \sim \nabla u$, these equations indeed imply $\nabla (\nabla u)^2 \sim T$ as we wanted from our discussion on the correct form of the Lagrangian.

In Hossenfelder's paper, this equation contains a mistake according to the paper by Yen-Kheng Lim and Qing-hai Wang [18] and the author of this report shares this opinion. This mistake comes from the interaction term Hossenfelder proposes, which is a factor 2 different from our interaction term. This mistake can be fixed by letting $\beta \rightarrow \frac{\beta}{2}$ in Hossenfelder's paper. This does not affect any results as this is simply a constant that is fixed later.

Before we move on to the other equations such as the interaction between the imposter field and the curvature of space-time, let us see whether we can solve the field equations 5.18 in the Newtonian limit.

5.3.1 The Newtonian Limit

It is time to make a couple of assumptions. First, we will assume that u^μ only consists of a temporal part, thus $u^\mu = (u^0, \mathbf{0})$, which we assume to be negative, as in Erik Verlinde's theory. The fact that we only consider the temporal part implies that we are working relatively close to the inertial frame of the imposter field. Stated simpler, we assume that the field moves

slowly, which was also used by Erik Verlinde in his glassy dynamics. This requirement is obviously not Lorentz invariant, but will suffice for our Newtonian considerations.

We will use a Newtonian approximation $g_{\mu\nu} \approx \eta_{\mu\nu}$ to get an idea for this field u^μ . We will also assume that the field moves very slowly, which implies that we ignore time derivatives $\partial_t u^\mu = 0$. In our analysis, we will make use of the short hand notation for the following matrix:

$$\nabla u^0 \begin{bmatrix} 0 & 1 \\ -1 & 0 \end{bmatrix} := \begin{bmatrix} 0 & \nabla u^0 \cdot \mathbf{e}_1 & \nabla u^0 \cdot \mathbf{e}_2 & \nabla u^0 \cdot \mathbf{e}_3 \\ -\nabla u^0 \cdot \mathbf{e}_1 & 0 & 0 & 0 \\ -\nabla u^0 \cdot \mathbf{e}_2 & 0 & 0 & 0 \\ -\nabla u^0 \cdot \mathbf{e}_3 & 0 & 0 & 0 \end{bmatrix} \quad (5.19)$$

Here \mathbf{e}_i are the unit vectors of our spatial coordinate system. It is simply the anti-symmetric matrix with as its temporal-spatial parts its spatial derivatives.

The first step in solving for the imposter field equations in CEG is always to calculate the strain $\epsilon_{\mu\nu}$ and stress $F_{\mu\nu}$ under the current approximation. Plugging our approximations in the formulas 5.3, the stress and strain tensors become:

$$F_{\mu\nu} = \nabla u^0 \begin{bmatrix} 0 & 1 \\ -1 & 0 \end{bmatrix} \quad \epsilon_{\mu\nu} = \nabla u^0 \begin{bmatrix} 0 & -1 \\ -1 & 0 \end{bmatrix} \quad (5.20)$$

Next, one solves for the simplifying tensors $A_{\mu\nu}$ and $B_{\mu\nu}$. For our field equations 5.18, we only need $B_{\mu\nu}$. For our simplifying tensor $B_{\mu\nu}$ (equation 5.17), our strain and stresses (equation 5.20) yield:

$$B^{\mu\nu} = \nabla u^0 \begin{bmatrix} 0 & b-d \\ b+d & 0 \end{bmatrix} \quad \chi = -(b+d) (\nabla u^0)^2 \quad (5.21)$$

Since we ignore time derivatives, the only non-trivial term in the imposter field equation 5.18 for u^μ is the $\nu = 0$ term, which gives:

$$(b+d) \sqrt{-b-d} \frac{3\alpha}{16\pi G} \nabla \cdot (|\nabla u^0| \nabla u^0) = \frac{\beta}{2} \rho \frac{u^0}{|u^0|} \quad (5.22)$$

From our Newtonian discussions, we now that what comes after ∇ is often the potential of the field. Thus, let us define the dark potential $\phi_D := \frac{\beta}{2} \sqrt{-u^\alpha u_\alpha} = \frac{\beta}{2} u$. Later on this will indeed be identified as the potential associated with this field such that the force of the field is $\mathbf{F} \sim \nabla \phi_D$.

Plugging our approximations for $u^\mu = (u^0, \mathbf{0})$ into our definition of the potential, we see that: $\phi_D = \frac{\beta}{2} |u^0|$. If we now use that we know from Erik Verlinde's paper that $u^0 \leq 0$ and insert the potential into the previous equation 5.22, we obtain:

$$(b+d) \sqrt{-b-d} \frac{4}{\beta^2} \nabla \cdot (|\nabla \phi_D| \nabla \phi_D) = -\frac{\beta}{\alpha} \frac{16\pi G}{6} \rho \quad (5.23)$$

In our discussion on the effective metric, we already saw that $\beta = \frac{2}{L}$ by comparing equation 5.7 and 5.8. In Hossenfelder's paper, she also assumed that $\alpha = \frac{1}{L^2}$ by dimensional analysis. This implies:

$$(b+d) \sqrt{-b-d} \nabla \cdot (|\nabla \phi_D| \nabla \phi_D) = -\frac{8}{6L} 4\pi G \rho \quad (5.24)$$

In order to fix b and d , let us use that in Erik Verlinde's paper, the Newtonian equations should be:

$$\nabla \cdot (|\nabla\phi_D|\nabla\phi_D) = -\frac{a_0}{6}4\pi G\rho \quad (5.25)$$

Equating the two expressions yields $b + d = -4$. Note that this set of constants is different from those obtained by Hossenfelder, but the resulting force is of course similar to that of Erik Verlinde [26]. We can fix b and d as follows. From our discussion on stresses and strains and equation 5.3, we see that b determines the strain and d the stress contribution to our equations. In Erik Verlinde's second paper [26], the strain in the medium was the main contributor to the force on the particle. Thus we assume that $d = 0$, which implies $b = -4$ and $d = 0$ in equation 5.4. This yields our Newtonian approximation of the field equations 5.18 as:

$$\nabla \cdot (|\nabla\phi_D|\nabla\phi_D) = \frac{a_0}{6}4\pi G\rho \quad (5.26)$$

An easy solution to the equation 5.26 is that of a particle of mass M at position $r = 0$. We can then simply solve equation 5.26 by using a Gaussian sphere around the mass. The results are:

$$\phi_D = \sqrt{\frac{GMa_0}{6}} \ln r + C_2 \quad (5.27)$$

Note that this was indeed the form of the equation we were looking for from our historical discussion as it yields a constant tangential velocity for circular orbits from the centripetal law if $\mathbf{F} \sim \nabla\phi_D$ in order to yield a flat velocity.

5.3.2 Newtonian Lagrangian

Our Newtonian discussion can also be accompanied by a Lagrangian for the field ϕ_D such that we produce equation 5.26. The correct Newtonian action is:

$$S_N = \iiint \left\{ \frac{2}{a_0} (\nabla\phi_D \cdot \nabla\phi_D)^{\frac{3}{2}} + 4\pi G\rho\phi_D \right\} dV dt \quad (5.28)$$

We see that the interaction term $4\pi G\rho\phi_D$ in 5.28 is similar to the interaction term in Electromagnetism (3.12) and in baryonic gravity. The source term $\frac{2}{a_0} (\nabla\phi_D \cdot \nabla\phi_D)^{\frac{3}{2}}$ is however fundamentally different from the source terms in either of these. This is also necessary to produce a force that goes as $\frac{1}{r}$ instead of $\frac{1}{r^2}$.

For completeness, we can also add the baryonic gravitational potential ϕ_B , to arrive at a total action of:

$$S_N = \iiint \left\{ \frac{2}{a_0} (\nabla\phi_D \cdot \nabla\phi_D)^{\frac{3}{2}} + 4\pi G\rho(\phi_D + \phi_B) + \nabla\phi_B \cdot \nabla\phi_B \right\} dV dt \quad (5.29)$$

We can again draw analogies from our single particle case. The equations of motion for the field ϕ_D are given by 5.26. These look similar to Newton's equations of for a single particle $\frac{d}{dt} \left(m \frac{dx}{dt} \right) = F$ with the substitutions, $x \rightarrow \phi$, $m \rightarrow \frac{6}{a_0} |\nabla\phi_D|$ and $\frac{d}{dt} \rightarrow \nabla$. The mass of the field (by analogy with the single particle case) is thus dependent on the value of the field: $m_\phi = \frac{6}{a_0} |\nabla\phi_D|$. For low accelerations $a \leq \frac{a_0}{6}$, the mass of the field is low, making it very responsive to the baryonic matter densities. The reverse is true for high accelerations $a \geq \frac{a_0}{6}$. This is of course exactly the behaviour we were looking for, as the rotation curves tended to deviate from our Newtonian predictions when $a \leq \frac{a_0}{6}$.

5.4 The Modified Einstein Equations

Now that we know how the imposter field reacts to baryonic matter, we can ask ourselves how the imposter field affects the curvature of space-time. This is done by varying the Action 5.15 with respect to the metric $g^{\mu\nu}$. Since every term in the action depends on the metric, this is not an easy task, as can be seen in the appendix A. The results are the modified Einstein equations:

$$R_{\mu\nu} - \frac{1}{2}g_{\mu\nu}R = 8\pi GT_{\mu\nu} - \frac{1}{2}g_{\mu\nu} \left[\alpha\chi^{\frac{3}{2}} + 8\pi G\beta \frac{u_\alpha u_\beta}{u} T^{\alpha\beta} \right] + \frac{3\alpha}{2}\chi^{\frac{1}{2}}A_{\mu\nu} - \frac{3\alpha}{2}\nabla_\alpha \left[\chi^{\frac{1}{2}} \left(B^\alpha_{(\mu} u_{\nu)} + u_{(\nu} B_{\mu)}^\alpha - B_{(\mu\nu)} u^\alpha \right) \right] - 8\pi G\beta \left[\frac{u_\alpha u_\beta}{2u^3} u_\mu u_\nu T^{\alpha\beta} + \frac{2u_\beta}{u} u_{(\mu} T_{\nu)}^\beta \right] \quad (5.30)$$

These equations provide the downward arrow from matter in figure 5.1 and show how both the imposter field and baryonic matter determine the normal metric $g_{\mu\nu}$. Don't worry, we will hardly need these equations throughout the rest of the report. The first three terms give the known Einstein equations and the all other terms stem from the interaction between $g^{\mu\nu}$ and the imposter field u^μ . These interactions arise from the Lagrangian of the imposter field u^μ , which contains both a source term and an interaction of the imposter field with the baryonic matter. These equations are rather large, but have already been solved for a Schwarzschild-like solution by Yen-Kheng Lim and Qing-hai Wang [18] under the assumption that $d = -1$ and $b = 0$.

There are several important points we would like to stress. Firstly, the motion of matter is primarily influenced by the effect u^μ has on the effective metric $\widetilde{g}_{\mu\nu}$ (5.8). The effect of u^μ on the modified Einstein equations are negligible in the Newtonian approximation. This is because the effect of the extra terms on the Einstein equations are incredibly small as $\frac{\alpha}{G} \approx 10^{-60}$ and $\frac{\beta}{G} \approx 10^{-25}$. Secondly, and more mathematically, we will see that the extra terms disappear in our linearisation of the modified Einstein equations.

Now that we have derived the equations of motion for the imposter field u^μ and the metric $g_{\mu\nu}$, the procedure to find the effective metric is clear. We have to solve both the system of equations for the imposter field equations 5.18 and the modified Einstein equations 5.30. From this we can construct an effective metric $\widetilde{g}_{\mu\nu}$. This is a rather hefty challenge, but we will see that the equations simplify immensely using perturbation theory.

The main attack in equations in CEG thus consists of first solving for the various tensors such as the stress and strain tensor 5.3 and the simplifying tensors 5.17 under the correct approximations for u^μ . The next step is to try to solve for the evolution of the imposter field through the imposter field equations 5.18. Subsequently, one solves for the metric $g_{\mu\nu}$ through the modified Einstein equations 5.30. Since these are all coupled differential equations, worst case scenario is that one needs to solve these all at once. From the metric and the imposter field, one then recovers the effective metric from equation 5.8. This effective metric determines the motion of matter, which is what we will tackle next.

5.5 The Equations of Motion

In order to obtain the equations of motion for a single particle, we place a single test particle in our space and vary its path to obtain its equations of motion. The particle adds a matter action of the form $S_m = \frac{m}{2} \int \sqrt{-g_{\mu\nu} \dot{x}^\mu \dot{x}^\nu} d\tau$. From our discussions on from Newtonian to

Einsteinian gravity, we know that the equation of motion are determined by the geodesic equations in general relativity. The equations of motions for the particle will be altered, since instead of a normal metric, we know have an effective metric. This can also be seen from the fact that our action 5.15 contains an interaction term between the field u^μ by $\frac{u_\mu u_\nu}{u} T^{\mu\nu}$.

The derivation of the equations of motion can be found in the relevant section of the appendix A. The imposter geodesic equations are:

$$\ddot{x}^\delta - \beta \frac{u^\delta u_\nu}{u} \dot{x}^\nu = \dot{x}^\mu \dot{x}^\nu \left(\beta C_{\mu\nu}^\delta - \Gamma_{\mu\nu}^\delta \right) \quad (5.31)$$

Here we have introduced the imposter Christoffel symbols $C_{\mu\nu}^\delta$ as is done by Yen-Kheng Lim and Qing-hai Wang [18]. These imposter Christoffel symbols are defined as:

$$C_{\mu\nu}^\delta = \frac{1}{2} g^{\delta\alpha} \left[\partial_\mu \left(\frac{u_\alpha u_\nu}{u} \right) + \partial_\nu \left(\frac{u_\alpha u_\mu}{u} \right) - \partial_\alpha \left(\frac{u_\mu u_\nu}{u} \right) \right] \quad (5.32)$$

Here the main contribution of the imposter field u^μ to the motion of our particle comes from the imposter Christoffel symbols $C_{\mu\nu}^\delta$ and not the modifications in the Einstein equations. In the Newtonian approximation, we defined the potential of the field as $\phi_D = \frac{\beta}{2} |u^0|$. From the imposter Christoffel symbols $C_{\mu\nu}^\delta$, we see that the force is indeed given by $\mathbf{F} \sim C_{\mu\nu}^\delta \sim \nabla \phi_D$. Thus the force is indeed given by the gradient of the potential. Note that the imposter geodesic equations 5.31 also imply that the gravitation force $\sim \Gamma_{\mu\nu}^\delta$ and the force due to the imposter field $\sim C_{\mu\nu}^\delta$ are additive.

These equations are illustrated by the arrow from the effective metric to matter in figure 5.1 and determine how the metric plus the imposter field determine the motion of matter.

Now that we know how masses move due to the imposter field, we can make use of the Newtonian approximation for the imposter field and study the motion of slow-moving particles.

Again, we consider the Newtonian limit. We assume that the metric is approximately Minkowskian, such that $g_{\mu\nu} \approx \eta_{\mu\nu}$ in formula 5.32 and formula 5.31. We also make the assumption that $u^\mu = (u^0, \mathbf{0})$. From our discussion on From Newtonian to Einsteinian gravity, we know that the Christoffel symbols are the 'acceleration' in general relativity. In fact, the radial acceleration for slow-moving particles in a circular orbit is determined by:

$$\ddot{r} - \omega^2 r = c^2 (\beta C_{00}^r - \Gamma_{00}^r) \quad (5.33)$$

Let us consider a slow-moving particle circling a much heavier particle with a mass M centered at the origin. This allows us to C_{00}^r from its defining equation 5.32 and our the imposter potential due to a point source 5.26. The effect of the Christoffel symbols are known from Newtonian gravity. Inserting both the Christoffel symbols and imposter Christoffel symbols in the radial acceleration equations 5.33 yields:

$$\ddot{r} - \omega^2 r = -\frac{GM}{r^2} - \sqrt{\frac{GMa_0}{6}} \frac{1}{r} \quad (5.34)$$

Thus for objects circling this mass, we obtain a tangential velocity by using the usual centripetal velocity law:

$$v^2 = -r^2 \omega^2 \implies v = \sqrt{-r\dot{r}} = \sqrt{\frac{GM}{r} + \sqrt{\frac{GMa_0}{6}}} \quad (5.35)$$

Thus our velocities should go to a constant at large radii:

$$v_{\text{flat}} = \left(\frac{GMa_0}{6} \right)^{\frac{1}{4}} \quad (5.36)$$

This is exactly the result obtained by Vera Rubin, namely that the rotation curves of galaxies appear to flatten for large radii. Since any mass distribution at large radii looks like a point source, we obtain a rather important result, namely that if the total mass in the galaxy is M , the rotation curves should tend to the value obtained above. This is an important experimentally verifiable result, but it is also an effect commonly attributed to dark matter.

The fact that the flat velocity obeys the scaling relation $M \sim v^4$ and is not dependent on other properties of the galaxy is an experimentally known fact (see Lelli et al. [13]), known as the Tully-Fisher relation. Thus we have obtained our first theoretical evidence for an experimentally observed phenomena. This phenomena is also explained by MOND. However, CEG derives it from entropic principles and MOND simply postulates a form that matches observations.

5.6 Perturbation theory

In the previous section, we ignored the contribution of the imposter field u^μ to the modified Einstein equations 5.30. This is fine in the Newtonian approximation that $g_{\mu\nu} \approx \eta_{\mu\nu}$ and for slow-moving particles, but may break down for particles with relativistic velocities.

The reason we would like to calculate whether the imposter field modifies the metric $g_{\mu\nu}$ is because we will study the bending of light in the next section. From the bending of light, we can calculate whether CEG predicts deviations of the bending angle of light with respect to the predicted value by Einstein's equations. This time we actually have to solve for the effective metric as light moves at such high speeds that the 'magnetic components' of the metric become important. However, since the bending angle is usually very small (in the order of arc seconds), we will use perturbation theory.

In order to find the appropriate bending of light, we will write the metric in terms of a Minkowskian part $\eta_{\mu\nu}$ plus a small perturbation $h_{\mu\nu}$, so that $g_{\mu\nu} = \eta_{\mu\nu} + h_{\mu\nu}$. Furthermore, we assume that the stress-energy tensor $T_{\mu\nu}$ is of the same order as the perturbation. This last assumption follows from the fact that we assume that the mass of the object must be small for the perturbation to be small.

From Erik Verlinde's theory we know that for spherical masses $\beta u_\mu = \frac{\phi_B}{c^2}$. This will turn out to be exactly $h_{\mu\nu}$, such that βu_μ and $h_{\mu\nu}$ are of the same order.

Now since $\alpha \sim \beta^2$ and $\beta \ll 1$, this also implies that $\sqrt{\chi}$ is of the same order as $h_{\mu\nu}$. Using these assumptions on the order of $h_{\mu\nu}$, $T_{\mu\nu}$ and u^μ , the right-hand side of the Modified Einstein equations (equation 5.30) up to first order in $h_{\mu\nu}$ becomes:

$$G_{\mu\nu} = 8\pi GT_{\mu\nu} \quad (5.37)$$

We see that we can neglect the interaction the imposter field has with the metric. Alternatively, we could also have stated that the extra terms in the modified Einstein equations are much smaller than the usual terms, as indicated in the section on the modified equations.

Equation 5.37 are the unmodified Einstein field equations. This confirms our statement that the influence of the imposter field u^μ mainly comes from the effective metric $\widetilde{g}_{\mu\nu}$, at least in the weak-field limit.

The linearization of the Einstein equations under the assumptions that the perturbation $h_{\mu\nu}$ is well known. For a pressure-less fluid (matter density without internal pressure), we know that $T_{\mu\nu} = \rho v^\mu v^\nu$. We will also assume that our matter does not move. Under these assumptions, the only non-zero component is $T_{00} = \rho$.

By plugging $h_{\mu\nu}$ and $T_{\mu\nu}$ into the perturbed modified Einstein equations 5.37, one can calculate the perturbed metric $h_{\mu\nu}$. This is done in any book on general relativity (for instance Sean Carroll [5]). The results are best formalized in a gravitational potential ϕ_B such that the metric becomes:

$$g_{\mu\nu} = \begin{bmatrix} -1 - 2\phi_B & 0 & 0 & 0 \\ 0 & 1 - 2\phi_B & 0 & 0 \\ 0 & 0 & 1 - 2\phi_B & 0 \\ 0 & 0 & 0 & 1 - 2\phi_B \end{bmatrix} \quad \text{with} \quad \nabla^2 \phi_B = 4\pi G\rho \quad (5.38)$$

Note that, if we were to plug this metric into the geodesic equation, this indeed leads to the Newtonian gravitational law for slow-moving particles.

From this perturbed metric, we can calculate the perturbed effective metric by equation 5.8. From our discussion on the Newtonian approximation of the imposter field u^μ , we know that:

$$u = \frac{2}{\beta} \phi_D \quad \text{with} \quad \nabla \cdot (|\nabla \phi_D| \nabla \phi_D) = \frac{a_0}{6} 4\pi G\rho \quad (5.39)$$

This yields an effective metric in equation 5.8 of:

$$\widetilde{g}_{\mu\nu} = \begin{bmatrix} -1 - 2\phi_B - 2\phi_D & 0 & 0 & 0 \\ 0 & 1 - 2\phi_B & 0 & 0 \\ 0 & 0 & 1 - 2\phi_B & 0 \\ 0 & 0 & 0 & 1 - 2\phi_B \end{bmatrix} \quad (5.40)$$

A few comments about this effective metric are in order. Firstly, the fact that the effective metric only differs from the metric by a temporal component is logical as we used that u^μ only has a temporal component. Secondly, this effective metric together with the geodesic equations (5.31) yield an effective Newtonian force of:

$$\mathbf{F}_{net} = -m\nabla\phi_B - m\nabla\phi_D \quad (5.41)$$

This is exactly what we found in our previous Newtonian analysis of the imposter geodesic equations 5.31. Let us offer a quick summary to collect our results and then move on to the bending of light.

5.6.1 Summary of the interactions from the imposter field

In the preceding chapters we found that matter feels an additional force next to the gravitational force. This force will be called the dark force and will have a potential ϕ_D . The normal gravitational force will have a potential ϕ_B with the B of Baryonic matter. The resulting force on a particle in the Newtonian approximation would simply be the sum of these forces. Thus our model obeys:

$$\mathbf{F}_{net} = -m\nabla\phi_D - m\nabla\phi_B \quad (5.42)$$

We know reintroduce the speed of light to make our results truly Newtonian. The differential equations for the potentials ϕ_D and ϕ_B are:

$$\nabla^2 \phi_B = 4\pi G\rho \quad \text{and} \quad \nabla \cdot (|\nabla \phi_D| \nabla \phi_D) = \frac{a_0}{6} 4\pi G\rho \quad (5.43)$$

These equations can be applied to slow-moving particles in CEG. In order to solve for relativistic particles such as light, we needed perturbation theory. Using perturbation theory and the assumption that $u^\mu = (u^0, \mathbf{0})$ and $\phi_D = \frac{\beta}{2}|u^0|$, we found that the effective metric is given by:

$$\widetilde{g}_{\mu\nu} = \begin{bmatrix} -1 - 2\frac{\phi_B}{c^2} - 2\frac{\phi_D}{c^2} & 0 & 0 & 0 \\ 0 & 1 - 2\frac{\phi_B}{c^2} & 0 & 0 \\ 0 & 0 & 1 - 2\frac{\phi_B}{c^2} & 0 \\ 0 & 0 & 0 & 1 - 2\frac{\phi_B}{c^2} \end{bmatrix} \quad (5.44)$$

The corresponding imposter geodesic equations are:

$$\ddot{x}^\delta - \beta \frac{u^\delta u_\nu}{u} \ddot{x}^\nu = \dot{x}^\mu \dot{x}^\nu (\beta C_{\mu\nu}^\delta - \Gamma_{\mu\nu}^\delta) \quad (5.45)$$

Here we have defined the imposter Christoffel symbols $C_{\mu\nu}^\delta$ as:

$$C_{\mu\nu}^\delta = \frac{1}{2} g^{\delta\alpha} \left[\partial_\mu \left(\frac{u_\alpha u_\nu}{u} \right) + \partial_\nu \left(\frac{u_\alpha u_\mu}{u} \right) - \partial_\alpha \left(\frac{u_\mu u_\nu}{u} \right) \right] \quad (5.46)$$

These equations can be applied to both slow-moving particles and light. For slow-moving particles, we found that at large radii, the velocity becomes a flat constant:

$$v_{\text{flat}} = \left(\frac{GMa_0}{6} \right)^{\frac{1}{4}} \quad (5.47)$$

This theoretical fact is also observed experimentally and captured in the Tully-Fisher relation [13].

Chapter 6 ● ■ ▲

Theoretical applications CEG

In this chapter we will explore two theoretical consequences of our general relativistic formulation of emergent gravity. These are gravitational lensing and an attempt at a cosmological model. Our gravitational lensing results are applicable to any lensing systems. In order to explain these results, we will however first focus on the bending of light in Newtonian gravity. Afterwards we will move on to bending of light in GR for point masses and subsequently general lensing systems.

Our cosmological model will consist of a vacuum dominated solution and a matter dominated solution. The vacuum dominated solution will turn out to yield a constant imposter field, whilst the matter dominated solution has a changing imposter field due to the changing matter content of the universe.

6th

6.1 Gravitational lensing

In this section we will use the previously obtained results to calculate the bending of light in an arbitrary mass distribution in CEG.

6.1.1 Newtonian Gravitational lensing

Long before Einstein, physicist had considered the bending of light due to large masses. In fact, in 1704 Newton wrote the following quote in his treatise on optics [22]:

"Do not Bodies act upon Light at a distance, and by their action bend its Rays, and is not this action strongest at the least distance?"

In GR, light curves around masses as masses bent the nearby space-time. In Newtonian gravity however, there is not a clear indication of why light should bent around masses. Light has no mass, thus it would not feel a force. Nevertheless, this does not stop us from saying that light feels an acceleration due to gravity, as masses cancel out in gravity. Let us therefore calculate the bending angle due to classical mechanics as a warm-up for the general relativistic case.

As the bending angle of light is extremely small in most cases (arcseconds or less), we will use perturbation theory. This implies that we act as if the light follows a straight line and simply moves a tiny bit in the direction of the mass.

In figure 6.1, we have sketched our situation. We consider a beam of light that passes the Sun at a distance b . As we are doing perturbation theory, we assume that the light travels almost entirely in the x -direction such that $\frac{dx}{dt} \approx c$. The y -direction is thus the direction with impact parameter b with the Sun. Let us calculate the acceleration in the y -direction:

$$\frac{d^2y}{dt^2} = \sin \theta |\nabla \phi| = \frac{b}{\sqrt{x^2 + b^2}} |\nabla \phi| \quad (6.1)$$

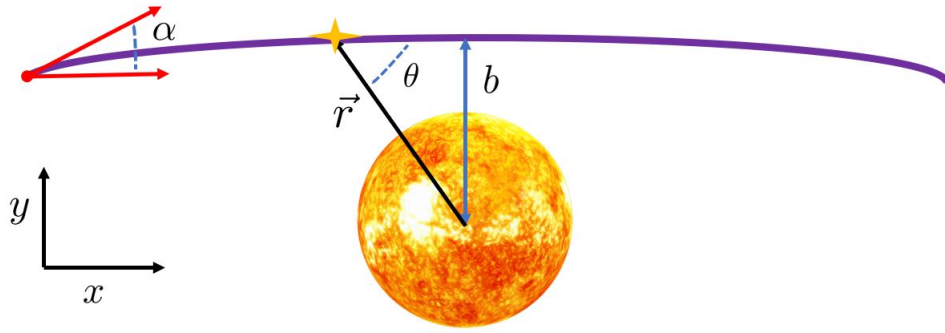


FIGURE 6.1: A light beam passing the Sun at an impact parameter b . The current position of the light is indicated by the yellow dot and its current angle with the Sun is indicated by θ . The initial angle of the light beam was α .

Here the angle θ is the angle $\sin \theta = \frac{y}{\sqrt{x^2+y^2}} \approx \frac{b}{\sqrt{b^2+x^2}}$ as indicated in figure 6.1.

Now the angle the path makes with respect to the x -axis at any point is given by:

$$\alpha = \frac{dy}{dx} = \frac{\frac{dy}{dt}}{\frac{dx}{dt}} = \frac{1}{c} \frac{dy}{dt} \quad (6.2)$$

The total deflection angle α in the y -direction is then the final angle minus the initial angle:

$$\alpha = \frac{1}{c} \left[\frac{dy}{dt} \Big|_{t_{\text{final}}} - \frac{dy}{dt} \Big|_{t=0} \right] = \frac{1}{c} \int \frac{d^2y}{dt^2} dt = \frac{1}{c} \int \frac{d^2y}{dt^2} \frac{dt}{dx} dx = \frac{1}{c^2} \int \frac{b}{\sqrt{b^2+x^2}} \nabla \phi_B dx \quad (6.3)$$

Note that this formula is valid for any matter distribution! We have substituted the acceleration from equation 6.1. Now let us evaluate this angle for the total deflection due the Sun for a light ray that started at $x = -\infty$ and ends at $x = +\infty$:

$$\alpha = \frac{1}{c^2} \int_{-\infty}^{\infty} \frac{b}{\sqrt{x^2+b^2}} \frac{GM}{x^2+b^2} dx = \frac{2GM}{bc^2} \approx 0.87'' \quad (6.4)$$

Here b was taken to be R_{\odot} , the radius of the Sun and the mass M as M_{\odot} , the mass of the Sun. This is already a remarkable result. In fact, we are only off by a factor of 2 with respect to the general relativistic case. One of the successes of Einstein's theory was to explain this missing factor. In fact Jaume Giné [6] showed in a recent paper that one recovers the general relativistic case if one uses a retarded gravitational potential.

6.1.2 Microlensing in CEG

We will now focus on the bending of light in GR. In special relativity, light moves at speed c . Thus a light ray that moves in the x -direction moves a distance $dx = c dt$ in a time dt . This is equivalent to $\eta_{\mu\nu} dx^{\mu} dx^{\nu} = 0$ or to $c^2 dt^2 - dx^2 = 0$. Similarly, in GR, light satisfies $g_{\mu\nu} dx^{\mu} dx^{\nu} = 0$. The following problem now arises: In our covariant emergent gravity, does light satisfy $g_{\mu\nu} dx^{\mu} dx^{\nu} = 0$ or $\widetilde{g}_{\mu\nu} dx^{\mu} dx^{\nu} = 0$. Yen-Kheng Lim and Qing-hai Wang chose the former, but we will argue for the latter.

Both the introduction of light and matter alter the distribution of entropy by their stress-energy tensor $T_{\mu\nu}$ in the interaction term. Since light alters the entropy distribution of the universe due to its energy, it should, like matter, feel an additional force. Thus we must demand that light satisfies $\widetilde{g}_{\mu\nu} dx^{\mu} dx^{\nu} = 0$ and use the imposter geodesic equation 5.31. Thus if light

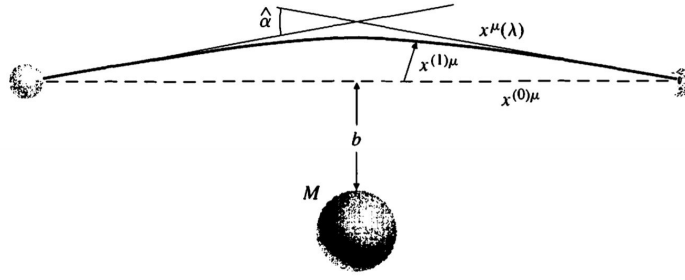


FIGURE 6.2: The deflection of light passing a lens of mass M at an impact parameter b . The path $x^{(0)\mu}$ is the unperturbed path and $x^{(1)\mu}$ the perturbation. The angle $\hat{\alpha}$ is the total deflection angle of the light geodesic. Credit to Sean Carroll [5]

follows a path $x^{\mu}(\lambda)$, it must satisfy the equations:

$$\widetilde{g}_{\mu\nu} dx^{\mu} dx^{\nu} = 0 \quad (6.5)$$

$$\ddot{x}^{\delta} - \beta \frac{u^{\delta} u_{\nu}}{u} \ddot{x}^{\nu} = \dot{x}^{\mu} \dot{x}^{\nu} \left(\beta C_{\mu\nu}^{\delta} - \Gamma_{\mu\nu}^{\delta} \right) \quad (6.6)$$

The dot represents the derivative with respect to the parameter λ of the path. Let the path of the photon also be a perturbation to an unaccelerated path:

$$x^{\mu}(\lambda) = x^{(0)\mu}(\lambda) + x^{(1)\mu}(\lambda) \quad (6.7)$$

A pictorial interpretation of this can be found in figure 6.2. The following discussions follows the discussion of Sean Carroll's book [5] on the bending of light with a few alterations to accommodate for the additional force. We denote the wave vectors as:

$$k^{\mu} = \frac{dx^{(0)\mu}}{d\lambda}, \quad \ell^{\mu} = \frac{dx^{(1)\mu}}{d\lambda} \quad (6.8)$$

We will again look for a vector that is perpendicular to the unaccelerated path. Thus a vector perpendicular to the space part \mathbf{k} of the vector of the path k^{μ} . In order to find such a vector, we first need to solve the set of equations 6.6 for the wave vectors at different orders. We will first solve for various order for the first equation of the set. If during this derivation, something is unclear, we advise the reader to return to the Newtonian lensing derivation (section 6.1.1).

At zeroth-order, the effective metric (equation 6.6) yields:

$$(k^0)^2 = \mathbf{k}^2 = k^2 \quad (6.9)$$

At first order, we obtain:

$$2\eta_{\mu\nu} k^{\mu} \ell^{\nu} + \widetilde{h}_{\mu\nu} k^{\mu} k^{\nu} = 0 \quad (6.10)$$

Equivalently:

$$-2k^0 \ell^0 + 2\boldsymbol{\ell} \cdot \mathbf{k} - (2\phi_B + 2\phi_D) (k^0)^2 - 2\phi_B \mathbf{k} \cdot \mathbf{k} = 0 \quad (6.11)$$

Using our zeroth-order equation 6.9 and equation 6.11, we obtain:

$$-k \ell^0 + \boldsymbol{\ell} \cdot \mathbf{k} = (2\phi_B + \phi_D) k^2 \quad (6.12)$$

Thus if we want to find a vector that is perpendicular to \mathbf{k} , we need to solve for ℓ^0 . We will now solve for $\frac{d\ell^{\mu}}{d\lambda}$ using the imposter geodesic equation of set 6.6. The zeroth order of this

equation simply states that k^μ (the zeroth order wavevector along the path) is an unaccelerated path. However, at first order we have:

$$\frac{d\ell^0}{d\lambda} - 2\phi_D \frac{dk^0}{d\lambda} = (k^0)^2 \partial_t \phi_D - 2k(\mathbf{k} \cdot \nabla \phi_B) - 2k(\mathbf{k} \cdot \nabla \phi_D) \quad (6.13)$$

Note that the k^μ wave vector does not change along the path and that we ignore time derivatives, thus the temporal component of the previous equation simplifies to:

$$\frac{d\ell^0}{d\lambda} = -2k(\mathbf{k} \cdot \nabla \phi_B) - 2k(\mathbf{k} \cdot \nabla \phi_D) \quad (6.14)$$

This allows us to solve for ℓ^0 by integrating the previous equation:

$$\ell^0 = \int \frac{d\ell^0}{d\lambda} d\lambda = -2k \int \mathbf{k} \cdot (\nabla \phi_B + \nabla \phi_D) d\lambda = -2k \int \frac{d\mathbf{x}}{d\lambda} \cdot (\nabla \phi_B + \nabla \phi_D) d\lambda = -2k(\phi_B + \phi_D) \quad (6.15)$$

Now that we have solved for ℓ^0 , we can find a vector that is perpendicular to the unaccelerated path's space vector \mathbf{k} by the dot product in equation 6.12 by substituting the results of equation 6.15 :

$$\boldsymbol{\ell} \cdot \mathbf{k} = (2\phi_B + \phi_D) k^2 + k \ell^0 = -\phi_D k^2 \quad (6.16)$$

Thus the vector perpendicular to \mathbf{k} is:

$$\mathbf{m} = \boldsymbol{\ell} + \mathbf{k}\phi_D \quad (6.17)$$

We will again use the acceleration in the direction of this vector to find the total deflection angle. Since \mathbf{m} contains the spatial components of the wave vectors, we will first solve for these using the geodesic equation of the set 6.6 at first order:

$$\frac{d\boldsymbol{\ell}}{d\lambda} = -k^2 \nabla \phi_D - 2k^2 \nabla_\perp \phi_B \quad \text{with} \quad \nabla_\perp \phi_B := \nabla \phi_B - k^{-2} (\mathbf{k} \cdot \nabla \phi_B) \mathbf{k} \quad (6.18)$$

In this equation, we have defined the perpendicular gradient $\nabla_\perp \phi_B$ as simply the component of the gradient perpendicular to the path. As in the classical case, the deflection angle vector α is again given by the initial angle the vector \mathbf{m} makes with the vector \mathbf{k} minus the final angle, which is given by:

$$\alpha = - \left(\frac{\mathbf{m}_{initial}}{k} - \frac{\mathbf{m}_{final}}{k} \right) = - \frac{\Delta \mathbf{m}}{k} \quad (6.19)$$

The minus sign is included to account for the fact that the observer sees minus this deflection angle. We can calculate $\Delta \mathbf{m}$ using our previous knowledge of the spatial components of $\boldsymbol{\ell}$ (equation 6.18) and \mathbf{k} :

$$\Delta \mathbf{m} = \int \frac{d\mathbf{m}}{d\lambda} d\lambda = \int \left[\frac{d\boldsymbol{\ell}}{d\lambda} + \mathbf{k} \frac{d\phi_D}{d\lambda} \right] d\lambda = \int \left[\frac{d\boldsymbol{\ell}}{d\lambda} + \mathbf{k} \frac{d\phi_D}{dx^\mu} \frac{dx^\mu}{d\lambda} \right] d\lambda \quad (6.20)$$

$$= k^2 \int [-\nabla \phi_D - 2\nabla_\perp \phi_B] d\lambda + \mathbf{k} \int (\mathbf{k} \cdot \nabla \phi_D) d\lambda \quad (6.21)$$

This can again be simplified using the perpendicular gradient:

$$\Delta \mathbf{m} = k^2 \int [-\nabla_\perp \phi_D - 2\nabla_\perp \phi_B] d\lambda \quad (6.22)$$

We are almost done. We only have to replace the parameter λ by the physical distance traveled on our path like in the classical case. The physical distance traveled up to zeroth order is:

$$s = \int \sqrt{\left(\frac{dx^\mu}{d\lambda}\right)^2} d\lambda = k\lambda \quad (6.23)$$

This allows us to re-express the deflection angle vector in equation 6.22 as:

$$\hat{\alpha} = \int [\nabla_\perp \phi_D + 2\nabla_\perp \phi_B] ds \quad (6.24)$$

From this equation it is clear that the amount of matter you would predict on the basis of lensing is different from the amount of matter you would predict from the rotation curves by the Newtonian force 5.42 as the baryonic and dark potential do not provide the same contribution to the deflection angle. This is an important conclusion. However, it also depends on the assumption that we are in a comoving frame with the imposter field $u_\mu = (u_0, \mathbf{0})$. Different assumptions would also lead to a more complicated imposter field equation, possibly altering the form of the imposter field and thus the dark force. Such a change however is not unlikely, as the theory is still in the early stages. The derivation of the lensing equation in this report can then be applied to the new model.

Before we look at the deflection angle caused by a point mass, let us first check if the formula makes sense. The Einsteinian deflection can be found by setting $\phi_D = 0$, which yields:

$$\alpha_{\text{class}} = 2 \int \nabla_\perp \phi_B ds \quad (6.25)$$

Interestingly, if one wants to calculate this angle deflection without GR, one finds the same formula without the factor of 2. This was because in Newton's theory, the magnetic components of the gravitational field were ignored even for light. These magnetic components are the spatial part of our perturbed metric and amount exactly to an extra factor of $\nabla_\perp \phi_B$. This also sheds light on why we don't recover this factor of 2 in front of ϕ_D , as the imposter field only affects the temporal part of our metric.

As a quick side note, it can be shown that the deflection angle (equation 6.24) is equivalent to having an index of refraction $n = 1 - 2\frac{\phi_B}{c^2} - \frac{\phi_D}{c^2}$. We could equivalently have done the whole analysis starting with this refractive index and solving for the extremes of the action $S = \int n ds$ and would have arrived at the same result for the deflection angle.

An important point is to be made on the boundary of the integrals. Since Erik Verlinde's theory consists of a Hubble sphere of radius L , the maximum result would be obtained if we integrated from $-L$ to L . However, for an object of a small size relative to this scale, all the deflection will happen when the light is very close to the object. Thus we can safely extend the limits to $-\infty$ to ∞ , as the only important contribution comes from the point of closest approach of the light.

6.1.3 Deflection due to the Sun

Let us calculate this deflection angle 6.24 in case of a point mass with mass M , using that:

$$\phi_B = -\frac{GM}{r} \quad \text{and} \quad \phi_D = \sqrt{\frac{GMa_0}{6}} \ln r + C \quad (6.26)$$

Suppose the background path was originally along the x -direction. Let the impact parameter be b , which is the point of closest approach. We then find:

$$\phi_B = -\frac{GM}{\sqrt{x^2 + r^2}} \implies \nabla_{\perp} \phi_B = \frac{GM}{(b^2 + x^2)^{\frac{3}{2}}} \mathbf{b} \quad (6.27)$$

In the same fashion:

$$\phi_D = \sqrt{\frac{GMa_0}{6}} \ln r \implies \nabla_{\perp} \phi_D = \sqrt{\frac{GMa_0}{6}} \frac{1}{(b^2 + x^2)} \mathbf{b} \quad (6.28)$$

Then our deflection angle in equation 6.24 becomes:

$$\hat{\alpha} = 2GMb \int \frac{dx}{(b^2 + x^2)^{\frac{3}{2}}} + b \sqrt{\frac{GMa_0}{6}} \int \frac{dx}{x^2 + b^2} \quad (6.29)$$

If we integrate this from one side of our Hubble sphere to the other, this becomes:

$$\hat{\alpha} = \frac{4GM}{bc^2} \left[\frac{L}{\sqrt{b^2 + L^2}} \right] + 2\sqrt{\frac{GM}{6c^2L}} \arctan \left(\frac{L}{b} \right) \quad (6.30)$$

The deflection in GR is usually determined by integrating from $-\infty$ to ∞ , which yields:

$$\hat{\alpha} = \frac{4GM}{bc^2} + \pi \sqrt{\frac{GM}{6c^2L}} \quad (6.31)$$

The normal maximum deflection due to the Sun is 1.75 arcseconds and is found by integrating from $-\infty$ to ∞ . The extra deflection acquired when we integrate the new formula from $-\infty$ to ∞ would be $0.91 \cdot 10^{-6}$ arcseconds. This was calculated using values as reported in the physical constants section. This extra deflection is comparable to the error in the deflection due to the error in the physical constants.

Let us see which astronomical objects do yield a significant impact. Using a constant density $M = \rho \frac{4}{3} \pi b^3$ and factoring common terms yields:

$$\hat{\alpha} = \frac{4GM}{bc^2} \left(1 + \frac{\sqrt{\pi}}{8\sqrt{2}} \sqrt{\frac{c^2}{G\rho bL}} \right) \quad (6.32)$$

Thus to find deviations due to CEG, we need to look for galaxies with a low density and light rays with small impact parameters. This is generally the regime of strong lensing. However, caution should also be taken at small impact parameters as the current CEG framework only deviates from Einstein at accelerations smaller than a_0 .

6.1.4 The lens equation

From the previous discussion, it might appear that these deflection angles are incredibly small. For instance we would need a telescope with an effective diameter of 10 kilometers at optical wavelengths to measure the deviation due to CEG. However, the previous calculated angle isn't the full story as we haven't accounted for the fact that the observer does not have to be co-linear with the source nor do source and lens.

This is depicted in figure 6.3. Let $\hat{\alpha}$ be the calculated deflection angle, θ be the observed angle of the image and β be its true angle. The measured deflection angle is related to these

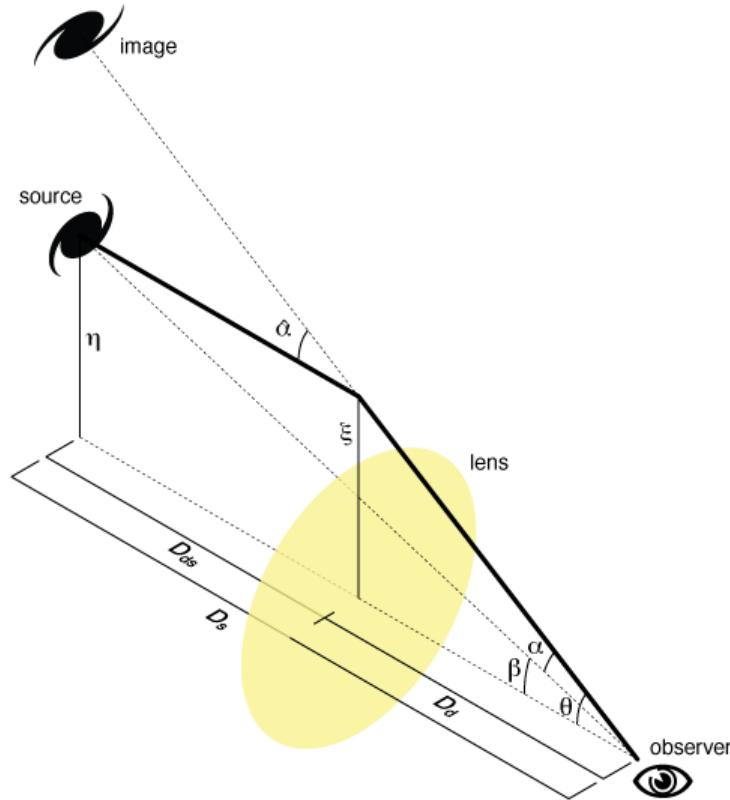


FIGURE 6.3: The geometry of gravitational lensing. The angle θ is the observed angle by the observer, whilst β is the observed angle when the gravitational mass is not present. The angle $\hat{\alpha}$ is the actual deflection angle and α the observed deflection angle. The parameter ξ is the impact parameter, which is denoted in this report by b . The distances are the angular diameter distances. "Michael Sachs." Wikipedia. Wikipedia.org, 6 June 2008, <https://commons.wikimedia.org/wiki/File:Gravitational-lensing-angles.png>. Accessed 30 June 2019.

by: $\alpha = \theta - \beta$. Let us call the vertical distance between source and lens S and between image and lens I . The angular distance between observer and lens is D_d , between source and lens D_{ds} and between source and observer D_s . From the geometry of the image and the fact that we are working with large distances, it follows that:

$$I - S = \theta D_s - \beta D_s \quad I - S = D_{ds} \hat{\alpha} \quad (6.33)$$

Thus we obtain the lens equation:

$$\beta = \theta - \frac{D_{ds}}{D_s} \hat{\alpha} \quad (6.34)$$

As a quick side note, as we are working with angular distances to account for the curvature of space-time between the various objects, the distances do not necessarily add: $D_s \neq D_{ds} + D_d$.

Suppose we now consider again our point source with mass M and a co-linear source lens and image, such that $\beta = 0$. The impact parameter b is then simply $D_d \theta$ and our deflection angle is given by 6.31. This yields a lens equation 6.34 of:

$$0 = \theta - \frac{D_{ds}}{D_d D_s} \frac{4GM}{\theta c^2} - \frac{D_{ds}}{D_d} \pi \sqrt{\frac{GM}{6c^2 L}} \quad (6.35)$$

This is a quadratic equation in θ . For convenience, let us define the Einstein angle and Verlinde angle:

$$\theta_E = \sqrt{\frac{D_{ds}}{D_D D_s} \frac{4GM}{c^2}} \quad \theta_V = \frac{D_{ds}}{D_d} \pi \sqrt{\frac{GM}{6c^2 L}} \quad (6.36)$$

Then the solution to the quadratic equation 6.35 becomes an Einstein-Verlinde ring at an angle:

$$\theta = \frac{\theta_V + \sqrt{\theta_V^2 + 4\theta_E^2}}{2} \quad (6.37)$$

This is a ring around the lens by all the light rays that were sent from the source. The other negative solution is not a true solution to the quadratic equation, as negative angles would also require us to shift $\theta_V \rightarrow -\theta_V$ due to the vector nature of equation 6.29. We obtain using the lens equation 6.34 for non-colinear sources ($\beta \neq 0$) two images at:

$$\theta_{\pm} = \frac{\beta \pm \theta_V \pm \sqrt{(\beta \pm \theta_V)^2 + 4\theta_E^2}}{2} \quad (6.38)$$

We thus see that the Einstein-Verlinde rings are slightly enlarged in comparison to the usual rings.

6.1.5 General lensing systems

For general lensing systems, the situation is a bit more complicated. For instance, when a source is lensed by a galaxy, the image will appear magnified and distorted, just as with a normal non-perfect lens. Two important quantities of such a general lens are its convergence κ and its shear γ . The convergence can be thought of as the power of the lens, thus it describes the focusing of the lens. The shear, is a measure of the distortion of the shape of the source. An often cited example is that circular sources can be distorted into elliptical ones. The convergence κ is clearly related to the mass along the path the light ray takes, whilst the shear is related to how the potential of the current path differs from a nearby light ray's path. In astrophysical situation, both the convergence and shear are calculated by investigating a large number of background sources of light and the way their pattern statistically deviates from a non-distorted shape due to a gravitational lens. It is therefore important to investigate the convergence and shear in CEG. However, this is similar to replacing $2\phi_B$ to $2\phi_B + \phi_D$ in the known formulas for shear and convergence in astrophysics. The theoretical framework for solving for general lensing systems can be found in any book on gravitational lensing or in Sean Carroll's book [5]. For the interested reader, we have provided a summary in appendix C that incorporates CEG.

The results are best summarised in terms of the lensing potential:

$$\psi(\theta) = \frac{D_{ds}}{D_d D_s} \int [\phi_D + 2\phi_B] ds \quad (6.39)$$

The converge then becomes:

$$\kappa(\theta) = \frac{1}{2} \nabla_{\theta}^2 \psi \quad \text{with} \quad \nabla_{\theta} = D_d \nabla_{\perp} \quad (6.40)$$

In order to state the shear, we will use the notational convenience:

$$\psi_{ij} = \frac{\partial^2 \psi}{\partial \theta^i \partial \theta^j} \quad (6.41)$$

If the light rays move along the z -direction, the convergence then becomes $\kappa = \frac{1}{2} [\psi_{11} + \psi_{22}]$. The shear γ in CEG then becomes:

$$\gamma = \pm \sqrt{\gamma_1^2 + \gamma_2^2} \quad \text{with} \quad \gamma_1 = \frac{1}{2} (\psi_{11} - \psi_{22}) \quad \text{and} \quad \gamma_2 = \psi_{12} \quad (6.42)$$

It is clear that the convergence is a measure of the amount of matter along the path of the light ray and the shear a measure of the difference between neighbouring light ray paths. These results could be used to test whether CEG provides an accurate description for the measured bending angle for light rays instead of theories of dark matter. Finally, the magnification M is given by the usual formula:

$$M = \frac{1}{(1 - \kappa)^2 - \gamma^2} \quad (6.43)$$

6.2 Cosmological model

Let us now try to solve for the imposter field u^μ in a more realistic metric; a Robertson Walker metric with zero curvature $\kappa = 0$:

$$g_{\mu\nu} dx^\mu dx^\nu = -dt^2 + f(t)^2 \left(dr^2 + r^2 d\theta^2 + r^2 (\sin \theta)^2 d\phi^2 \right) \quad (6.44)$$

Sabine Hossenfelder [11] already solved for u^μ in an empty Robertson-Walker universe, but we will also solve for the evolution of the imposter field in a matter dominated universe by means of the imposter field equations 5.18. This section is not meant to represent a true cosmological model, but merely to investigate the evolution of the imposter field in the existing cosmological models and the impact this has on the geodesic equations and properties of the space. We will also show that the assumption that the imposter field does not contribute to the modified Einstein equations 5.30 no longer holds in cosmology and that the imposter field may actually yield an important contribution to the evolution of the Hubble parameter in our current dark energy dominated cosmological era.

As Hossenfelder did, we take the comoving ansatz:

$$u_\mu = (u(t), 0, 0, 0) \quad (6.45)$$

This simply states that the density of the imposter field increases/decreases in an expanding universe, which is true for all densities, such as matter, radiation and vacuum densities. Inserting this expression into the strain and stress tensors (equation 5.3) yields for the strain tensor:

$$\epsilon_{\mu\nu} = \begin{bmatrix} 2\dot{u} & 0 & 0 & 0 \\ 0 & -2uf\dot{f} & 0 & 0 \\ 0 & 0 & -2uf\dot{f}r^2 & 0 \\ 0 & 0 & 0 & -2uf\dot{f}r^2(\sin \theta)^2 \end{bmatrix} \quad (6.46)$$

The stress tensor $F_{\mu\nu}$ vanishes. Inserting the expression for the strain and stress tensor into our expression for the imposter scalar field 5.4 and using that $3a + b = 0$ yields:

$$\chi = -\frac{b}{6} \left(2\dot{u} + 6u\frac{\dot{f}}{f} \right)^2 + \frac{b}{2} 4 \left((\dot{u})^2 + 3 \left(u\frac{\dot{f}}{f} \right)^2 \right) \quad (6.47)$$

Simplifying this result and introducing the Hubble parameter as $H = \frac{\dot{f}}{f}$ in equation 6.47 yields:

$$\chi = \left(\frac{4}{3} b \dot{u}^2 - 4 b u \dot{u} H \right) \quad (6.48)$$

We can also solve for our auxiliary tensors in equation 5.17 by inserting our expression of the strain and stress tensor into equation 5.17:

$$B^{\mu 0} = \delta_0^\mu \left(\frac{b}{3} (2\dot{u} + 6uH) + 2b\dot{u} \right) = \delta_0^\mu \left(\frac{8}{3} b \dot{u} + 2buH \right) \quad (6.49)$$

Plugging our imposter scalar field into the imposter field equations 5.18 yields:

$$\boxed{\frac{3\alpha}{4\pi G} \partial_0 \left[\sqrt{\frac{b}{3} \dot{u}^2 - bu\dot{u}H} \left(\frac{4}{3} b \dot{u} + buH \right) \right] = \frac{\beta}{2} \rho} \quad (6.50)$$

These equations are valid whether the Friedman equations apply or not.

To make headway in solving these equations, we assume that the impact of the imposter field on the Einstein equations 5.30 is negligible, such that the Hubble parameter is determined by the Friedman equation:

$$H^2 = \frac{8\pi G}{3} \rho + \frac{\Lambda}{3} \quad (6.51)$$

Before we move on to solving equation 6.50 for the various universes, we can derive some intuitive analytical results for the various densities in our universe. For instance, let ρ be the density of matter in our universe at a certain time t . After a while, space has expanded by a factor $f(t)$. The density thus decreases as $\rho(t) = \rho_0 [f(t)]^{-3}$. This can be stated in terms of the Hubble parameter as $\frac{\dot{\rho}}{\rho} = -3H$.

Actually, from the conservation equations of the baryonic components, it follows that all baryonic densities scale as power laws given by $\rho \propto f^{-n}$ or $\frac{\dot{\rho}}{\rho} = -nH$. We will now move on to solving the evolution equation of the imposter density in various universes.

6.2.1 Vacuum dominated universe

Now we touch upon an important concept. The constants α and β are determined by the current value of the size of the universe $L = \frac{1}{H_0}$. The question is whether we let our constants α and β evolve as H evolves or not. From our earlier analysis, we know that $\frac{\dot{\beta}}{\beta} = 2H_0$. Note that the question whether we let the constants evolve does not matter in a vacuum dominated universe, as $H = H_0$ is constant in such a universe.

In a vacuum dominated universe with cosmological constant Λ , we have $H = H_0$ and $\rho = 0$. The imposter field equations 6.50 then become:

$$0 = \partial_0 \left[\sqrt{\frac{b}{3} \dot{u}^2 - bu\dot{u}H_0} \left(\frac{4}{3} b \dot{u} + buH_0 \right) \right] \quad (6.52)$$

An easy solution to this equation is of course a constant imposter field $u(t) = u_0$ such that $\dot{u} = 0$. Upon integration (introducing the integration constant κ) and squaring, we find:

$$\kappa = \left(\frac{b}{3} \dot{u}^2 - bu\dot{u}H_0 \right) \left(\frac{4}{3} b \dot{u} + buH_0 \right)^2 \quad (6.53)$$

Another interesting solution is provided by $\kappa = 0$ and $\frac{\dot{u}}{u} = -nH$ with $n = 3$. Both solutions make the imposter scalar χ vanish in equation 6.48. Note that the constant solution makes sense. The Hubble constant is fixed and thus the Hubble horizon doesn't move, implying no stress in the medium.

Inserting this solutions into the Einstein equations 5.30 yields no contribution of the Imposter field. As Hossenfelder also noted, the only way for the imposter field u^μ to make a contribution in a vacuum dominated universe is by adding a mass term to the Lagrangian [11]. At the very least, it is comforting to see that the field equations for the imposter field have a constant solution in the case that it should be constant according to EG.

6.2.2 Matter dominated universe

In a matter dominated universe, the Hubble parameter varies as $H = \frac{1}{t}$. It is not clear what the constants α and β should be, as no vacuum energy is present and the Hubble parameter varies with time. However, we will still assume that $\frac{\beta}{\alpha} = 2H_0$. Substituting our choice into the imposter field equation 6.50, we find that:

$$\left(-\frac{1}{2H_0 t} + \kappa\right) = \sqrt{\frac{b}{3}\dot{u}^2 - bu\dot{u}\frac{1}{t}} \left(\frac{4}{3}b\dot{u} + bu\frac{1}{t}\right) \quad (6.54)$$

Again, easy solutions are found when the integration constant $\kappa = 0$. We assume that $b = -4$ from our Newtonian discussion in CEG. This yields the more instructive solution:

$$u = -\left(\frac{3}{20}\right)^{\frac{3}{4}} \left(\frac{t}{H_0}\right)^{\frac{1}{2}}, \quad n = -\frac{1}{2} \quad (6.55)$$

Inserting this back into our expression for the scalar field 6.48, we find that:

$$\chi = \frac{1}{H_0 \sqrt{\frac{20}{3}} t} \quad (6.56)$$

Note that $\chi \sim \frac{H}{H_0}$. We find that we can only ignore the contribution of the imposter field to the modified Einstein equations (5.30) when the density ρ has the property that $G\rho \gg H^{\frac{3}{2}} H_0^{\frac{1}{2}}$. In our matter-dominated universe, the matter density is estimated to satisfy $G\rho \sim H^2$. We thus see that our initial assumption that we can ignore the contribution of the imposter field to the Einstein equations is only valid when $H \gg H_0$ or simply times much smaller than the age of our universe.

The physical interpretation of the fact that u (the one with the upstairs indices) is increasing is as follows. We know that when we introduce matter to our De Sitter space, the entropy content of our universe decreases due to the fact that the size of our universe went from $L \rightarrow L + u(L)$. As time moves on, the baryonic density $\rho \sim t^{-2}$ decreases. This causes the size of our universe to slowly return to its initial size $L = \frac{1}{H_0}$, which is similar to a positive shift $u^0 = -u(t)$.

If we were to combine both the vacuum-dominated and matter-dominated universe solutions, we see that for early times ($H \gg H_0$ when matter/radiation dominates), the imposter field $u \sim \sqrt{t}$. For later times $H \sim H_0$, the imposter field becomes a constant.

6.2.3 Effective metric

If one is able to solve for the imposter field in an FLR-metric using the imposter field equations 5.18 and the modified Einstein equations 5.30, then the following procedure shows the effects of this imposter field.

According to the previous solutions, the effective metric will be of the form:

$$\widetilde{g}_{\mu\nu} dx^\mu dx^\nu = -(1 + \beta u) dt^2 + f(t)^2 \left(dr^2 + r^2 d\theta^2 + r^2 (\sin \theta)^2 d\phi^2 \right) \quad (6.57)$$

This can be transformed back into a Robertson-Walker metric using the transformation $(dt^*)^2 = (1 + \beta u) dt^2$ or $t^* = \int \sqrt{1 + \beta u} dt$. We thus recover an effective metric of the form:

$$\widetilde{g}_{\mu\nu} dx^\mu dx^\nu = -(dt^*)^2 + f[t(t^*)]^2 \left(dr^2 + r^2 d\theta^2 + r^2 (\sin \theta)^2 d\phi^2 \right) \quad \text{with} \quad t^* = \int \sqrt{1 + \beta u(t)} dt \quad (6.58)$$

Thus we see that the effect of the imposter field is to modify the evolution of the scale factor. The scale factor may also be further changed through the modified Einstein equations 5.30. For the vacuum-dominated universe, it is obvious that the constant imposter field solution does not alter the dynamics of space-time as t^* and t have a constant ratio.

In case of the matter-dominated universe, we find that $t^* \sim t^{\frac{5}{4}}$. From our analysis, we know that in a matter-dominated universe, $f(t) \sim t^{\frac{2}{3}}$. Thus we see that $f(t^*) \sim [t^*]^{\frac{8}{15}}$. As $\frac{2}{3} \geq \frac{8}{15}$, we see that the effect of the imposter field is thus to decrease the expansion of space and thus the redshift of light in the early universe $H \gg H_0$. In this new coordinate system, the Hubble parameter $H(t^*) \sim \left[\frac{1}{t^*} \right]^{\frac{4}{5}}$.

Actually integrating and solving for t^* in equation 6.58 yields:

$$t^* = \frac{4}{5} \left(\frac{3}{20} \right)^{\frac{1}{8}} \left(\frac{3H_0}{5} \right)^{\frac{1}{4}} t^{\frac{5}{4}}, \quad H(t^*) = \left(\frac{20}{3} \right)^{\frac{1}{10}} \left(\frac{5}{3H_0} \right)^{\frac{1}{5}} \left(\frac{5}{4t^*} \right)^{\frac{4}{5}} \quad (6.59)$$

Of course, we can again calculate the age of the universe by setting $H(t^*) = H_0$, which yields an age of $14.7 \cdot 10^9$ years, which is slightly older than the age of our universe using current models of $13.2 \cdot 10^9$ years. However, as we assumed $H \ll H_0$ in our matter-dominated universe, this is of course not a true representation of the age but just an estimate. A full solution for a cosmological model can be obtained by numerically integrating the field equations 6.50 together with the modification the imposter field makes to the Einstein equations 5.30.

Caution should however be taken. Remember that we chose the constants a, b, d in equation 5.4 in order to make a constant solution for the imposter field possible, a.k.a. Hossenfelder's way of fixing the constants. This is not a problem because at present no other way is known to fix these constants and all we are now saying is that there exists a set of constants such that a constant solution is possible.

Chapter 7 ● ■ ▲

Fourier-Bessel methods & results

In this chapter we will provide the numerical framework which we will use to solve gravitational problems in MOND and CEG. Firstly, we will develop a numerical method that can be used to solve the non-linear differential equation for the imposter potential (5.43). The methods we will develop are applicable to cylindrical matter density distributions and will make use of an iterative algorithm with Bessel and Fourier transformations to solve the non-linear differential equations. This methods could also be used to solve for the potentials in MOND. As not much research has gone into numerical methods to solve for the MOND equations, this makes the developed numerical methods interesting beyond the context of CEG.

We will apply our developed algorithm to both a spherical case (the sun) as on galaxy NGC6503. Both cases will be used to analyse the effectiveness of the algorithm.

7th

7.1 Theoretical Summary

In this section we provide a theoretical summary of the theory that we will test numerically. For a full description of CEG, we recommend the relevant section in the theoretical chapter. We will also introduce another theory, MOND, which is a rival theory to CEG that makes similar predictions.

In the preceding chapters we found that matter in CEG feels an additional force next to the gravitational force. This force will be called the dark force and will have a potential ϕ_D . The normal gravitational force will have a potential ϕ_B with the B of baryonic matter. The resulting force on a particle in the Newtonian approximation would simply be the sum of these forces. Thus the particles in our model obey:

$$F_{net} = -m\nabla\phi_D - m\nabla\phi_B \quad (7.1)$$

These potentials satisfy the following differential equations:

$$\boxed{\nabla^2\phi_B = 4\pi G\rho \quad \text{and} \quad \nabla \cdot (|\nabla\phi_D|\nabla\phi_D) = \frac{a_0}{6} 4\pi G\rho} \quad (7.2)$$

The non-linear differential equation for ϕ_D will be solved using the numerical algorithm we will develop in the next sections.

The important prediction of CEG was that the speed of the stars and gas in galaxies would become a constant far away from the center. A graph of the speed of these components is called a rotation curve. In the theoretical chapter (equation 5.36), it was found that the dark potential ϕ_D would lead to a velocity contribution to the rotation curves that only depends on

the mass M of the galaxy as:

$$V_{\text{dark}} = \left(\frac{GMa_0}{6} \right)^{\frac{1}{4}} \quad (7.3)$$

These equations completely determine the path of non-relativistic particle in the Newtonian approximation and are all that we need from the theoretical section on CEG.

The predictions of CEG are similar to those of Modified Newtonian Dynamics (MOND). This is a theory invented by Mordehai Milgrom [2] to explain why the rotation curves of galaxies tend to flatten when the acceleration drops below $a_m = 1.2 \cdot 10^{-10} \text{ ms}^{-2}$. This constant is usually called a_0 , but that name is already reserved in CEG with the approximate relation $a_0 \approx 6 a_m$. Like CEG, MOND also has a relativistic formulation called Tensor-Vector-Scalar gravity (TeVeS) [3], which was developed by Jacob Bekenstein in 2004.

In MOND there is only one potential, which we will call ϕ_m . This potential satisfies the equation:

$$\nabla \cdot \left(\mu \left(\frac{|\nabla \phi_m|}{a_m} \right) \nabla \phi_m \right) = 4\pi G \rho \quad (7.4)$$

The interpolation function $\mu(x)$ is chosen such that when the acceleration is much larger than a_m , $\mu(x) \rightarrow 1$, such that $\phi_m = \phi_B$ to mimic Newtonian behaviour at high accelerations. At accelerations much smaller than a_m , the function is chosen such that $\mu(x) \rightarrow x$, mimicking the behaviour of the dark potential. A common choice for the interpolating function is the standard interpolating function:

$$\mu(x) = \frac{x}{\sqrt{1+x^2}} \quad (7.5)$$

It is clear that for $x \rightarrow 0$, $\mu(x) \rightarrow x$, such that the defining equation for the potential ϕ_m in MOND (equation 7.4) becomes similar to the equation for the dark potential ϕ_D in equation 7.2 with the approximate relation $a_m = \frac{a_0}{6}$. This implies that the flat part of the rotation curves in MOND become:

$$v_{\text{flat}} = (GMa_m)^{\frac{1}{4}} \quad (7.6)$$

It is clear that both MOND and CEG predict similar behaviours in the regimes in which the acceleration is much larger than a_0 or much smaller. An important test would be to test their behaviours in the intermediary region. This region coincides with the measurements of the rotation curves of 175 galaxies done by the SPARC project [15]. We will thus compare the two theories against the observations. This will be done in the next chapter. First we will introduce the numerical method developed during this project to solve for the potentials ϕ_B and ϕ_D in cases that the baryonic density is known.

7.2 Numerical baryonic potential

Before stating the numerical methods we use, we would like to note the following: The transformation laws and the numerical algorithm to solve for the dark and baryonic potential were mainly developed by my supervisor Dr. P. M. Visser during this project and I claim no ownership over the results of this section.

7.2.1 Fourier-Bessel transform for scalars

Let us first solve for the baryonic potential ϕ_B in equation 7.2, as this is the easiest of the pair. There are several ways to solve for the baryonic potential ϕ_B using equation 7.2 otherwise known as Poisson's equation. A subset of these methods include Bessel functions, Green's

function and Fourier transforms. One of the most common methods is to use the three dimensional Fourier transform:

$$\mathcal{F}(\phi) = \iiint \phi(\mathbf{r})e^{-i\mathbf{r}\cdot\mathbf{k}}d^3\mathbf{r} \quad (7.7)$$

If we then Fourier transform Poisson's equation 7.2, we obtain the following equation for the Fourier transform:

$$\mathcal{F}(\nabla^2\phi_B) = 4\pi G\mathcal{F}(\rho) \implies -(k_x^2 + k_y^2 + k_z^2)\mathcal{F}(\phi_B) = 4\pi G\mathcal{F}(\rho) \quad (7.8)$$

This yields the straightforward solution:

$$\mathcal{F}(\phi_B) = -\frac{4\pi G\mathcal{F}(\rho)}{(k_x^2 + k_y^2 + k_z^2)} \quad (k \neq 0) \quad (7.9)$$

We are thus able to convert differential equations in the spatial domain to algebraic equations in the Fourier domain. Inverting this transform then yields the baryonic potential corresponding to that specific density. Such a method however requires a lot of computational memory, as we will show next. If we were to choose a three dimensional grid with size $N \times N \times N$, our Fourier transforms would also be of size N^3 . For instance, if we take a grid with $N = 1000$ points along each dimension, then our Fourier transform would take up 1GB of memory if we count each entry as a bit, which is a severe underestimation. Nonetheless, we also tested this method in the numerical results section next to the method we will develop next.

Since the three dimensional Fourier transform would prove to be too computationally heavy, we can make use of the symmetries we have in our system. Suppose we are working in a two dimensional world in which we will be using polar coordinates (r, θ) and let $f(r, \theta) = f(r)$ be a circular symmetric function. Then the two dimensional Fourier transform of $f(r)$ is:

$$\mathcal{F}[f(\mathbf{r})] = \iint f(\mathbf{r})e^{-i\mathbf{r}\cdot\mathbf{k}}d^2\mathbf{r} \quad (7.10)$$

Transforming to polar coordinates and picking a system such that the \mathbf{k} -vector lies on the $\theta = 0$ axis, we find that:

$$\mathcal{F}[f(\mathbf{r})](\mathbf{k}) = \int_0^\infty \int_0^{2\pi} f(r)e^{-irk\cos\theta} r d\theta dr = 2\pi \int_0^\infty f(r)r J_0(kr) dr \quad (7.11)$$

By using the symmetry of our function f , we have turned a two dimensional Fourier transform into a one dimensional Hankel transform. For three-dimensional functions with cylindrical symmetry, we can do the same trick. Let us choose cylindrical coordinates r, θ, z and a density function ρ that is cylindrical symmetric $\rho(r, \theta, z) = \rho(r, z)$. Using the previous result, the three dimensional Fourier transform of a cylindrical symmetric function $\rho(r, z)$ is equivalent to the two dimensional Fourier-Bessel transform:

$$\mathcal{F}[\rho(r, z)](k, \ell) = 2\pi \int_{-\infty}^\infty \int_0^\infty \rho(r, z)r J_0(kr) e^{-i\ell z} dr dz \quad (7.12)$$

We have found a different way of solving the Poisson equation 7.2 for cylindrical symmetric potentials. Instead of using a three dimensional Fourier transform, we will use a two dimensional Fourier-Bessel transform. This allows us to calculate the gravitational potential on a large grid without taking up too much memory. We will indicate the transformation of a function $f(r, z)$ by the Fourier-Bessel transformation simply by $\tilde{f}(k, \ell)$ and it satisfies the

transformation rules:

$$f(r, z) = \int_0^\infty \int_{-\infty}^\infty k J_0(kr) e^{i\ell z} \tilde{f}(k, \ell) d\ell dk \quad (7.13)$$

$$\tilde{f}(k, \ell) = \frac{1}{2\pi} \int_0^\infty \int_{-\infty}^\infty r J_0(kr) e^{-i\ell z} f(r, z) dz dr \quad (7.14)$$

In an analogous fashion, we can now calculate the Fourier-Bessel transformation of the Laplace operator:

$$\widetilde{\nabla^2 \phi} = (-k^2 - \ell^2) \tilde{\phi}(k, \ell) \quad (7.15)$$

This again allows us to solve for the baryonic potential ϕ_B using equations 7.12, 7.14 and 7.15:

$$\tilde{\phi}_B(k, \ell) = \frac{-4\pi G}{k^2 + \ell^2} \tilde{\rho}(k, \ell) \quad (7.16)$$

These results are all very similar to their 3D Fourier counterpart. We are now able to solve for the baryonic potential using the Fourier-Bessel transformation (equation 7.12). However, if we also want to solve for the dark potential ϕ_D in equation 7.2, we will need a bit more machinery. For instance, we will see that the Fourier-Bessel transform of vectors isn't quite as simple as its scalar counterpart.

7.2.2 Bessel-Fourier transform of vectors

We will now look at the Fourier-Bessel transformation of vectors. Since our density will have cylindrical symmetry, so will all our relevant vectors. Thus we can write a vector and its Fourier-Bessel transform as:

$$\mathbf{F}(r, z) = \hat{\mathbf{r}} F_1(r, z) + \hat{\mathbf{z}} F_2(r, z) \quad (7.17)$$

$$\tilde{\mathbf{F}}(k, \ell) = \hat{\mathbf{r}} \tilde{F}_1(k, \ell) + \hat{\mathbf{z}} \tilde{F}_2(k, \ell) \quad (7.18)$$

The following set of vector transformation laws were proposed by my supervisor Dr. P. M. Visser:

$$\mathbf{F}(r, z) = \int_0^\infty \int_{-\infty}^\infty \left[\hat{\mathbf{r}} i J_1(kr) \tilde{F}_1(k, \ell) + \hat{\mathbf{z}} J_0(kr) \tilde{F}_2(k, \ell) \right] k e^{i\ell z} d\ell dk \quad (7.19)$$

$$\tilde{\mathbf{F}}(k, \ell) = \frac{1}{2\pi} \int_0^\infty \int_{-\infty}^\infty \left[-\hat{\mathbf{r}} i J_1(kr) F_1(r, z) + \hat{\mathbf{z}} J_0(kr) F_2(r, z) \right] r e^{-i\ell z} dz dr \quad (7.20)$$

These transformations are conjugate symmetric (up to a factor of 2π). A curious reader might now wonder why we would use J_1 instead of J_0 for the radial transformation. The reason for this, is that we want the derivatives of the transform to be of the same form as the transform itself. Otherwise, we would not be able to use them on an equation such as the non-linear differential equation for ϕ_D in 7.2. If we had just used J_0 , the derivative of J_0 would be J_1 and we would not be able to relate this derivative of the transformation back to our original transformation. This issue was not present in the scalar case, as the unwanted terms exactly cancel for the second derivative.

We will now compute the divergence and curl of a vector field in terms of these transformations in order to solve the non-linear differential equation 7.2. But, let us first state several important identities of the Bessel functions:

$$J_1' + \frac{J_1}{x} = J_0 \quad \text{and} \quad J_0' = -J_1 \quad (7.21)$$

Using these identities and the transformation laws proposed in 7.20, one can show that the divergence of a vector field satisfies:

$$-i \nabla \cdot \mathbf{F} = \int_0^\infty \int_{-\infty}^\infty \left(k \tilde{F}_1 + \ell \tilde{F}_2 \right) k J_0(kr) e^{i\ell z} d\ell dk \quad (7.22)$$

Since the gradient is a scalar, this is simply the transformation rule (equation 7.14) for a scalar in terms of its vector components in the Fourier-Bessel domain:

$$\widehat{-i \nabla \cdot \mathbf{F}} = k \tilde{F}_1 + \ell \tilde{F}_2 \quad (7.23)$$

Similarly, one can find the transformation of the curl of a vector:

$$-i \nabla \times \mathbf{F} = \hat{\theta} \int_0^\infty \int_{-\infty}^\infty \left(k \tilde{F}_2 - \ell \tilde{F}_1 \right) k J_1(kr) e^{i\ell z} d\ell dk \quad (7.24)$$

This expression is not directly related to any of the transformations we have discussed before due to the $\hat{\theta}$ component. This will not bother us however, as we will only need the transformation of the gradient. Now that we know the transformation rules for vectors, we can finally attempt to solve the non-linear differential equation for the dark potential.

7.3 Numerical dark potential

A common way to solve a non-linear differential equation such as 7.2, is by starting with a trial solution and using an iterative algorithm. We will use our newly found transformation rules for the Fourier-Bessel transform to construct such an iterative algorithm for ϕ_D , but first let us think of a trail solution. Instead of working with the dark potential, let us define a new dark vector \mathbf{F} :

$$\mathbf{F} := |\nabla \phi_D| \nabla \phi_D \quad \implies \quad \nabla \cdot \mathbf{F} = \frac{a_0}{6} 4\pi G \rho \quad (7.25)$$

The implication follows from equation 7.2.

If we are able to solve for \mathbf{F} , we can find the gradient of the dark potential from the inverse relation:

$$\nabla \phi_D = \frac{1}{\sqrt{|\mathbf{F}|}} \mathbf{F} \quad (7.26)$$

Thus our main goal will be to solve for \mathbf{F} such that it satisfies 7.25. Right from the start, a great trial solution would be to use the gravitational field vector $\mathbf{g} = -\nabla \phi_B$, since this vector already satisfies the equation $\nabla \cdot \mathbf{g} = -4\pi G \rho$ by Poisson's equation 7.2. We therefore propose to start our iterative algorithm with the trail solution:

$$\mathbf{F}_0 = -\frac{a_0}{6} \mathbf{g} \quad (7.27)$$

In fact for spherical symmetric distributions, this would already be the exact solution. One can check that equation 7.26 is indeed the same solution that we found in equation 5.27 for a spherical symmetric distribution.

However, in general this might not be the true solution for \mathbf{F} . This is because the right-hand side of equation 7.26 might not be a true gradient, as it might still have a non-zero curl. We should create a new vector \mathbf{F}_1 from \mathbf{F}_0 , such that equation 7.26 yields a true potential for \mathbf{F}_1 . This can be easily done by only keeping the divergence part of $\frac{1}{\sqrt{|\mathbf{F}|}} \mathbf{F}$.

However, when we only keep the divergence part, we face the new problem that this new vector would not necessarily satisfy its defining equation 7.25. Thus we create a new vector \mathbf{F}_2 from \mathbf{F}_1 such that it satisfies equation 7.25 etc. It is clear that we are going in circles, but hopefully for our uses, we can develop an iterative algorithm that converges. The aim of the algorithm is thus to let the vector \mathbf{F} both satisfy its defining equation (7.25) as to make sure that equation 7.26 is a true potential.

Before we lay out the algorithm, let's first remind ourselves of an important theorem in Analysis: Helmholtz theorem. Helmholtz theorem states that any vector field \mathbf{F} satisfying certain well behaved boundary conditions can be decomposed into a part with zero curl and a part with zero divergence as:

$$\mathbf{F} = \nabla\phi + \nabla \times \mathbf{A} \quad (7.28)$$

In which ϕ is a scalar function called the potential and $\nabla \times \mathbf{A}$ is called the magnetic part, which we will denote by $\mathbf{B} := \nabla \times \mathbf{A}$ and \mathbf{A} is called a vector potential. In practice, all vector fields that we are interested in satisfy these boundary conditions as it was shown by Milgrom and Bekenstein [2] that for finite bodies the magnetic part decreases faster with radius r as $\frac{1}{r^3}$ and the decrease of $\nabla\phi$ for finite bodies goes as $\frac{1}{r^2}$ or faster. The gradient of the potential and magnetic part are uniquely specified by respectively the divergence of \mathbf{F} and the curl of \mathbf{F} .

Since we know that the divergence of \mathbf{F} is up to a constant equal to the divergence of the gravitational field vector \mathbf{g} by equation 7.25, we can actually solve for the divergence part of \mathbf{F} . Since the gravitational field vector has zero curl, we find using equation 7.25 and Helmholtz theorem, that we can always write:

$$\mathbf{F} = -\frac{a_0}{6}\mathbf{g} + \mathbf{B} \quad (7.29)$$

This will always be our base equation to satisfy, along with finding a true potential in equation 7.26. For cases of high symmetry, such as spherical, cylindrical or planar, the magnetic field vanishes. This is easy to show using a Gaussian surface to solve for equation 7.2.

7.3.1 The Fourier-Bessel method for the dark potential

It is time to introduce the algorithm. In order to keep the following discussion clear, we have included a table 7.1 with the name of each vector, the equation it satisfies and its use. We have also included a figure 7.1 which can be read alongside the following discussion. The main aim of the algorithm is to keep removing unwanted aspect of vectors in the Fourier-Bessel domain such as their divergence or curl.

Name	Symbol	Def.	Use
Gravitational contr.	\mathbf{g}	$\mathbf{g} = \nabla\phi_B$	In 7.29
Dark vector	\mathbf{F}	$\mathbf{F} = \nabla\phi_D \nabla\phi_D$	$\mathbf{F} = -\frac{a_0}{6}\mathbf{g} + \mathbf{B}$
Magnetic contr.	\mathbf{B}	$\mathbf{B} = \mathbf{F} + \frac{a_0}{6}\mathbf{g}$	In 7.29
Dark potential vector	\mathbf{f}	$\mathbf{f} = \frac{\mathbf{F}}{\sqrt{ \mathbf{F} }}$	$\mathbf{f} = \nabla\phi_D$

TABLE 7.1: Table showing the definitions of the various vectors used in the Fourier-Bessel method

We will use the same initial solution as discussed earlier. Once we have solved for the bright potential using Fourier-Bessel transformations, we can calculate the gravitation field vector

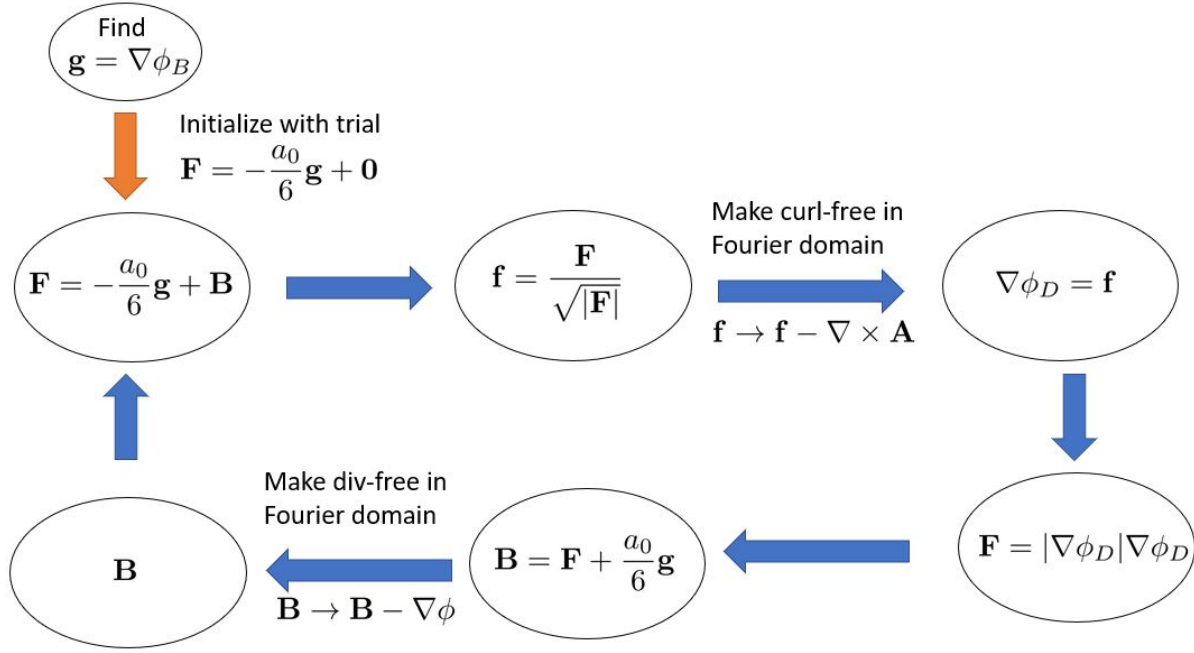


FIGURE 7.1: Illustration of the Fourier-Bessel method.

\mathbf{g} . Thus we will start with our trail solution:

$$\mathbf{F}_0 = -\frac{a_0}{6}\mathbf{g} \quad (7.30)$$

Our trial solution is simply the vector \mathbf{F} with zero magnetic component in equation 7.29. From this vector we can construct a new vector according to right-hand side of equation 7.26:

$$\mathbf{f}_0 = \frac{1}{\sqrt{|\mathbf{F}_0|}} \mathbf{F}_0 \quad (7.31)$$

Again, from Helmholtz theorem we know that we can write \mathbf{f}_0 as the sum of a potential and magnetic part:

$$\mathbf{f}_0 = \nabla\phi_0 + \nabla \times \mathbf{A} \quad (7.32)$$

We are only interested in the potential part by equation 7.26. If we were able to remove the magnetic part from this vector \mathbf{f}_0 , we would obtain a true potential and would indeed satisfy equation 7.26. We can remove unwanted components using our Fourier-Bessel transform. We will now show how one can obtain just the divergence part of 7.32. This is repeatedly done in the following way:

We know that the divergence of the curl part in equation 7.32 is zero, thus:

$$\nabla \cdot \mathbf{f}_0 = \nabla^2 \phi_0 \quad (7.33)$$

We can solve for the potential by Fourier-Bessel transforming both sides, which yields using equation 7.15 and 7.23:

$$\tilde{\phi}_0(k, \ell) = \frac{1}{i(k^2 + \ell^2)} \left(k\tilde{f}_1 + \ell\tilde{f}_2 \right) \quad (7.34)$$

In which the 1 and 2 indicate the components of the transform of \mathbf{f}_0 . Inverting this transform yields the divergence part of \mathbf{f}_0 in equation 7.32.

Thus we now satisfy equation 7.26 with our new $\mathbf{f}_0 \rightarrow \nabla\phi_0$. However, we also need to check whether we still satisfy our base equation 7.29. This is done by reconstructing \mathbf{f} and \mathbf{F} by:

$$\mathbf{f}_1 = \nabla\phi_0 \quad \text{and} \quad \mathbf{F}_1 = |\mathbf{f}_1| \mathbf{f}_1 \quad (7.35)$$

We can then check whether we satisfy our base equation 7.29 by checking whether \mathbf{B} is a true magnetic field with zero divergence. We find this vector from 7.29 by:

$$\mathbf{B}_1 = \mathbf{F}_1 + \frac{a_0}{6} \mathbf{g} \quad (7.36)$$

To check whether this is a true magnetic field, we solve for its potential using the same trick as before:

$$\nabla \cdot \mathbf{B}_1 = \nabla^2 \phi \quad (7.37)$$

If this is zero, we can stop and we have found our previous solution for \mathbf{F} was correct. If not, we find this potential using our Fourier-Bessel transform:

$$\tilde{\phi}(k, \ell) = \frac{1}{i(k^2 + \ell^2)} \left(k \tilde{B}_1 + \ell \tilde{B}_2 \right) \quad (7.38)$$

In which the 1 and 2 denote the components of the Fourier-Bessel transform of \mathbf{B}_1 . We then subtract the gradient of this potential from our magnetic field, to find a true magnetic field:

$$\mathbf{B}_2 = \mathbf{B}_1 - \nabla\phi \quad (7.39)$$

We now know that we satisfy our base equation 7.29 since this is a true magnetic field. From this magnetic field, we can again construct \mathbf{F} by using our base equation 7.29:

$$\mathbf{F}_3 = -\frac{a_0}{6} \mathbf{g} + \mathbf{B}_2 \quad (7.40)$$

However, we find ourselves where we started. We have a certain \mathbf{F} that satisfies our base equation 7.29, but we do not know whether equation 7.26 yields a true potential. Thus we repeat the same algorithm over again until we have converged to a solution that satisfies both equation 7.29 and equation 7.26.

Thus our algorithm consists of 9 steps:

1. Initialize with the trail vector for \mathbf{F} :

$$\mathbf{F} = -\frac{a_0}{6} \mathbf{g} \quad (7.41)$$

2. Construct the vector \mathbf{f} :

$$\mathbf{f} = \frac{1}{\sqrt{|\mathbf{F}|}} \mathbf{F} \quad (7.42)$$

3. Find the potential part $\nabla\phi$ of \mathbf{f} by solving for ϕ in the Fourier-Bessel domain:

$$\tilde{\phi}(k, \ell) = \frac{1}{i(k^2 + \ell^2)} \left(k \tilde{f}_1 + \ell \tilde{f}_2 \right) \quad (7.43)$$

4. Construct the new vectors \mathbf{f} and \mathbf{F} :

$$\mathbf{f} \rightarrow \nabla\phi \quad \text{and} \quad \mathbf{F} = |\mathbf{f}| \mathbf{f} \quad (7.44)$$

5. Construct the magnetic field \mathbf{B} from:

$$\mathbf{B} = \mathbf{F} + \frac{a_0}{6} \mathbf{g} \quad (7.45)$$

6. Solve for the potential part $\nabla\phi$ of this magnetic field using the Fourier-Bessel transform:

$$\widetilde{\phi}(k, \ell) = \frac{1}{i(k^2 + \ell^2)} \left(k\widetilde{B}_1 + \ell\widetilde{B}_2 \right) \quad (7.46)$$

7. Construct a new magnetic field without the divergence part:

$$\mathbf{B} \rightarrow \mathbf{B} - \nabla\phi \quad (7.47)$$

8. The new trail function for \mathbf{F} will be:

$$\mathbf{F} = -\frac{a_0}{6} \mathbf{g} + \mathbf{B} \quad (7.48)$$

9. Go to step 2

This loop continuous until the magnetic field \mathbf{B} has converged. The potential of the final vector \mathbf{f} is then our dark potential ϕ_D . We will test our algorithm by applying it to the case of a spherical density, for which it is known that the magnetic field vanishes.

From the bright potential ϕ_B and dark potential ϕ_D we can calculate the tangential velocity by using the net force law (equation 7.1) and the approximation that stars move in nearly circular orbits, such that $|\mathbf{F}_{net}| = m \frac{|v|^2}{r}$ according to the centripetal law.

7.3.2 Altered Fourier-Bessel method for the dark potential

We will also present an altered version of this algorithm and test this altered version against the previously introduced version. The aim of this altered version is to avoid using the vector transformation laws and to only use the scalar transformation laws. Such an alteration only requires an easy change to our algorithm. For instance, in equation 7.33, we solved for the divergence of \mathbf{f} in the Fourier-Bessel domain. This was done by first transforming \mathbf{f} into the Fourier-Bessel domain using vector transformation laws and subsequently calculating the divergence in this frequency domain. This is shown on the right hand side of equation 7.34. Thus we first convert a vector into the frequency domain and then convert it into a scalar.

However, we can also simply first calculate the divergence $\nabla \cdot \mathbf{f}$ in the spatial domain such that we only have to transform a scalar. Subsequently, we transform this scalar into the Fourier-Bessel domain. Thus instead of solving equation 7.34, we solve the equation:

$$\widetilde{\phi}(k, \ell) = \frac{-1}{k^2 + \ell^2} \widetilde{\nabla \cdot \mathbf{f}}(k, \ell) \quad (7.49)$$

In which we have already solved for $\nabla \cdot \mathbf{f}$ in the spatial domain such that we only have to transform scalars. A similar change can be applied to calculating the divergence component of the magnetic contribution. Such a change allows us to only transform scalars, reducing the complexity of the algorithm and the need for the vector transformation laws. The alterations only affect steps 3 and steps 6 of the algorithm with the substitutions $(k\widetilde{f}_1 + \ell\widetilde{f}_2) \rightarrow -i\widetilde{\nabla \cdot \mathbf{f}}(k, \ell)$ and $(k\widetilde{B}_1 + \ell\widetilde{B}_2) \rightarrow -i\widetilde{\nabla \cdot \mathbf{B}}(k, \ell)$ using equation 7.23. This is effectively doing nothing but

it allows us to calculate $\nabla \cdot \mathbf{f}$ in the spatial domain and then convert to the Fourier-Bessel domain instead of calculating the Fourier-Bessel vector components \tilde{f}_1 and \tilde{f}_2 using 7.20.

7.3.3 Software and Implementation

We have implemented the software into Matlab R2018b as we had to work with large matrices and matrix multiplications. The Fourier transforms were done using the FFT algorithm already present in Matlab. No such algorithm exists in Matlab for the Bessel transformations. The Bessel transformations are therefore done by using the quasi-discrete Hankel transform developed by Guizar-Sicairos and Gutiérrez-Vega [10] for solving field propagation problems in optics. This transform was implemented by Chouinard and Baddour [1] into Matlab.

7.4 Testing the numerical algorithm; Spherical symmetric case

7.4.1 Numerical bright potential

In this section we present the results of the numerical algorithm as applied to the Sun. We will use the symbols M_\odot for the solar mass and R_\odot for the solar radius. The true solution for the baryonic gravitational force in the plane $z = 0$ is:

$$\mathbf{g}_{\text{bar}}(r, 0) = \begin{cases} -\frac{GM_\odot}{r^2} \hat{\mathbf{r}} & \text{for } r \geq R_\odot \\ -\frac{GM_\odot r}{R_\odot^3} \hat{\mathbf{r}} & \text{for } r \leq R_\odot \end{cases} \quad (7.50)$$

The analytical and numerical solution for g_{bar} and V_{bar} for the Sun are plotted for a grid with maximum grid radius of $10R_\odot$ and $100R_\odot$ in figure 7.2 and 7.3 respectively. Both use a grid with twice as many points in the z -direction, such that the maximum z -value coincides with the maximum r -value. For both figures a grid of size 8000×4000 was used. The numerical solutions are indistinguishable upon visual inspection from the analytical solutions except for at the boundary. Such boundary effects are expected for Fourier transforms and Bessel transforms as both have to cover a jump discontinuity at the boundary with a finite sum of continuous functions. The boundary effects are almost unnoticeable in g_{bar} , but can be easily identified in the velocity graphs.

Despite diverging at the boundaries, the analytical and numerical solution are in good agreement with a RMS value for the error of 0.3103 for the solution at a maximum radius of $10R_\odot$. The numerical solution is however always larger than the analytical one making the error not uniformly distributed. This is further quantified by a rejection based at a 5% significance level from both a χ^2 and Kolmogorov-Smirnov test between the numerical and analytical gravitational potentials.

We will also test the Fourier-Bessel method against a 3D Fourier based method using the same ideas as in the Fourier-Bessel method. This is done in figure 7.4 for the Sun, on a grid of size $400 \times 400 \times 400$ for the 3D Fourier method and a grid with size 400×200 for the Fourier-Bessel method. For numerical calculations, both the Fourier method and Fourier-Bessel method yield accurate results with a rms value of 5.3486 for the Fourier method and a rms value of 0.9941 for the Fourier-Bessel method. However, the Bessel method calculated velocities are in much better agreement with the analytical velocities with a rms value of $1.0110 \cdot 10^4$, whilst the Fourier method had a rms value of $3.2196 \cdot 10^4$ with the main error coming from boundary effects.

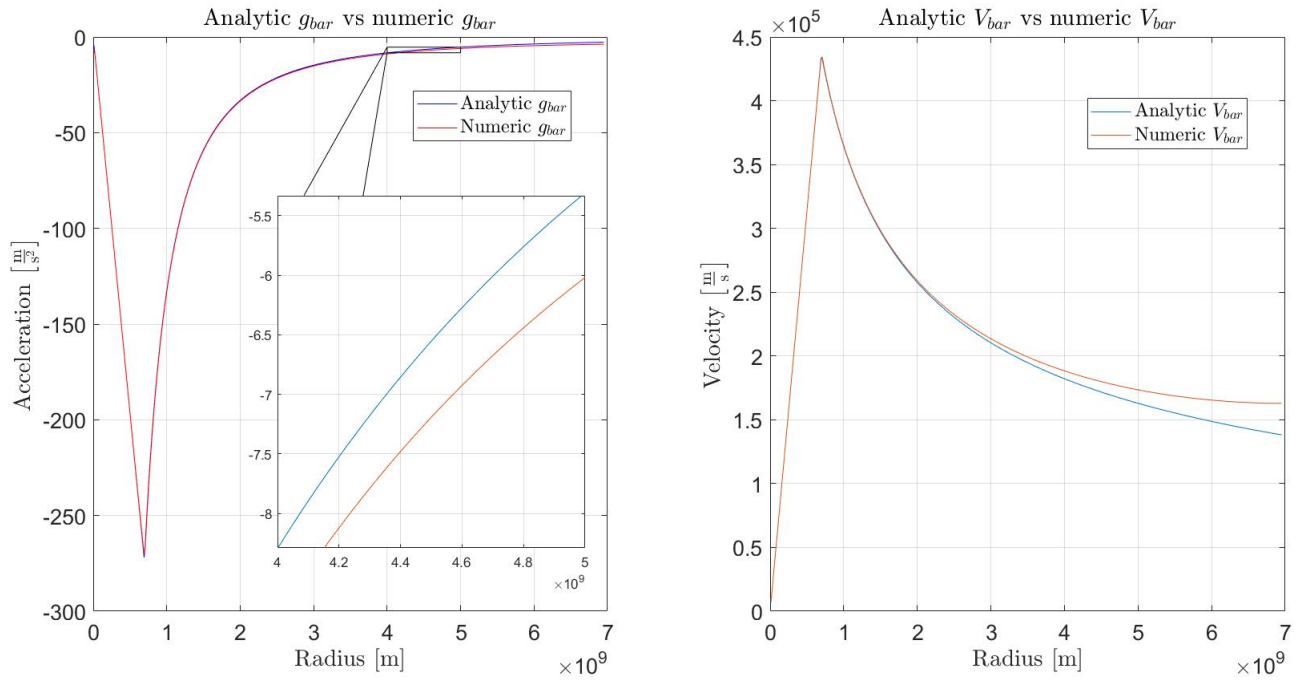


FIGURE 7.2: Comparison between the analytical solution for the sun and the numerical solution using the Fourier-Bessel algorithm. The left figure shows a comparison between the analytical and numerical solution for g_{bar} . The right figure shows a comparison between the analytical and numerical solution for V_{bar} as computed by the centripetal law. A grid of $[z, r] = 400 \times 200$ points was used with a maximum radius of $R = 10R_{\odot}$ and similar maximum height.

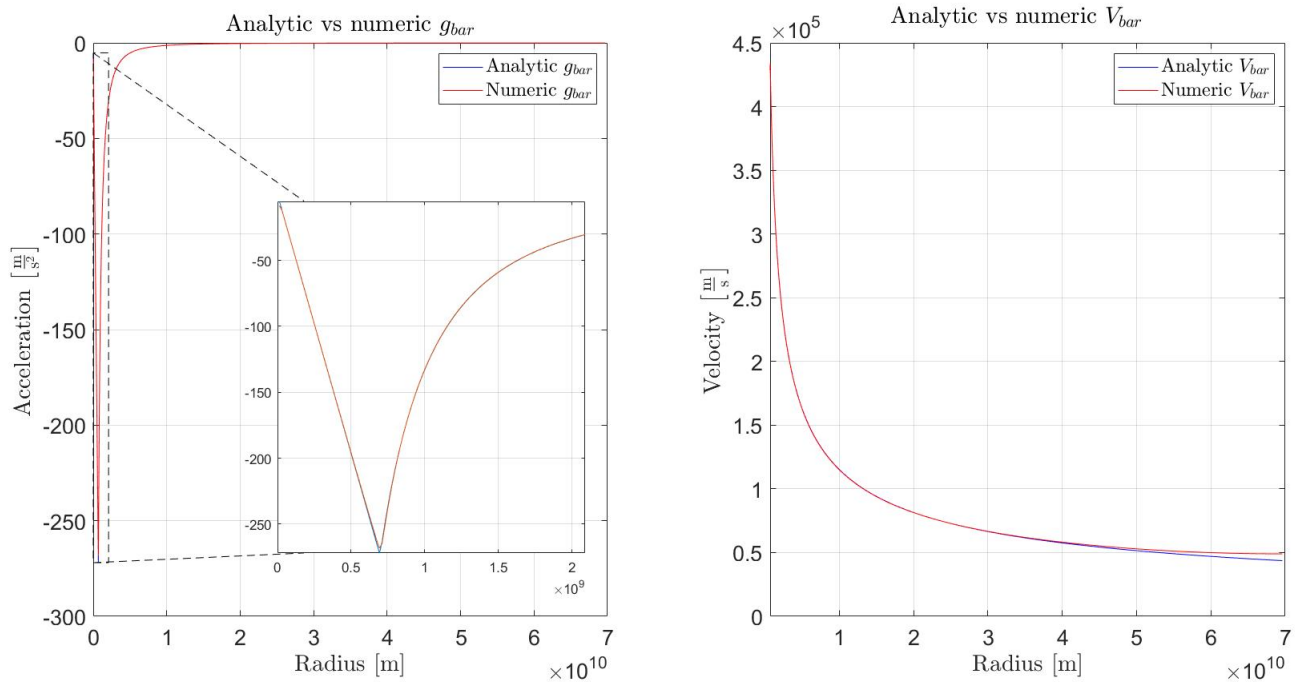


FIGURE 7.3: Same as figure 7.2, except for a domain of size $100 R_{\odot}$.

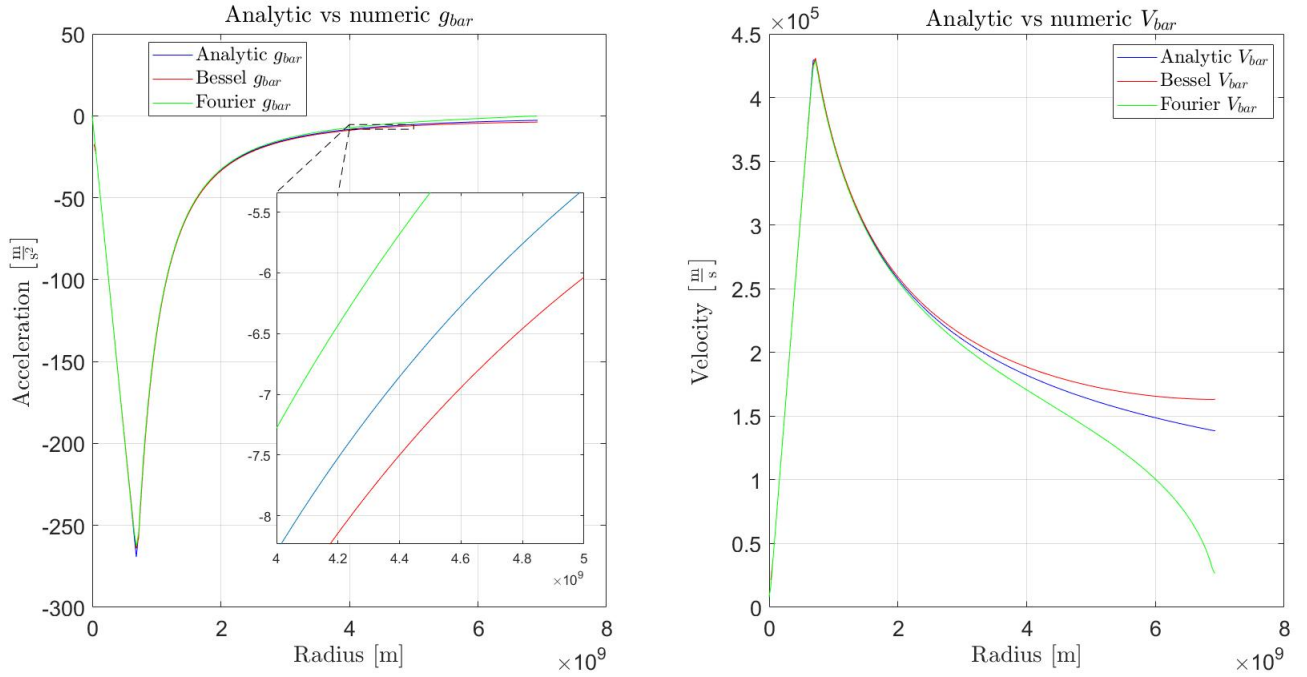


FIGURE 7.4: Comparison between the analytical solution for the sun and the numerical solution using the Fourier-Bessel algorithm and a similar algorithm based on 3D Fourier methods. The left figure shows a comparison between the analytical solution for g_{bar} and the numerical solutions as obtained by the Bessel-Fourier and 3D Fourier method. The right figure shows a comparison between the analytical solution for V_{bar} as computed by the centripetal law and the numerical solutions as obtained by the Bessel-Fourier and 3D Fourier method. A grid of size $[x, y, z] = 400 \times 400 \times 400$ was chosen for the 3D Fourier method and $[z, r] = 400 \times 200$ for the Bessel-Fourier method.

It is thus clear that the Fourier-Bessel method outperforms the Fourier method even on smaller grid sizes. Another advantage is that the Fourier-Bessel method also allows for much larger grid sizes due to the fact that we only need a two-dimensional grid. We also calculated the deflection angle for a right ray passing the sun at an impact parameter of $b = R_{\odot}$. This was calculated by using equation 6.29 by numerically integrating a path with impact parameter $b = R_{\odot}$. The bending angle was found to be $\alpha = 1.7402''$ for the Fourier-Bessel method, matching the theoretical value closely. This makes the Fourier-Bessel algorithm an interesting algorithm to calculate deflection angles.

7.4.2 Dark potential

Less accurate results were obtained for the dark potential. For a spherical symmetric system one can easily calculate the dark potential ϕ_D from equation 7.2 using a Gaussian sphere and using spherical symmetry. This yields for the dark potential:

$$g_{\text{dark}} = -\sqrt{-\frac{a_0}{6}} g_{\text{bar}} \quad (7.51)$$

The solution for the dark acceleration g_{dark} and dark velocity V_{dark} is plotted in figure 7.5. It is clear that the boundary effects have a larger impact on the dark force and velocity. To calculate the dark acceleration, we used the numerically determined bright force from the previous section. Using the analytical bright force yielded similar boundary effects. Once again, the boundary effects are most prevalent in the velocity plots.

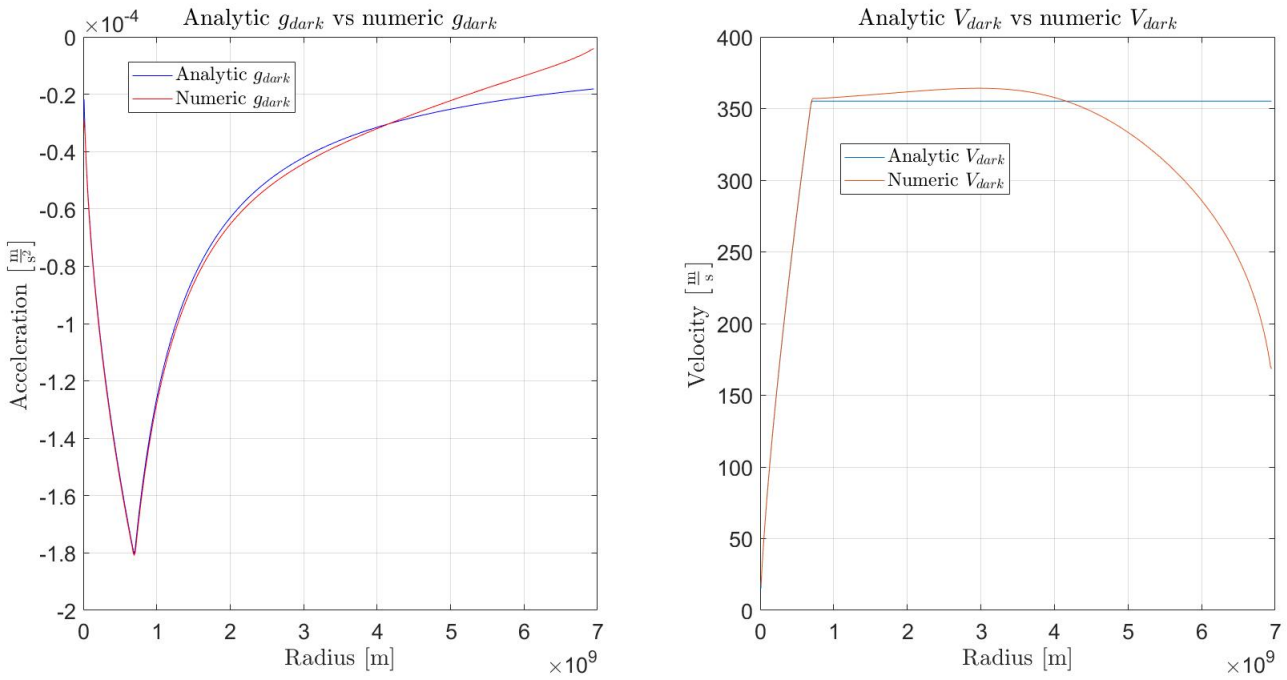


FIGURE 7.5: Comparison between the analytical solution for the dark force for the sun and the numerical solution using the Fourier-Bessel algorithm. The left figure shows a comparison between the analytical and numerical solution for g_{dark} . The right figure shows a comparison between the analytical and numerical solution for V_{dark} as computed by the centripetal law. A grid of $[z, r] = 400 \times 200$ points was used with a maximum radius of $R = 10R_{\odot}$ and similar maximum height. Large boundary effects are visible due to the Fourier-Bessel methods in both figures.

7.4.3 Alteration to Fourier-Bessel method

In order to avoid the boundary effects in figure 7.5, we will use our altered Fourier-Bessel method. It was noticed during the numerical simulations that the boundary effects depend heavily on the number of operations performed in the frequency domain. The alterations to the algorithm as proposed in the section on the altered dark potential algorithm yield better results, as shown in figure 7.6. In both cases (figure 7.5 and 7.6), a maximum radius of $10R_{\odot}$ was chosen to show the boundary effects clearly. When a maximum radius of $100R_{\odot}$ was chosen, the boundary effects produced the exact same deviations. This shows that both methods can still be used to study gravitational systems as long as the maximum radius is chosen large enough to avoid boundary effects.

A comparison of both the Fourier-Bessel method and the altered Fourier-Bessel method is shown in figure 7.7. In the left figure, we have plotted \mathbf{B} and $-\frac{a_0}{6}\mathbf{g}_{bar}$ to show their contribution to $\mathbf{F} = -\frac{a_0}{6}\mathbf{g}_{bar} + \mathbf{B}$. It is clear that for both methods the magnetic contribution is negligible inside the sun but yields a significant contribution at the boundary for the first method (non-altered algorithm) and a non-zero contribution to the second (altered algorithm). The second figure shows the logarithm of the rms value of the differences between magnetic fields of consecutive iterations. The logarithmic graph shows that both methods converge extremely fast. As the alteration to the algorithm shows better results, we will use this version throughout the rest of this chapter.

We conclude that the method provides a good fit to the bright potential, but fails to replicate the flat velocity profile for the dark potential. This can be mitigated by choosing a large enough grid such that the effects of the divergence is small.

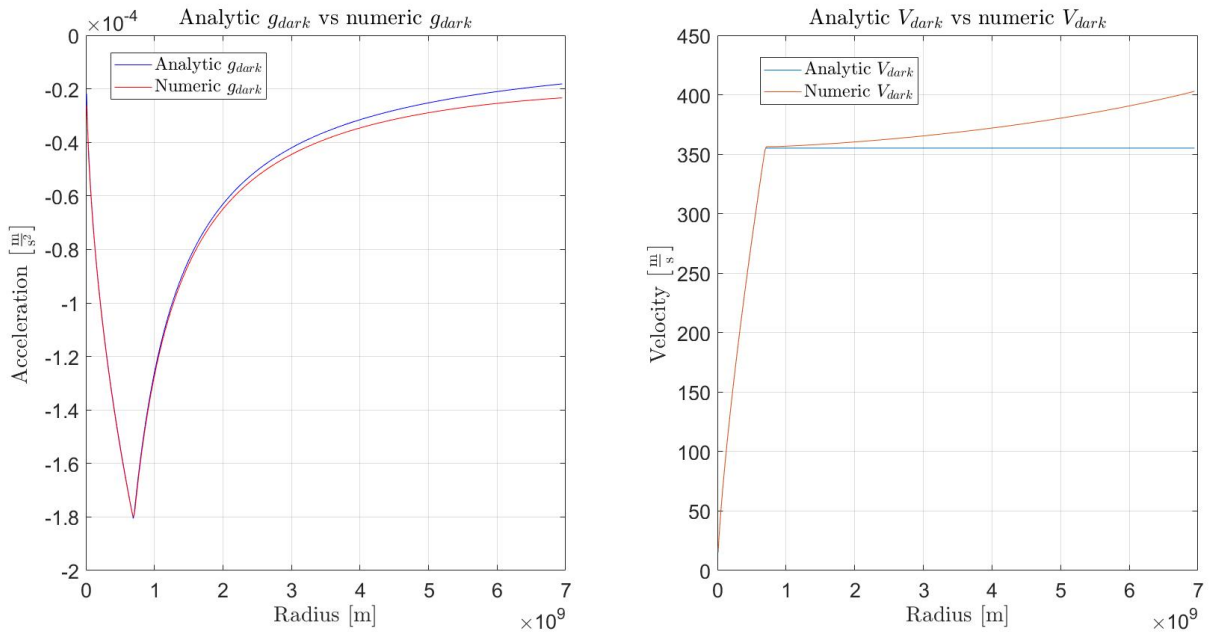


FIGURE 7.6: Comparison between the analytical solution for dark force for the sun and the numerical solution using the altered Fourier-Bessel algorithm. The left figure shows a comparison between the analytical and numerical solution for g_{dark} . The right figure shows a comparison between the analytical and numerical solution for V_{dark} as computed by the centripetal law. A grid of $[z, r] = 400 \times 200$ points was used with a maximum radius of $R = 10R_{\odot}$ and similar maximum height. Boundary effects are visible due to the Fourier-Bessel methods in both figures.

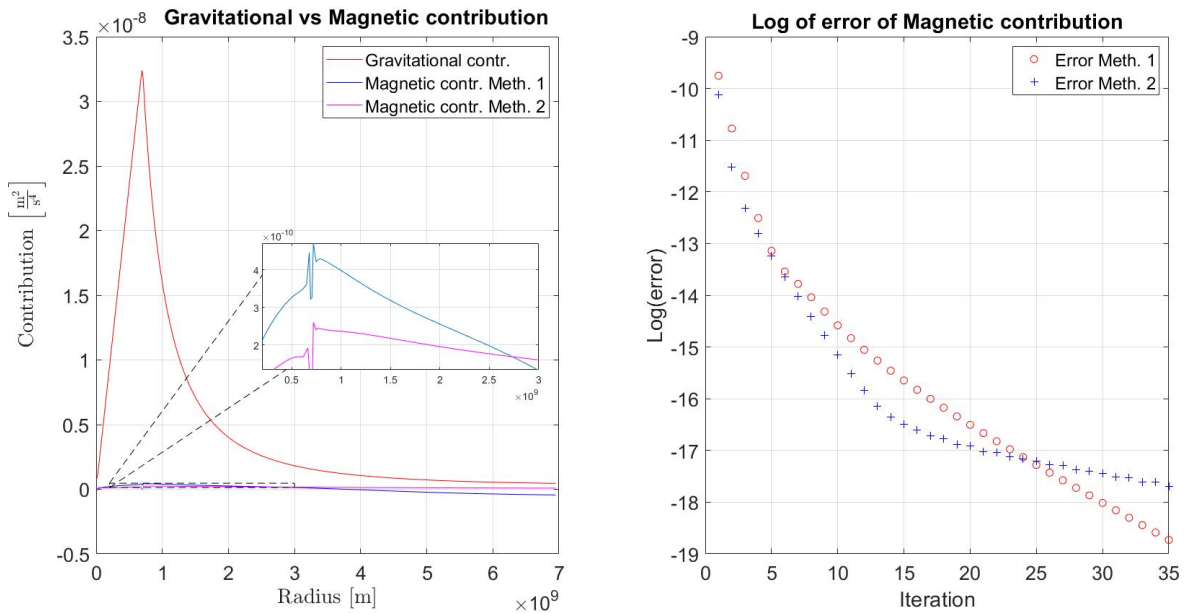


FIGURE 7.7: The left figure shows both the value of gravitational contribution $-\frac{a_0}{6} \mathbf{g}_{bar}$ and the magnetic contribution \mathbf{B} to the dark vector $|\nabla\phi_D|\nabla\phi_D = -\frac{a_0}{6} \mathbf{g}_{bar} + \mathbf{B}$. All vectors were calculated using a grid representing the sun. It is clear that the magnetic contribution is negligible except for at the boundary. The right figure shows the convergence of the magnetic contribution \mathbf{B} with respect to the number of iterations for the Fourier-Bessel method (meth. 1) and the altered Fourier-Bessel method (meth. 2). The error is the difference between successive values of the magnetic contributions. The values were calculated using a base 10 logarithm.

7.5 Spiral galaxy NGC6503

We will now apply the altered Fourier-Bessel method to our favorite galaxy, namely NGC6503, a dwarf spiral galaxy in the constellation Dragon. This is one of the few galaxies in SPARC for which our density profiles accurately fit the baryonic velocities as calculated by SPARC. The density profiles for the stellar disk and gas components were discussed in the section on the SPARC data set in the chapter on astrophysics and galaxies. We would like to note that the purpose of this section is not to accurately fit those density profiles, but to test our method in a case that they do.

7.5.1 Mass-to-light ratio

We will fix the mass-to-light ratio for the stellar disk by using the flat velocity V_{flat} to calculate the total stellar mass. This is done in the following fashion:

We can calculate the mass-to-light ratio of a galaxy if we know the total mass of the galaxy M as $M = \gamma_{\text{disk}} L_* + M_{\text{gas}}$ with L_* the observed total luminosity of the stellar disk. We also know that there exists a direct link between the velocity contribution V_{dark} of the dark potential ϕ_D and the total mass as $V_{\text{dark}} = \left(\frac{a_0}{6} GM\right)^{\frac{1}{4}}$ by equation 7.3. We therefore propose to calculate the velocity contribution the dark potential ϕ_D makes to the observed flat velocity of the rotation curve V_{flat} . If the baryonic velocity contribution to the flat part of the rotation curve is V_{bar} , the dark velocity is given by $V_{\text{dark}}^2 = V_{\text{flat}}^2 - V_{\text{bar}}^2$. Of course, V_{bar} also depends on the mass-to-light ratio by from equation 2.10. Setting the two expressions for V_{dark} in this discussion equal, yields:

$$\sqrt{\frac{a_0}{6} G (\gamma_{\text{disk}} L_* + M_{\text{gas}})} = \sqrt{\frac{a_0}{6} GM} = V_{\text{dark}}^2 = V_{\text{flat}}^2 - V_{\text{bar}}^2 = V_{\text{flat}}^2 - V_{\text{gas}} |V_{\text{gas}}| - \gamma_{\text{disk}} V_{\text{disk}}^2 \quad (7.52)$$

As we know V_{flat} , V_{disk} and V_{gas} from the SPARC data, we can solve the mass-to-light ratio γ_{disk} . We then use the stellar luminosity profile and scale this appropriately such that the integral over the volume yields the total stellar mass. This fixes our stellar mass density profile. For the gas density profile we use the same luminosity profile as in the baryonic calculation. We then solve for the bright and dark potential with the algorithm and calculate the rotation curves as predicted by MOND and CEG and compare them with the actual observed rotation curves of the galaxy in question. This entire section is therefore to test our numerical algorithm on real examples.

We would like to note that we do not fit a single parameter. This makes the approach we followed highly valuable for both CEG and MOND like density reconstructions from the flat velocity and the luminosity profiles.

7.5.2 Results NGC6503

In figure 7.8 two plots are shown. We will first focus on the left plot. In this plot the Newtonian/baryonic velocity is plotted as V_{bar} as calculated by the SPARC team for a light-to-mass ratio of unity. From our density profiles, we calculated the baryonic velocities as predicted by our profiles, which is plotted as V_{kep} . We also plotted the baryonic contribution to the rotation curve of the disk V_{disk} and of the gas V_{gas} . It is clear that the reason that our density profile works so well is because the disk dominates the dynamics of the galaxy, for which we have an exact luminosity profile. The second plot in figure 7.8 shows the observed velocity in NGC6503 corrected for inclination and distance. We also plotted the predicted velocity in CEG based on our altered Fourier-Bessel method. The mass of the disk was estimated as indicated in the numerical theory section, yielding a mass-to-light ratio of $\gamma = 0.4090 \frac{M_{\odot}}{L_{\odot}}$.

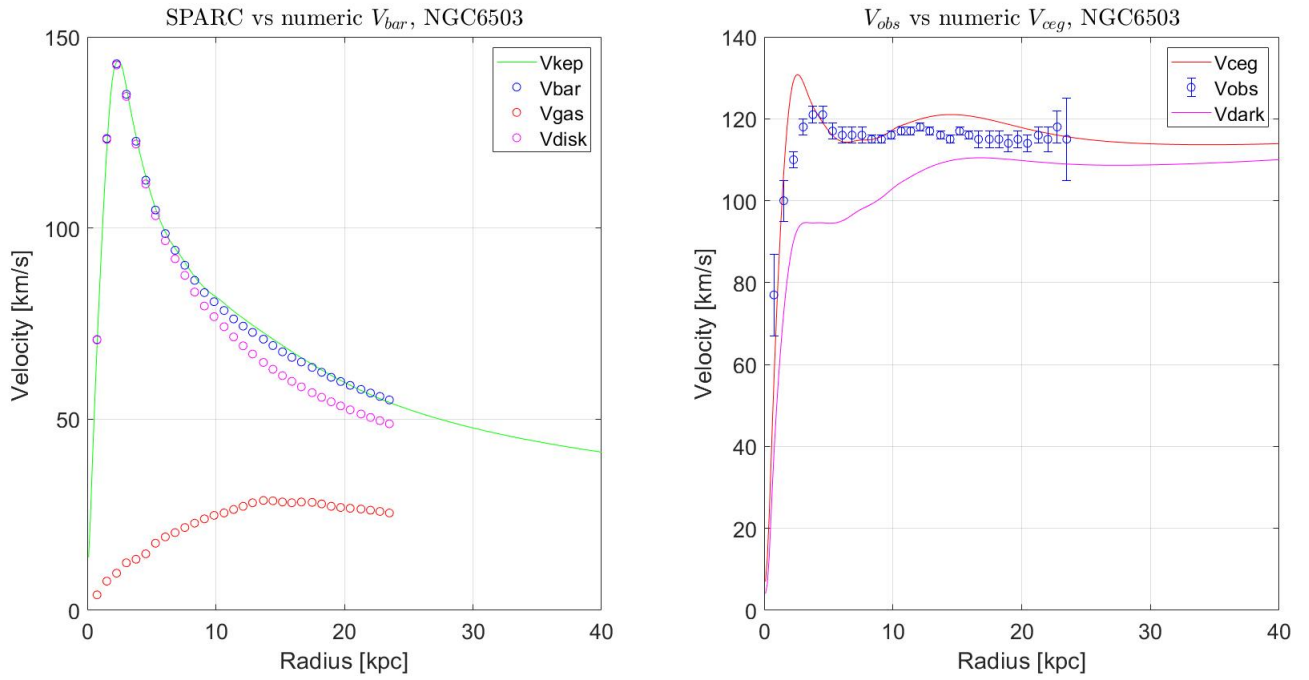


FIGURE 7.8: The left figure shows both the calculated baryonic velocity V_{bar} calculated by the SPARC team as the numerical baryonic velocity as calculated by the altered Fourier-Bessel algorithm based on the assumed density profiles for galaxy NGC6503. The gas contribution V_{gas} and disk contribution V_{disk} to V_{bar} were calculated by the SPARC team based on the measured luminosity profiles. The values were calculated using a disk mass-to-light ratio of unity. The right figure shows the observed velocities V_{obs} as in the SPARC database vs the calculated velocities V_{ceg} in CEG based on the altered Fourier-Bessel algorithm and the assumed density profiles. We also plotted the dark velocity V_{dark} , the velocity contribution due to the dark potential. The mass-to-light ratio was calculated as explained in the numerical theory section.

Several important conclusions can be drawn from baryonic velocities as calculated by the SPARC team. Firstly, we see that V_{gas} is non-zero when the rotation curves have become flat. This implies that the velocity in CEG will drop below the flat velocity of the rotation curve as the baryonic contribution of the gas drops. Thus the flat velocity in CEG will drop further as the baryonic contribution drops, making the velocity not exactly flat. In general, the baryonic contribution is non-zero when the rotation curve is already flat for all SPARC galaxies, making a good case for transition theories such as MOND or dark matter.

We also see that due to the fact that CEG is an additive theory ($g_{\text{obs}} = g_{\text{bar}} + g_{\text{dark}}$), the CEG velocity shows the same peak at 2.2 times the disk scale length of the disk as V_{disk} . This peak is usually not present in the rotation curves of galaxies, indicating that the mass-to-light ratio for the disk has to be small in CEG, such that this peak is suppressed.

We would also like to note that the overestimation of CEG at 15 kpc might be caused by the fact that we overestimate the density at 15 kpc, as is clear from the left figure (7.8).

Now we will consider the magnetic contribution and the error. We have again plotted the Magnetic \mathbf{B} and Gravitational contribution $\frac{a_0}{6} \mathbf{g}_{\text{bar}}$ to \mathbf{F} in equation 7.29 and the error between consecutive magnetic fields in figure 7.9. This plot is a great insight into the magnetic contribution in disk galaxies. Firstly, the magnetic contribution is highest when the density is largest. This is clear from the form of the non-linear differential equation 7.2; higher densities imply that more potentials of individual point masses overlap, creating extra pairwise contributions to the magnetic contribution.

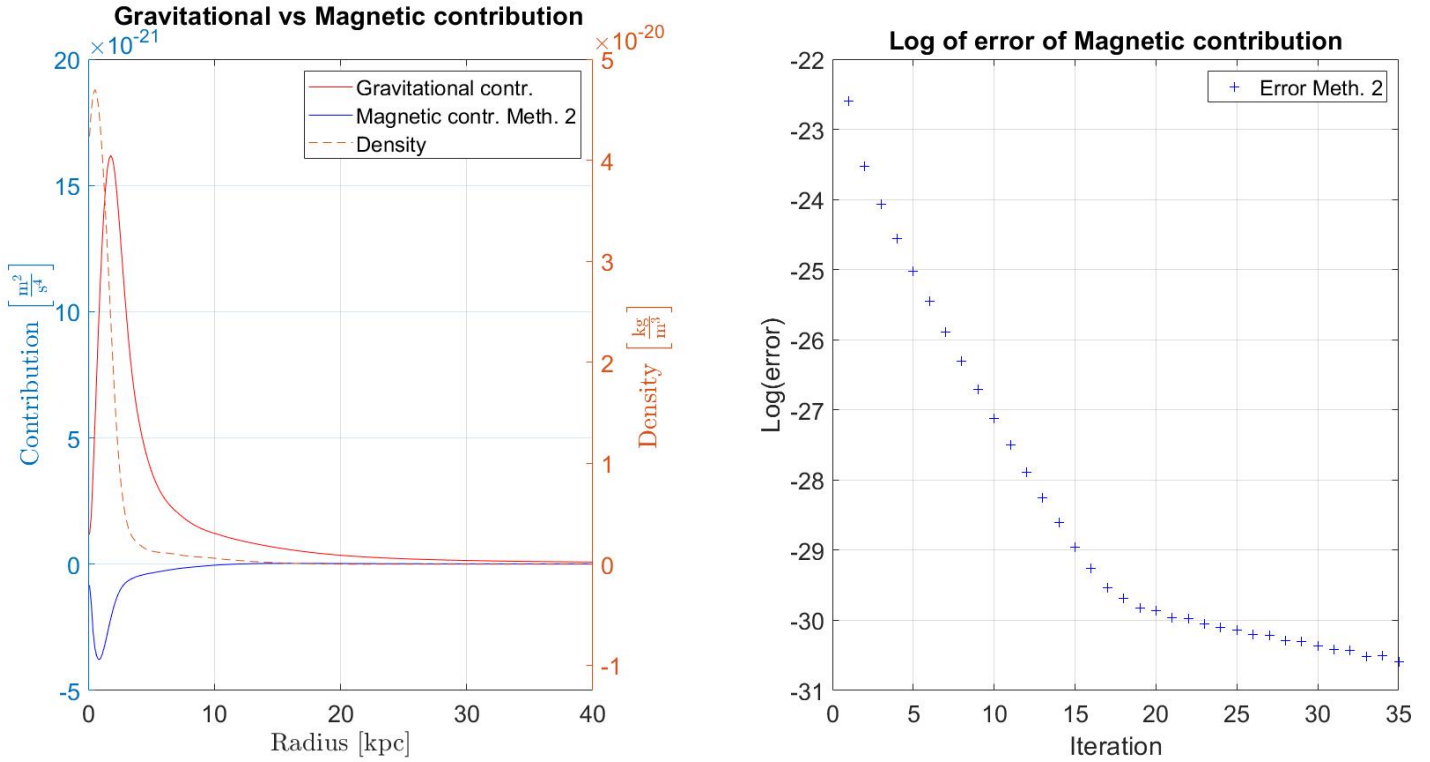


FIGURE 7.9: The left figure shows both the value of gravitational contribution $-\frac{a_0}{6} \mathbf{g}_{\text{bar}}$ and the magnetic contribution \mathbf{B} to the dark vector $|\nabla\phi_D|\nabla\phi_D = -\frac{a_0}{6} \mathbf{g}_{\text{bar}} + \mathbf{B}$. All vectors were calculated using assumed density profiles describing galaxy NGC6503. The right figure shows the convergence of the magnetic contribution \mathbf{B} with respect to the number of iterations. The error is the difference between successive values of the magnetic contributions for the altered Fourier-Bessel method (meth. 2). The values were calculated for a base 10 logarithm.

The right plot in figure 7.9 shows that the magnetic contribution converges similar to the spherical case. In order to test the effect of the magnetic contribution, we will also calculate a velocity that ignores the magnetic contribution solely based on the predicted mass-to-light ratio and the baryonic velocity. This velocity is called V_{fit} . This velocity is not dependent on the density profiles but just on the baryonic velocities V_{bar} from SPARC. In the next chapter we will explain how one should calculate such a velocity, but all we need to know right now is that this velocity is not dependent on our density profiles and just on the SPARC data. We have plotted this velocity V_{fit} against the rotation curves of CEG and the observed rotation curves in figure 7.10. The velocity is in good agreement with the predictions of the Fourier-Bessel method, except at the points that we overestimate the density. This shows that the magnetic contribution is negligible in this galaxy and that our numerical method works well.

However, there are several reasons why we cannot draw conclusions from the SPARC database. Firstly, our density profiles only match the SPARC velocities when the velocities are dominated by the disk velocity, indicating that our gas velocity does not fit the data. Secondly, the produced velocities are dependent on the chosen maximum grid radius. This is because the density profiles change slightly when we alter the maximum radius due to the finite grid. Thirdly, as in CEG the velocity is not truly flat, it is hard to estimate the mass-to-light ratio from formula 7.52. In conclusion, there are too many variables that can be varied to make a general conclusion about CEG from our density profile. This is why we will fit CEG and MOND velocity curves to the rotation curves in the next section.

Nonetheless, the convergence of the magnetic contribution and the match between V_{ceg} and

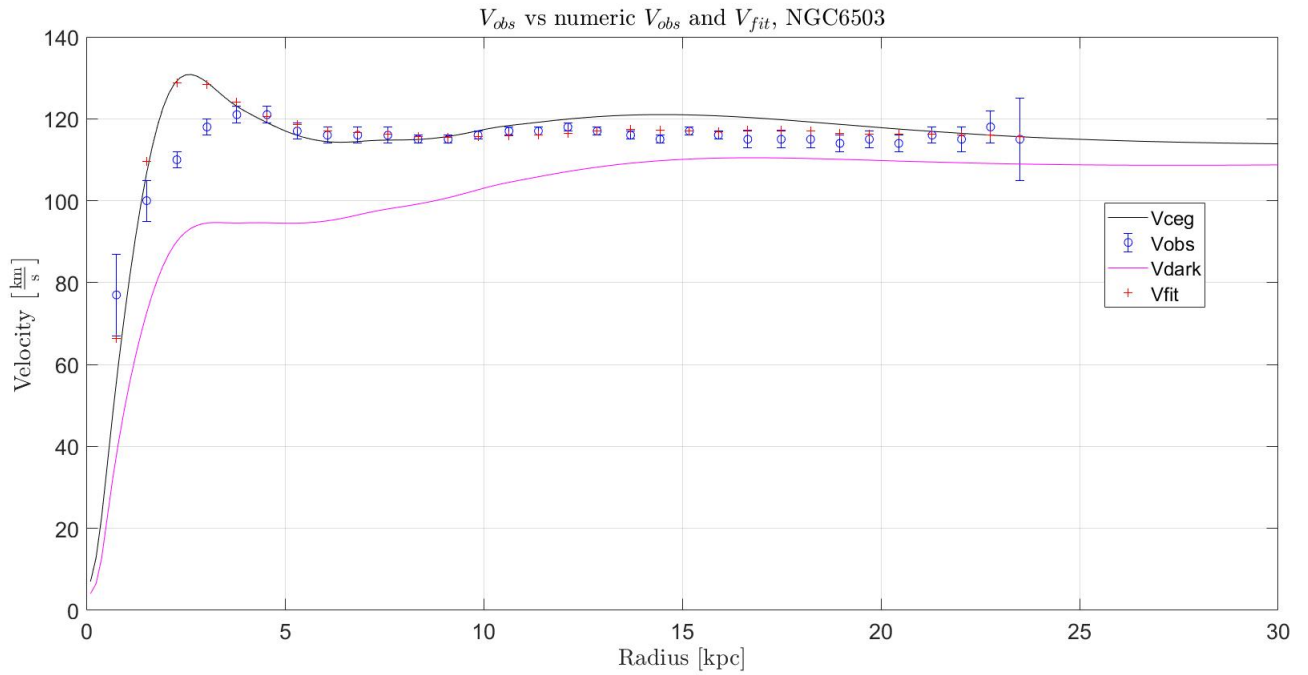


FIGURE 7.10: The figure shows the observed velocities V_{obs} as in the SPARC database vs the calculated velocities V_{ceg} in CEG based on the altered Fourier-Bessel algorithm and the assumed density profiles for galaxy NGC6503. We also plotted the dark velocity V_{dark} , the velocity contribution due to the dark potential and the velocity V_{fit} . The latter velocity is the velocity based solely on g_{bar} as calculated by SPARC and equation 8.3. The mass-to-light ratio was calculated as indicated in the numerical theory section.

V_{obs} shows that our altered Fourier-Bessel method can be used to calculate both CEG and MOND rotation curves in cases that the actual density profiles are known.

Chapter 8 ● ■ ▲

Testing MOND and CEG to observed rotation curves

In this chapter we will describe the fits of MOND and CEG to the SPARC database of 175 galaxies. We will use this database to test both the prediction of CEG and MOND against the actual observed rotation curves by fitting both theories to the rotation curves. We will use three fit parameters: the mass-to-light ratio, the disk inclination and galactic distance. We will fit these parameters to the observed rotation curves using a Markov Chain Monte Carlo (MCMC) algorithm. Our fitting procedures are described in this chapter as well as the results.

8.1 MOND and CEG fits

The previous chapter was thus to test our algorithm on real examples. However, in order to make quantitative statements about the overall effectiveness of MOND and CEG, we will also fit both theories to the rotation curves. Of the 175 SPARC galaxies, we will only use the galaxies that do not have a significant bulge and a quality flag of $Q = 1, 2$. This reduces our fitting set to 131 galaxies. Such fittings for CEG are interesting, because it was shown by Lelli. et al that EG did not describe the rotation curves well [16].

In these fits, we will only use the baryonic calculated acceleration by the SPARC team to explain the observed acceleration. The baryonic acceleration at a galactic radius R is given by:

$$g_{\text{bar}} = \frac{\gamma_{\text{disk}} V_{\text{disk}}^2 + V_{\text{gas}} |V_{\text{gas}}|}{R} \quad (8.1)$$

The symbols we use throughout this chapter were explained in the section on the SPARC data set in the chapter on astrophysics and galaxies. We advise the reader to return to this chapter for definitions of the various symbols.

From this baryonic acceleration, one can calculate the acceleration due to MOND, g_{mond} , and due to CEG, g_{ceg} , in a straightforward manner. From our section on the bright and dark potential in the Fourier-Bessel method chapter, we know that the potential of the modified theories (equation 7.29) are related to the baryonic potential as:

$$\mu\left(\frac{|g_{\text{mond}}|}{a_m}\right) g_{\text{mond}} = g_{\text{bar}} + \nabla \times \mathbf{A}_{\text{mond}} \quad , \quad |g_{\text{dark}}| g_{\text{dark}} = \frac{a_0}{6} g_{\text{bar}} + \nabla \times \mathbf{A}_{\text{ceg}} \quad (8.2)$$

In their 1984 joint paper, Milgrom and Bekenstein showed that the magnetic component ($\nabla \times \mathbf{A}$) decreases as $\mathcal{O}(r^{-3})$. For our current purposes, this implies that we can neglect this terms contribution to the actual velocity, as the other terms scale as $\mathcal{O}(r^{-2})$. Thus we effectively set ($\nabla \times \mathbf{A} = 0$ in equation 8.2. This implies that both the acceleration in MOND

and CEG can be predicted from the baryonic acceleration g_{bar} as:

$$g_{\text{mond}} = g_{\text{bar}} \left(\frac{1}{2} + \frac{1}{2} \sqrt{1 + \left(\frac{2a_m}{g_{\text{bar}}} \right)^2} \right)^{\frac{1}{2}}, \quad g_{\text{ceg}} = g_{\text{bar}} + \sqrt{\frac{a_0}{6}} g_{\text{bar}} \quad (8.3)$$

These predictions for the acceleration are compared against the actual observed acceleration in SPARC:

$$g_{\text{obs}} = \frac{V_{\text{obs}}^2}{R} \quad (8.4)$$

Such a fitting procedure as described above, in which the observed acceleration is fitted against other theories of gravity using just the baryonic acceleration, is more commonplace in astrophysics than the density profile procedure described earlier. For instance, fitting with different fit parameters were done for other modified gravity theories such as neo-MOND [23] and MOG [9]. A CEG fit was also performed by Hossfelder [12] with only a_0 as fit parameter. Our approach will be similar to the approach taken in [17], but then applied to MOND and CEG.

8.1.1 Fitting parameters

Since both V_{gas} and V_{disk} are known, we seem to have only one fitting parameter: the mass-to-light ratio γ_{disk} of the disk in equation 8.1. However, as was done in [17], we will also fit the galactic distance to the galaxy D and the inclination i of the galaxy disk. This is done because the 5 different methods in SPARC to estimate the galactic distance D have an error of 5% to 15%. Similarly, the inclination i also has non-negligible errors in the SPARC database. We will thus leave these parameters (the distance and inclination) as free parameters in our fit model. We will now discuss how varying these parameters with respect to their values in SPARC impacts our dataset as was done in [17].

Since the observed rotation velocity V_{obs} are determined based on line-of-sight velocity, changing the inclination from $i \rightarrow i'$ changes the observed velocities and its error by:

$$V'_{\text{obs}} = V_{\text{obs}} \frac{\sin i}{\sin i'}, \quad \delta V'_{\text{obs}} = \delta V_{\text{obs}} \frac{\sin i}{\sin i'} \quad (8.5)$$

Since we are working with small angles, changing the galactic distance from $D \rightarrow D'$ changes the radius R and baryonic velocities as:

$$R' = R \frac{D'}{D}, \quad V'_{\text{bar}} = V_{\text{bar}} \sqrt{\frac{D'}{D}} \quad (8.6)$$

Changing the distance does not affect the observed velocities. Notice that these transformations (equation 8.6) do not affect the baryonic acceleration $g'_{\text{bar}} = g_{\text{bar}}$ in equation 8.1. However, taking both the inclination change (8.5) and galactic distance change (8.6) into account implies g_{obs} in equation 8.4 changes as:

$$g'_{\text{obs}} = \left(\frac{\sin i}{\sin i'} \right)^2 \frac{D}{D'} g_{\text{obs}} \quad (8.7)$$

Thus changing the inclination (equation 8.5) and galactic distance (equation 8.6) only changes the observed values and does not change our baryonic values. We will next describe the fitting method we use. In our fits we will thus compare the observed acceleration g'_{obs} corrected for

our new inclination i' and distance D' to the MOND and CEG accelerations (equation 8.2). The latter does not change when we change the distance and inclination of the galaxy.

8.1.2 Fitting procedure

Due to the degeneracy's in 8.7 between the fitting parameters i and D , cftool cannot obtain good bounds on these parameters, even when we constrain them to be in the intervals $D' \in [D - \delta D, D + \delta D]$ and similarly $i' \in [i - \delta i, i + \delta i]$ in which D is the original galactic distance and δD the error as calculated by SPARC.

Instead, we will use a Markov Chain Monte Carlo (MCMC) algorithm or as it is known in less formal company: the MCMC Hammer algorithm. We use a Matlab implementation of Goodman & Weare's Affine Invariant Markov chain Monte Carlo Ensemble sampler [8] as implemented by Aslak Grinsted. The following approach is similar to the approach taken by the SPARC team [17] applied to their radial acceleration theory.

A MCMC sampler starts by initiating a set of random walkers at a set of randomly chosen points in the parameter space of the fit parameters. The goal is to have these random walkers converge to a desired equilibrium distribution around the desired parameter values. This is done by defining a log likelihood function. When the parameters that the random walkers currently have yield a rotation curve that matches the observed velocities well, the log likelihood function is high and visa versa. The random walkers then respond to this log likelihood function by walking to fit parameters that have a high log likelihood function. The log likelihood function is thus designed to let the random walkers converge to the fit parameters that fit the curve best.

Next to a log likelihood function, we should also make sure that the random walkers cannot converge to undesirable or nonphysical values in the parameter space. This is done by introducing a prior distribution for the fitted variables γ_{disk} , D and i . These prior distributions ensure that our parameters stay close to the actual SPARC parameters and deviate only from these parameters within the error range of these parameters as calculated by SPARC. For instance, the prior distribution for the galactic distance D is a Gaussian with as mean the SPARC value and as standard deviation the error SPARC calculated for this distance.

The log likelihood function thus ensures that our random walkers converge to fit parameters that match the observed rotation curves. The prior distributions ensure that our fit parameters stay reasonable. The eventual Markov chain of all the random walkers will then have as its distribution the equilibrium distribution of the actual parameter set of that specific galaxy.

In our MCMC sampler, we wish to minimize the difference between the observed rotation curve and the calculated rotation curve. This is done by minimizing the function:

$$\chi_v^2 = - \sum_R \frac{[g_{\text{obs}}(R) - g_{\text{tot}}(R)]^2}{(N - f) \sigma_{\text{obs}}^2} \quad (8.8)$$

In which g_{tot} is either g_{mond} or g_{ceg} . In this function we have already corrected for the new inclination and distance. N is the amount of data points and f the degrees of freedom of the fit (3). Notice that we simply minimize the error between our rotation curve and the observed rotation curve weighted by the error in the observed value. The minus sign is introduced to ensure that when the error between our curve and the observed curve is low, our function χ_v^2 is largest etc. This will be our log likelihood function.

We calculate the error in the observed data σ_{obs} as:

$$\sigma_{\text{obs}} = 2V_{\text{obs}} \frac{\delta V_{\text{obs}}}{R} \quad (8.9)$$

In which we also correct for the new inclination and distance.

As priors for γ_{disk} , D and i , we will use Gaussian distributions centered at the measured SPARC values for D and i and a mean of $0.5 \frac{M_{\odot}}{L_{\odot}}$ for γ_{disk} . The distance and inclination priors will have standard deviations given by the error in the SPARC data. The standard deviation for γ_{disk} will be $0.2 \frac{M_{\odot}}{L_{\odot}}$. This last deviation is based on assuming a uniform distribution for γ_{disk} in our universe and on the measured values for γ_{disk} ranging from $0.1 \frac{M_{\odot}}{L_{\odot}}$ to $0.8 \frac{M_{\odot}}{L_{\odot}}$ according to [20].

Note that the actual value of the deviation is not important, but it should be high enough to allow for changes in the Markov chains. We will also require that our parameters remain physical, thus $\gamma_{\text{disk}} > 0$, $D > 0$ and $0^{\circ} < i < 90^{\circ}$. The first 500 steps of the chain will be considered as burn-in and a total number of steps for the total of the random walkers of 10^5 . After the simulation we will discard another 20% of the data as burn-in.

8.2 Fitting CEG and MOND

In this section we will present the results from the MCMC fits to SPARC. The actual fitted parameters for all 131 SPARC galaxies can be found in appendix D.

Out of the 131 fits, 9 fits (7%) were poor fits ($R^2 < 0$) and 62 galaxies (47%) were excellent fits ($R^2 > 0.9$) and 94 good fits ($R^2 > 0.7$). Because we used three fitting parameters, we also present the adjusted R^2 -value. These yielded similar results with 54 galaxies excellent adjusted R^2 -values and 86 good fits by previous definitions.

The poor fits can be due to several reasons. Firstly, the standard deviations we imposed for the priors on the inclination i and galactic distance D may be too tight or the errors were underestimated in the SPARC data. Secondly, the galaxies might have dust contents that shroud the disk luminosity profiles, reducing g_{disk} . Thirdly, the baryonic acceleration was based on the calculated baryonic velocities from the SPARC team, which they calculated from luminosity profiles taken from other groups (mainly (75%) PHD theses from RUG). This introduces room for human error that we have not taken into account as the calculated acceleration is very sensitive to changes in the baryonic velocity. The SPARC team also released a paper [17] on their radial acceleration equation, in which only 10% of the galaxies were a poor fit. We should however add that we use smaller subsets from the SPARC data with better quality. They considered all SPARC galaxies, which includes galaxies with quality flag $Q = 3$ and bulges. In cases of bulge galaxies they introduced another fitting parameter γ_{bulge}

For 15 additional galaxies that were a good fit, the error in γ_{disk} was larger than the actual value. This does not imply that the fit was poor, as can be seen for galaxy DDO161 in figure 8.1 and galaxy NGC4214 in figure 8.2. Such a large error in γ_{disk} might be indicative that the gas dominates the rotation curves and that the disk contribution to the velocity is thus negligible. This is supported by the fact that the large errors in the mass-to-light ratio mainly occurred for galaxies with $\gamma_{\text{disk}} < 10^{-3}$. This indicates that these errors happen when the gas contribution dominates the rotation curve. We have also included galaxy IC2574 in figure 8.3, which is traditionally hard to fit by dark matter theorems [17]. We find R^2 values of 0.9839 and 0.9860 for CEG and MOND respectively for IC2574.

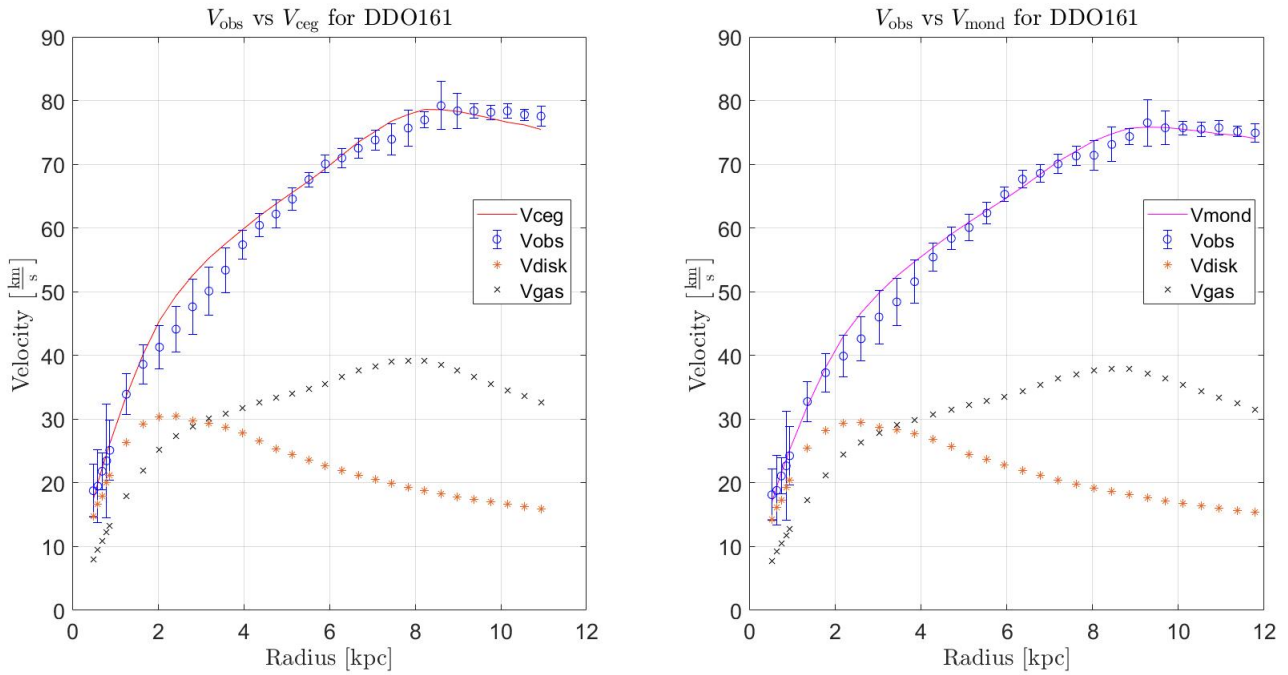


FIGURE 8.1: The figures show the fits of the velocities as calculated by CEG (V_{ceg}) and MOND (V_{mondd}) to the observed velocities V_{obs} by SPARC of gas dominated galaxy DDO161 respectively. We used the three fit parameters in a MCMC fitting algorithm based on the baryonic calculated acceleration g_{bar} and Gaussian priors on the fit parameters and a log-likelihood maximization. We fitted the mass-to-light ratio γ_{disk} , distance D and inclination i based on priors and estimates by SPARC. The velocities and errors are corrected for the distance and inclination and we also show the gas velocity contribution V_{gas} and the disk contribution V_{disk} for a mass-to-light ratio of unity.

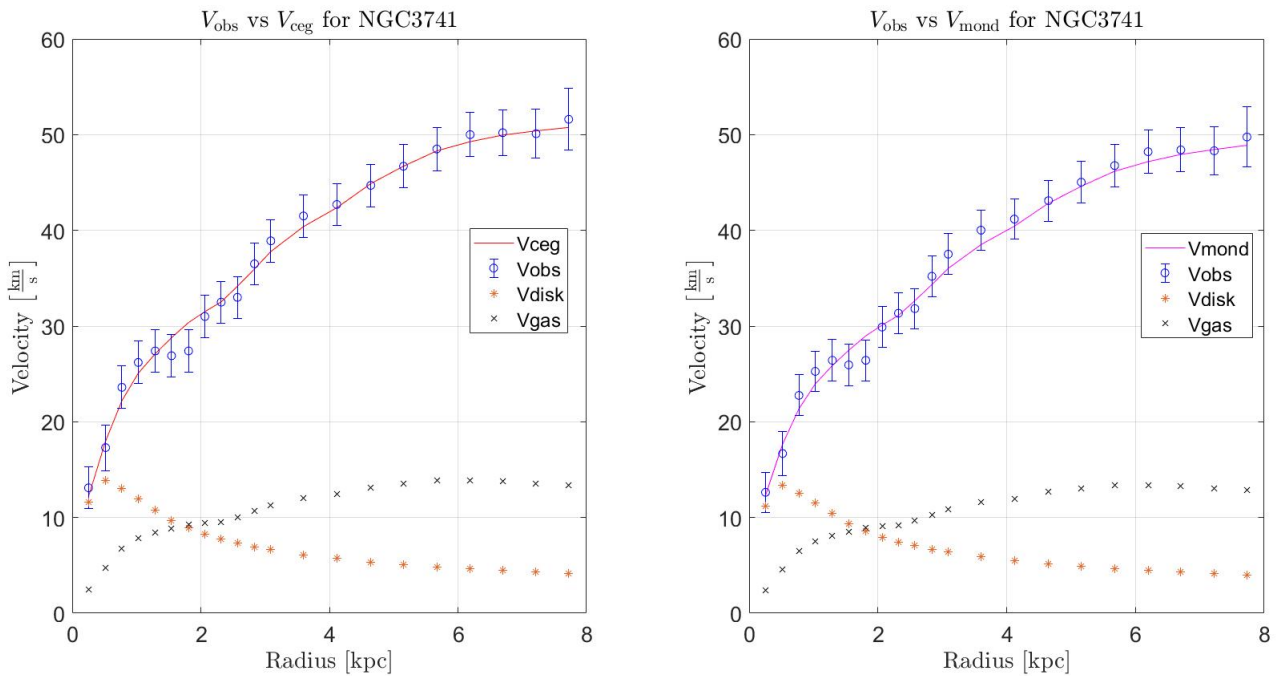


FIGURE 8.2: Same as figure 8.1 but for SPARC galaxy NGC3741.

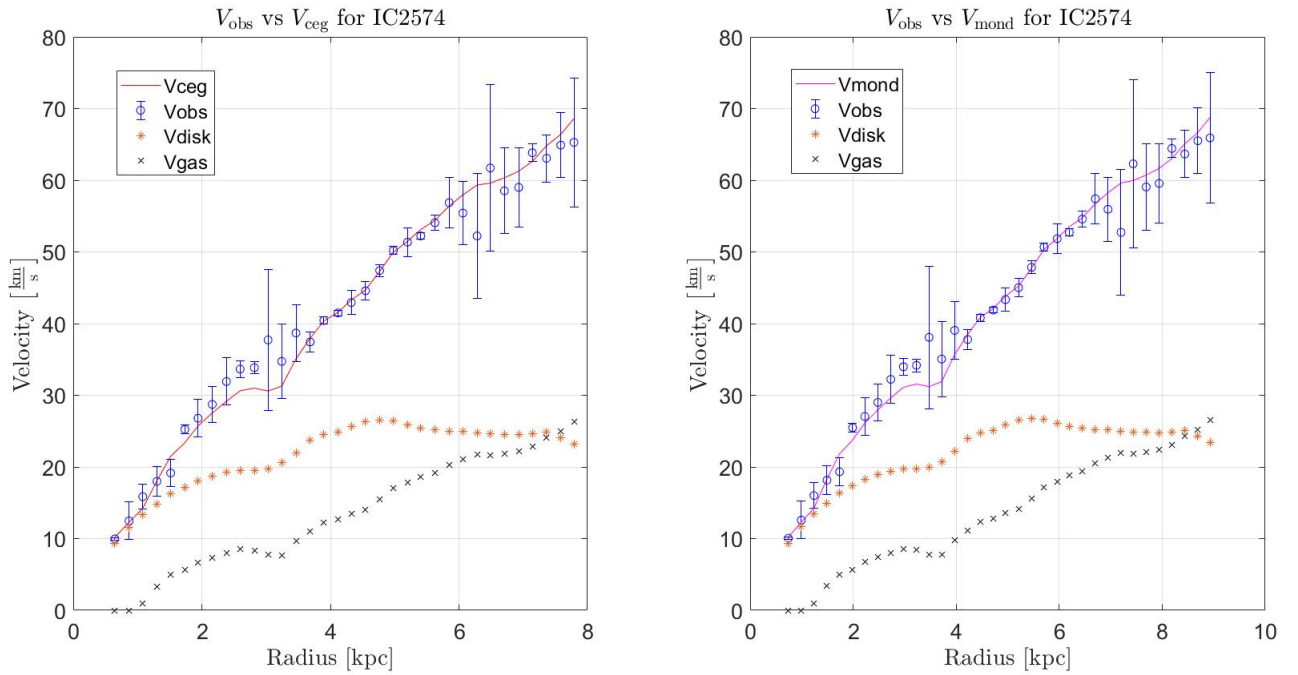


FIGURE 8.3: Same as figure 8.1 but for SPARC galaxy IC2574.

8.2.1 Fit results

In figure 8.4 the residuals of both fits are plotted. These residuals were best fitted by a sum of two Gaussian:

$$y = \sum_{i=1}^2 a_i e^{-\left(\frac{x-b_i}{c_i}\right)^2} \quad (8.10)$$

For both CEG and MOND fits, these Gaussians had means close to zero, indicating that the fits do not over/underestimate the data. The CEG double gaussian had a R^2 value of 0.9953 and the MOND had a R^2 value of 0.9949 indicating good fits. We fitted a double Gaussian similarly to [17], due to the fact that there are two main contributions to the error in the observed velocity. The first error in V_{obs} comes from fitting a disk to the luminosity profile to estimate the inclination by the SPARC team. The second error in V_{obs} is due to the asymmetry between velocities in the approaching and receding sides of the galaxy (which were averaged over) [17].

We will now consider the mass-to-light ratio of both CEG and MOND both plotted in figure 8.5. We will ignore the galaxies that were a poor fit ($R^2 < 0$). We also plotted the line $\gamma = 0.5 \frac{M_{\odot}}{L_{\odot}}$, which is the value predicted by current population synthesis models, indicated by a red vertical line. We calculated the trimmed mean at 95%. For CEG, this yielded $\gamma_{\text{disk}} = 0.4675 \frac{M_{\odot}}{L_{\odot}}$ and MOND $\gamma_{\text{disk}} = 0.6896 \frac{M_{\odot}}{L_{\odot}}$. However, as this mean might be influenced by the error due to the gas dominated galaxies, we will also present the medians, which are $0.4810 \frac{M_{\odot}}{L_{\odot}}$ and $0.7054 \frac{M_{\odot}}{L_{\odot}}$ for CEG and MOND respectively. However, the mass-to-light ratio is not constant from galaxy to galaxy as metal-rich galaxies tend to have a larger mass-to-light ratio. Further increasing the standard deviation in the prior of γ_{disk} did not significantly affect our results, but decreasing it yielded smaller values of γ_{disk} . This is because the random walkers are less likely to travel do to the smaller standard deviation.

Next, we will consider the similarities and differences between the MOND and CEG fits. In figure 8.6 we have plotted the CEG vs MOND scatter plots for the mass-to-light ratio,

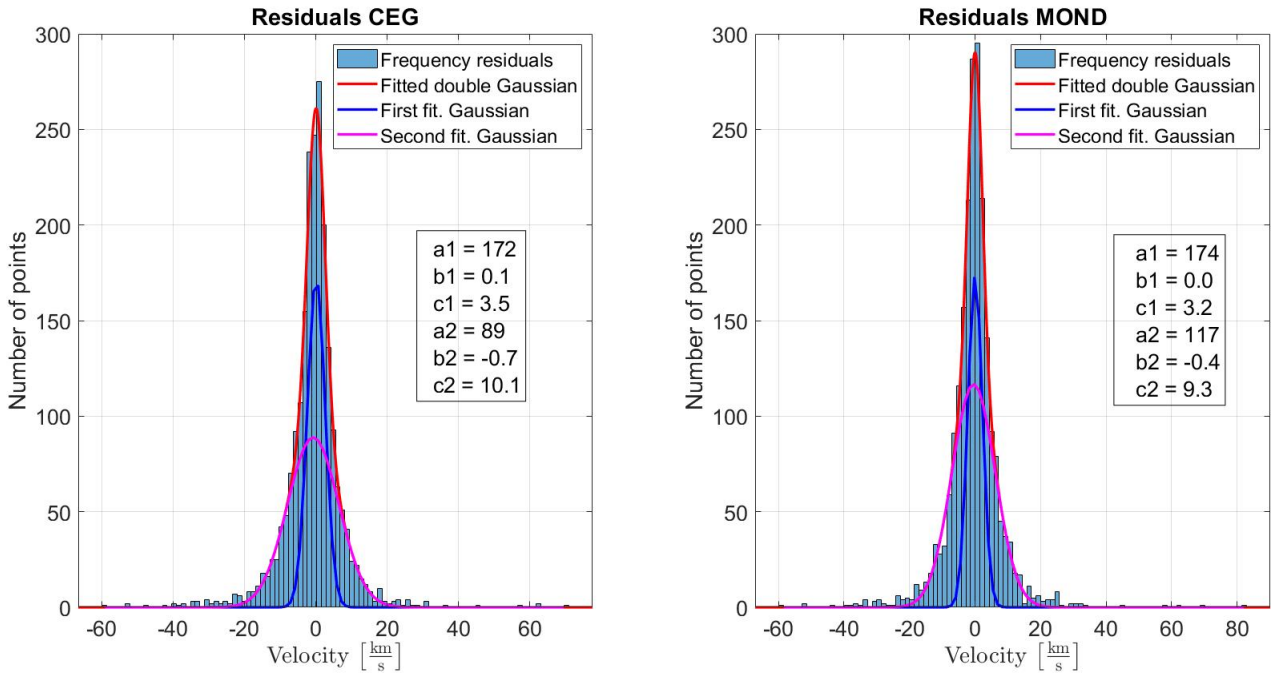


FIGURE 8.4: The left and right figure show the residuals of the fitted velocities to the SPARC observed velocities of CEG and SPARC respectively. We also fitted a double Gaussian as there are two main contributions to the error as indicated in the text with resulting fit parameters as indicated in the figure.

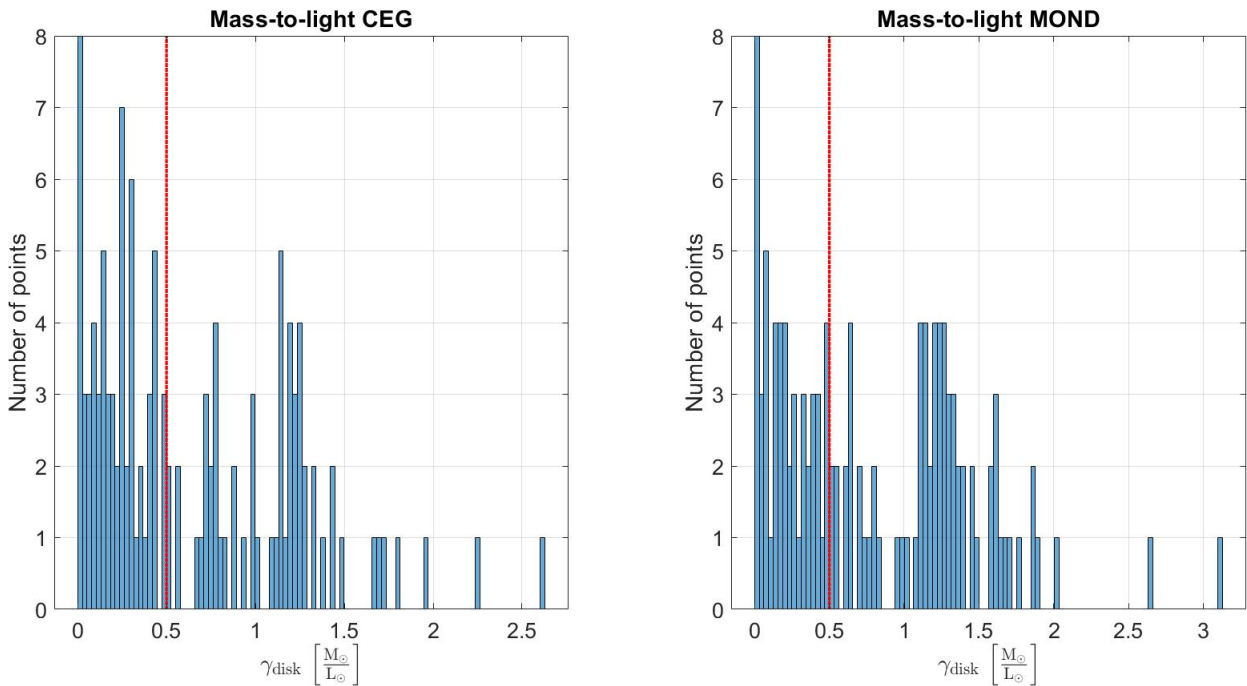


FIGURE 8.5: The left and right figures show respectively the mass-to-light of stellar disk of CEG and MOND for 122 SPARC galaxies as fitted by the MCMC algorithm based on three fit parameters with Gaussian priors. We excluded 9 galaxies that were a poor fit ($R^2 < 0$) of the original 131 galaxies. The median values of both plots are $0.4810 \frac{M_{\odot}}{L_{\odot}}$ and $0.7054 \frac{M_{\odot}}{L_{\odot}}$ for CEG and MOND respectively. We also plotted a red line indicating the stellar population synthesis model value of $0.5 \frac{M_{\odot}}{L_{\odot}}$.

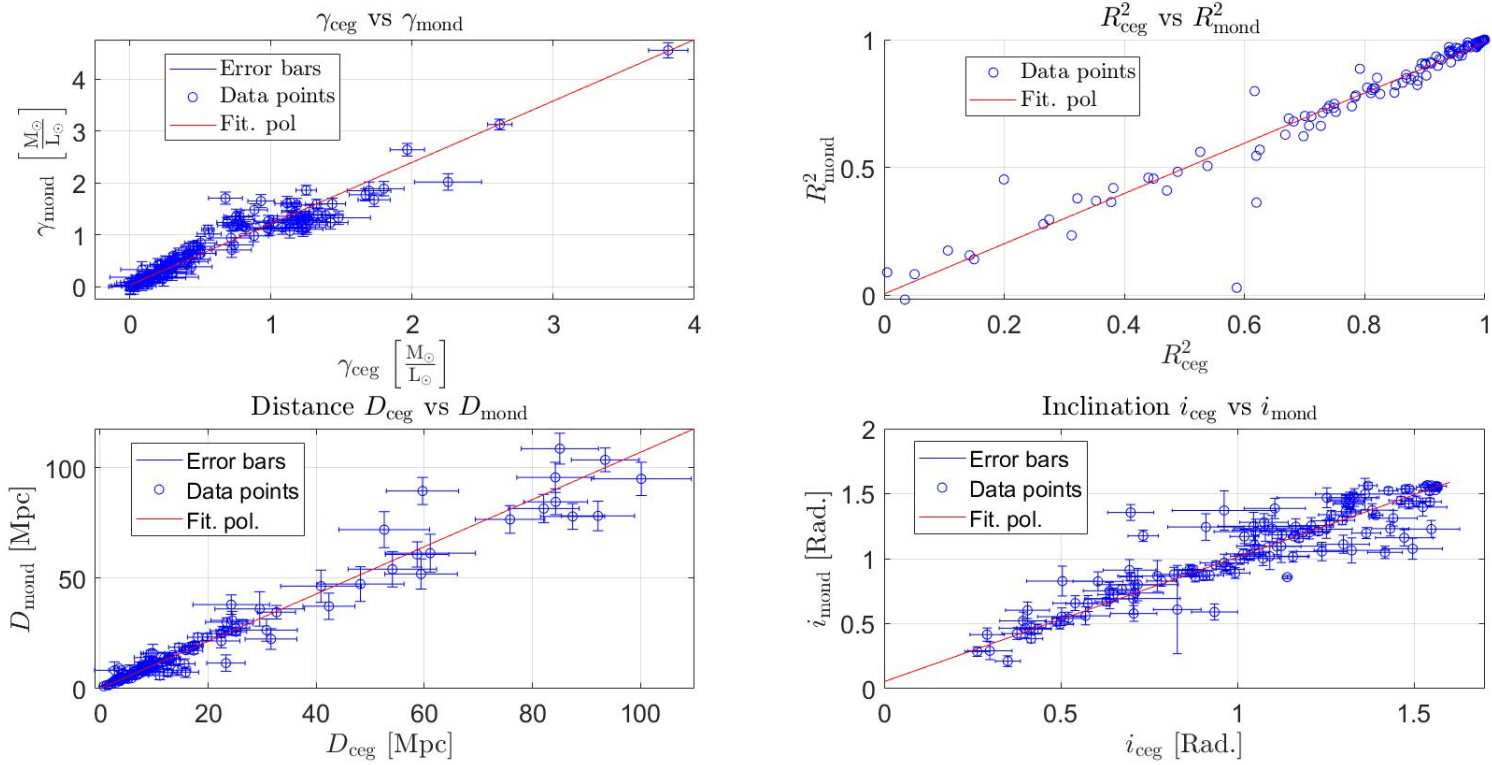


FIGURE 8.6: The figures shows scatter plots between MOND and CEG based on three fitted parameters of the MCMC algorithm applied to 131 galaxies of the SPARC database. We excluded 9 galaxies that were a bad fit ($R^2 < 0$). The top left plot shows the scatter plot between the mass-to-light ratios of the different models. A good fit of the form $y = ax + b$ was obtained with parameters $R^2 = 0.9954$, $a = 1.18 \pm 0.03$, $b = 0.03 \pm 0.02$. The upper right plot shows the scatter between the R^2 values. A good fit was obtained by a line $y = ax + b$ with $R^2 = 0.9311$, $a = 0.98 \pm 0.02$, $b = 0 \pm 0.02$. The bottom left plot shows the scatter between the calculated distances by CEG and MOND. A good fit was obtained by a straight line $y = ax + b$ with $R^2 = 0.9256$, $a = 1.07 \pm 0.03$, $b = 0.1 \pm 0.1$. The bottom right plot shows the inclinations as predicted by both models. We also found a good fit by a straight line $y = ax + b$ with $R^2 = 0.9120$, $a = 0.96 \pm 0.03$, $b = 0.05 \pm 0.04$. The displayed errors are the errors based on the MCMC fittings.

R^2 -value, distance and inclination. In all scatter plot we only considered curves that were good fits ($R^2 > 0$). To all plots we have also fitted a straight line with the errors produced in the fits as weights. The plot in the left upper corner shows the relation between the two mass-to-light ratios, with an excellent fit $R^2 = 0.9954$ provided by a straight line $y = ax + b$ with $a = 1.18 \pm 0.03$ and $b = 0.03 \pm 0.02$. The intersect is almost zero, as it should be, and the slope indicates that MOND has slightly higher mass-to-light ratios. This is already clear from formula 8.3 as CEG has an extra factor of g_{bar} compared to MOND in the Deep-MOND regime ($g_{\text{mon}} \approx \sqrt{a_0 g_{\text{bar}}}$), which yields a lower mass-to-light ratio for CEG. The upper right plot shows the relation between the R^2 -values of the plots. This plot shows that when either MOND or CEG fit the rotation curve, so will the other theory, as the line has a slope of $a = 0.98 \pm 0.02$. This will make it hard to differentiate between the theories on the basis of rotation curves.

A similar story is told by the two lower plots. These plots again have slopes close to unity, showing that the two theories make similar corrections to the distance and inclination. The median correction to the distance of CEG was 0.9208 times the original distance and 0.9635 for MOND. The median correction to the inclination was smaller with 0.9937 for CEG and

1.0208 for MOND. Again, this shows that it will be hard to differentiate between MOND and CEG on the basis of rotation curves.

The results for the inclination and distance are also indicative of the way in which distances and inclinations were determined by the SPARC team. The distance of a galaxy were determined by SPARC using the distances of the galaxy group it is in or the relevant Hubble flow with estimated errors ranging from 5% to 10%. The inclination however, was determined by fitting a tilted-ring to the H_1 velocity profile. This makes the inclination results much more accurate, which is shown in the median values close to unity by CEG and MOND.

We conclude that it is hard to differentiate between MOND or CEG on the basis of rotation curves, even if both the inclination and distance are more accurately known. Other scatter plots were also studied, such as γ_{disk} , Luminosity, Hubble type, error in distance D or inclination i or other variations, but none showed a significant correlation.

Chapter 9 ●■▲

Discussion & Conclusion

In this chapter, we will discuss the consequences and results of CEG as a framework for the gravitational force. This chapter will be split into a discussion on the theoretical chapter and a discussion on the numerical results.

9.1 Theoretical discussion & conclusions

In the theoretical chapters, Verlinde's theory [27] [26], which describes gravity as an emergent phenomenon, was translated into a covariant action formalism using Hossenfelder's CEG [11]. This amounted to introducing a new imposter field u^μ that exerts an extra force on matter through the imposter geodesic equations. This extra force was due to the fact that the introduction of matter into a de Sitter space shifts the horizon and thereby changes the de Sitter entropy of the space. The evolution of the imposter field was thus determined by the baryonic matter via the imposter field equations 5.18.

This new framework came at the cost of introducing an effective metric $\widetilde{g}_{\mu\nu}$ and altering the Einstein field equations 5.30. Whereas we could conveniently ignore the alterations to the Einstein equations, the effective metric proved fundamental to the theory. However, having two metrics raises some ambiguities and questions. These include: 'Which metric describes space-time?' and 'Do existing cosmological models describe the effective or usual metric?'. In the CEG framework, it seems that the metric $g_{\mu\nu}$ is reduced to a mere mathematical tool to raise and lower operators and translate between the imposter field and the effective metric. These questions might be solved by removing the need for an effective metric and having the usual metric satisfy different equations such that the extra force of the imposter field is already present in the usual metric. This might already be possible from the modified Einstein equations 5.30 for the usual metric and imposter field equations 5.18 as presented in this report. Using these two equations, one might be able to find Einstein equations for the effective metric. If such an equation is found, the effective metric could be promoted to the overall metric that is also used to raise and lower operators, nullifying the need for another metric. Attempts to solve for such equations by this author have proven futile.

We also provided a general lensing equation using perturbation methods, yielding a lensing potential, convergence and shear for general lensing systems. We showed that under the usual assumption that the imposter field has only a temporal part, that the amount of matter as predicted by lensing should differ from the amount of matter as predicted by the rotation curves. Such a result could be experimentally verified using data from both rotation curves and strong lensing. Weak lensing does not suffice as the effects are usually so small that only the effects of a large cluster of galaxies can be measured. We would like to note that this derivation was dependent on the assumptions on the imposter field. However, dropping the assumption of u^μ having only a non-zero temporal component would inevitably lead to cross-terms in the effective metric, which would non-trivially alter the path of geodesics

and thus the additional force. This implies that the imposter field equation 5.18 would also become more complicated to solve, possibly altering the form of the imposter field and thus the dark force. Such a change however is not unlikely, as the theory is still in the early stages. The lensing equation derivation in this report can then be applied to the new model.

A cosmological model was also presented in the theoretical section. This model is in its very early stages and the full effects of the imposter field on a cosmological scale should be explored by also considering its contribution to the modified Einstein equations. Such a work is beyond the scope and aim of this report, but could provide an interesting follow-up thesis, considering the ties that the imposter field provides between dark matter and dark energy. Such a report could aim to explain the current discrepancy between the Hubble constant measurements.

9.2 Experimental discussion & conclusions

In the chapters dealing with numerics and observations, we presented both our Fourier-Bessel method to solve for cylindrical symmetric systems in CEG or MOND and our fits of CEG and MOND to the rotation curve from SPARC. Our Fourier-Bessel method provided an excellent method for solving for gravitational problems for cylindrical symmetric densities, as would be expected from such methods. However, a significant deviation in our numerical solution for the dark potential due to boundary effects yielded large deviations in our predicted dark velocities. An altered Fourier-Bessel method was presented, that was significantly less dominated by boundary effects. We then used the latter method to solve for the velocity profile in one of the SPARC galaxies, showing good results. This makes the presented method useful in solving for cylindrical symmetric systems in CEG or MOND, especially in cases that the magnetic term in equation 7.29 provides a non-negligible contribution. Interesting topics to research using this method include the evolution of the galaxy disk and systems in which the magnetic contribution is non-negligible.

In addition, we fitted CEG and MOND to the SPARC database using an MCMC algorithm. Out of the 131 fits, 9 fits (7%) were poor fits ($R^2 < 0$) and 62 galaxies (47%) were excellent fits ($R^2 > 0.9$) and 94 good fits ($R^2 > 0.7$). Because we used three fitting parameters, we also presented the adjusted R^2 -value. These yielded similar results with 54 galaxies excellent adjusted R^2 -values and 86 good fits by previous definitions. We conclude that both theories provided good fits to the rotation curves of the SPARC database. This is in contrast to EG, which was shown to be a bad fit by Lelli et al. [16].

However, the scatter plots between CEG and MOND also showed that it will be hard to differentiate between the two based on the rotation curves of galaxies. Since the Newtonian acceleration as predicted by MOND and CEG are similar, it is also to be expected that CEG inherits several observation difficulties of MOND such as the velocity dispersion profile of globular structures and the temperature profile of galaxy clusters. A true distinction must thus be based on the difference between the covariant versions of the two theories. Such a theoretical investigation is another topic for further research.

The main goal of this thesis was to learn EG and CEG and identify experimentally verifiable results. We conclude that it will be very hard to differentiate between MOND and CEG in Newtonian regimes following our fits of CEG and MOND to 131 galaxies. One should thus focus on covariant differences, such as our lensing formalism or cosmological model.

References

- [1] Baddour, Natalie, and Chouinard, Ugo. “Matlab Code for the Discrete Hankel Transform”. In: *Journal of Open Research Software* 5 (1 2017).
- [2] Bekenstein, Jacob, and Mordehai Milgrom. “Does the missing mass problem signal the breakdown of Newtonian gravity?” In: *Astrophysical Journal* 286 (1984).
- [3] Bekenstein, Jacob D. “Relativistic gravitation theory for the modified Newtonian dynamics paradigm”. In: *Physical Review D* 70 (8 2004).
- [4] Brouwer, Margot M., et al. “First test of Verlinde’s theory of emergent gravity using weak gravitational lensing measurements.” In: *Monthly Notices of the Royal Astronomical Society* 466 (3 2017).
- [5] Carroll, Sean. *Spacetime and Geometry : An Introduction to General Relativity*. San Francisco, Calif: Addison Wesley, 2008.
- [6] Giné, Jaume. “On the origin of the deflection of light”. In: *Chaos, Solitons Fractals* 35 (1 2008).
- [7] Goldstein, Herbert and Poole, Charles and Safko, John. *Classical mechanics*. Addison Wesley, 2002.
- [8] Goodman, Jonathan, and Weare, Jonathan. “Ensemble samplers with affine invariance”. In: *Commun. Appl. Math. Comput. Sci.* 5 (1 2010).
- [9] Greene, Martin A. and Moffat, John W. “Modified Gravity (MOG) fits to observed radial acceleration of SPARC galaxies”. In: *Physics of the Dark Universe* 25 (2019).
- [10] Guizar-Sicairos, Manuel, and Julio C. Gutiérrez-Vega. “Computation of quasi-discrete Hankel transforms of integer order for propagating optical wave fields”. In: *Journal of the Optical Society of America A* 21 (1 2004).
- [11] Hossenfelder, S. “Covariant version of Verlinde’s emergent gravity”. In: *Physical Review D* 95 (12 2017).
- [12] Hossenfelder, Sabine, and Mistele, Thomas. “The Redshift-Dependence of Radial Acceleration: Modified Gravity versus Particle Dark Matter”. In: *International Journal of Modern Physics D* 27 (14 2018).
- [13] Lelli, Federico and McGaugh, Stacy S and Schombert, James M and Desmond, Harry and Katz, Harley. “The baryonic Tully–Fisher relation for different velocity definitions and implications for galaxy angular momentum”. In: *Monthly Notices of the Royal Astronomical Society* 484.3 (2019).
- [14] Lelli, Federico, et al. “Dynamics of starbursting dwarf galaxies: I Zw 18s”. In: *Astronomy & Astrophysics* 537 (2012).
- [15] Lelli, Federico, Stacy S. McGaugh, and James M. Schombert. “SPARC: Mass Models for 175 Disk Galaxies with Spitzer Photometry and Accurate Rotation Curves”. In: *The Astronomical Journal* 152 (6 2016).
- [16] Lelli, Federico, Stacy S. McGaugh, and James M. Schombert. “Testing Verlinde’s Emergent Gravity with the Radial Acceleration Relation”. In: *Monthly Notices of the Royal Astronomical Society Letters* 468 (1 2017).

- [17] Li, Penfei, et al. “Fitting the radial acceleration relation to individual SPARC galaxies”. In: *Astronomy & Astrophysics* 615 (2018).
- [18] Lim, Y. and Wang, Q. “Field equations and particle motion in covariant emergent gravity”. In: *Physical Review D* 98 (12 2018).
- [19] Martinsson, Thomas P. K., et al. “The DiskMass Survey. X. Radio synthesis imaging of spiral galaxies”. In: *Astronomy & Astrophysics* 585 (2016).
- [20] McGaugh, Stacy S., and James M. Schombert. “Color-Mass-to-Light-ratio relations for disk galaxies”. In: *The Astronomical Journal* 148 (5 2014).
- [21] McGaugh, Stacy S., and James M. Schombert. “Weighing galaxy disks with the baryonic Tully–Fisher relation”. In: *The Astrophysical Journal* 802 (1 2015).
- [22] Newton, Isaac. *A Treatise of the Reflections, Refractions, Inflections Colours of Light*. New York: Dover, 1979.
- [23] Roscoe, David. “Modelling the SPARC galaxies using a neo-MOND formalism, and the subsequent derivations of the baryonic Tully-Fisher relation and Freeman’s Law”. In: *arXiv preprint arXiv:1812.03490* (2018).
- [24] Schroeder, Daniel V. *An Introduction to Thermal Physics*. San Francisco, CA: Addison Wesley, 2000.
- [25] Starkman, Nathaniel, et al. “A new algorithm to quantify maximum discs in galaxies”. In: *Monthly Notices of the Royal Astronomical Society* 480 (2 2018).
- [26] Verlinde, Erik P. “Emergent Gravity and the Dark Universe”. In: *SciPost Phys.* 2 (3 2017).
- [27] Verlinde, Erik P. “On the Origin of Gravity and the Laws of Newton”. In: *Journal of High Energy Physics* 29 (4 2011).
- [28] Visser, Matt. “Conservative entropic forces”. In: *Journal of High Energy Physics* 140 (2011).
- [29] Wang, Tower. “Modified entropic gravity revisited”. In: *Science China Physics, Mechanics Astronomy* 57 (9 2014).
- [30] Werner, Michael W., et al. “The Spitzer space telescope mission”. In: *The Astrophysical Journal Supplement Series* 154 (1 2004).

Appendix A

Derivation of the field equations

In this chapter we will derive the field equations from the action 5.15. This section is rather heavy on the algebra, but can also be insightful for readers who are unfamiliar with varying actions in curved space-time.

This part will consist of varying the Lagrangian by means of the Euler-Lagrange equations in curved coordinates. For a single particle with path $x^\mu(\tau)$ parametrized by a parameter τ , the Euler-Lagrange equations in curve space-time are the same as in classical mechanics:

$$\frac{\partial L}{\partial x^\mu} = \frac{d}{d\tau} \frac{\partial L}{\partial(\dot{x}^\mu)} \quad (\text{A.1})$$

The Euler-Lagrange field equations for a field ϕ in curved coordinates are:

$$\frac{\partial \hat{\mathcal{L}}}{\partial \phi} = \nabla_\nu \left(\frac{\partial \hat{\mathcal{L}}}{\partial(\nabla_\nu \phi)} \right) \quad (\text{A.2})$$

The action we are interested in is was formulated in the chapter on the field equations in the report and is stated here for convenience:

$$S(g^{\mu\nu}, u_\mu, \rho, v^\mu) = \iiint \sqrt{-g} \left[\frac{1}{16\pi G} R + \frac{\alpha}{16\pi G} \chi^{\frac{3}{2}} + \frac{\beta}{2} \frac{u_\mu u_\nu}{u} T^{\mu\nu} \right] dx^\gamma + S_m \quad (\text{A.3})$$

A.1 Geodesic Equation

Before we calculate the imposter field equations and modified Einstein equations by varying the action A.3, we will first focus on the imposter geodesic equations. This is because these equations are easier to derive, as we can simply use the known Euler-Lagrange equations, and will serve as a warm-up for the tensor algebra needed to derive the field equations later.

The imposter field equations can be found by varying our action with respect to the path x^μ a single particle takes, thus varying with respect to δx^μ . The only terms in our action A.3 that depends directly on the path of the particle are the interaction and mass terms. As we saw in the report, the interaction action was chosen such that the interaction action plus the mass action yields a total action of:

$$S = \int \sqrt{-\widetilde{g}_{\mu\nu} \dot{x}^\mu \dot{x}^\nu} d\tau \quad (\text{A.4})$$

This is simply a normal action for a single particle but this time with respect to the effective metric. This was because we wanted particles to follow geodesics with respect to this effective metric. According to Sabine Hossenfelder [11], the particles feels an effective metric

$$\widetilde{g}_{\mu\nu} = g_{\mu\nu} - \beta \frac{u_\mu u_\nu}{u} \quad (\text{A.5})$$

This implies that the corresponding action for a single particle is indeed:

$$S = \int L d\tau \quad L = \sqrt{-\widetilde{g}_{\mu\nu}\dot{x}^\mu\dot{x}^\nu} \quad (\text{A.6})$$

We now choose the parametrization such that $\widetilde{g}_{\mu\nu}\dot{x}^\mu\dot{x}^\nu = -1$, which we will call τ for convenience. As this is not a Lagrangian density but simply a Lagrangian, we must satisfy the usual Euler-Lagrange equations from classical mechanics, which are stated in formula A.1. The first derivative yields:

$$\frac{\partial L}{\partial x^\alpha} = \frac{1}{\sqrt{-\widetilde{g}_{\mu\nu}\dot{x}^\mu\dot{x}^\nu}} \left(-\frac{1}{2}\dot{x}^\mu\dot{x}^\nu \frac{\partial}{\partial x^\alpha} \widetilde{g}_{\mu\nu} \right) = \left(-\frac{1}{2}\dot{x}^\mu\dot{x}^\nu \frac{\partial}{\partial x^\alpha} \widetilde{g}_{\mu\nu} \right) \quad (\text{A.7})$$

The derivative with respect to τ yields the following expression using our parametrization:

$$\frac{d}{d\tau} \frac{\partial L}{\partial (\dot{x}^\alpha)} = \frac{d}{d\tau} \left[\frac{1}{\sqrt{-\widetilde{g}_{\mu\nu}\dot{x}^\mu\dot{x}^\nu}} (-\dot{x}^\nu \widetilde{g}_{\alpha\nu}) \right] = -\ddot{x}^\nu \widetilde{g}_{\alpha\nu} - \dot{x}^\nu \frac{d}{d\tau} \widetilde{g}_{\alpha\nu} \quad (\text{A.8})$$

The the Euler-Lagrange equations then lead to:

$$\ddot{x}^\nu \widetilde{g}_{\alpha\nu} + \dot{x}^\nu \frac{d}{d\tau} \widetilde{g}_{\alpha\nu} = \frac{1}{2} \dot{x}^\mu \dot{x}^\nu \frac{\partial}{\partial x^\alpha} \widetilde{g}_{\mu\nu} \quad (\text{A.9})$$

As we still raise and lower using the normal metric, these equation are not equivalent to the geodesic equations for the normal metric replaced with the effective metric. Reintroducing the field u^μ yields:

$$\ddot{x}^\nu (g_{\alpha\nu} - \beta \frac{u_\alpha u_\nu}{u}) + \dot{x}^\nu \frac{d}{d\tau} (g_{\alpha\nu} - \beta \frac{u_\alpha u_\nu}{u}) = \frac{1}{2} \dot{x}^\mu \dot{x}^\nu \frac{\partial}{\partial x^\alpha} (g_{\alpha\nu} - \beta \frac{u_\alpha u_\nu}{u}) \quad (\text{A.10})$$

This equation can be simplified by introducing the inverse metric: Let $g^{\mu\nu}$ denote the inverse metric of $g_{\mu\nu}$. Upon multiplying with the inverse metric:

$$\ddot{x}^\delta - \beta \frac{u^\delta u_\nu}{u} \ddot{x}^\nu + \dot{x}^\nu g^{\delta\alpha} \frac{d}{d\tau} (g_{\alpha\nu} - \beta \frac{u_\alpha u_\nu}{u}) = \frac{1}{2} \dot{x}^\mu \dot{x}^\nu g^{\delta\alpha} \frac{\partial}{\partial x^\alpha} (g_{\alpha\nu} - \beta \frac{u_\alpha u_\nu}{u}) \quad (\text{A.11})$$

Upon reintroducing the familiar Christoffel symbols $\Gamma_{\mu\nu}^\delta$, we obtain:

$$\ddot{x}^\delta - \beta \frac{u^\delta u_\nu}{u} \ddot{x}^\nu + \dot{x}^\nu g^{\delta\alpha} \frac{d}{d\tau} (-\beta \frac{u_\alpha u_\nu}{u}) = -\dot{x}^\mu \dot{x}^\nu \Gamma_{\mu\nu}^\delta + \frac{1}{2} \dot{x}^\mu \dot{x}^\nu g^{\delta\alpha} \frac{\partial}{\partial x^\alpha} (-\beta \frac{u_\mu u_\nu}{u}) \quad (\text{A.12})$$

As is done by Yen-Kheng Lim and Qing-hai Wang, we simplify these equations by using the imposter Christoffel symbols:

$$C_{\mu\nu}^\delta = \frac{1}{2} g^{\delta\alpha} \left[\partial_\mu \left(\frac{u_\alpha u_\nu}{u} \right) + \partial_\nu \left(\frac{u_\alpha u_\mu}{u} \right) - \partial_\alpha \left(\frac{u_\mu u_\nu}{u} \right) \right] \quad (\text{A.13})$$

The equations then become:

$$\ddot{x}^\delta - \beta \frac{u^\delta u_\nu}{u} \ddot{x}^\nu = \dot{x}^\mu \dot{x}^\nu \left(\beta C_{\mu\nu}^\delta - \Gamma_{\mu\nu}^\delta \right) \quad (\text{A.14})$$

Thus the main contribution of the imposter field u^μ to the motion of our particle comes from the tensor $C_{\mu\nu}^\delta$. The effects of the modification of the geodesic equations due to the imposter field are studied in the relevant sections of the report.

We can actually apply the Lagrangian method, namely formula A.2, theory to the field u^μ to recover the field equations. However, this method can not be used to derive the Einstein equations for $g^{\mu\nu}$ as varying these equations also changes the term $\sqrt{-g}$ in the integral of the action, which is not taken into account when deriving the Euler-Lagrange field equation.

A.2 The imposter field equations

Now that we know how particles respond to the effective metric, it is time to determine the effective metric by finding the field equations for u_μ and $g^{\mu\nu}$. We will do this step by step, starting by analysing how the field χ varies with respect to the imposter field u_μ . Firstly, we introduce a set of tensors, which were taken from the paper of Yen-Kheng Lim & Qing-hai Wang [18]. The paper of Yen-Kheng Lim & Qing-hai Wang only stated the endresults, which is why we have included a derivation in this paper. Let us first introduce several important tensors, starting with the imposter field scalar:

$$\chi = \bar{a}(\nabla_\mu u^\mu)^2 + \bar{b}(\nabla_\mu u_\nu)(\nabla^\mu u^\nu) + \bar{d}(\nabla_\mu u_\nu)(\nabla^\nu u^\mu) \quad (\text{A.15})$$

Let us further introduce the strain tensor as:

$$\epsilon_{\mu\nu} = \nabla_\mu u_\nu + \nabla_\nu u_\mu \quad (\text{A.16})$$

And the stress tensor is defined as:

$$F_{\mu\nu} = \nabla_\mu u_\nu - \nabla_\nu u_\mu \quad (\text{A.17})$$

This enables us to write $\nabla_\mu u_\nu = \frac{\epsilon_{\mu\nu} + F_{\mu\nu}}{2}$. These two tensors allow use to write the imposter field scalar χ in terms of strains and stresses. Upon substitution in equation A.15 and noting that $F^{\mu\mu} = 0$ and that $\epsilon_{\mu\nu}F^{\mu\nu} = -\epsilon_{\mu\nu}F^{\mu\nu} = 0$ for $\mu = 0, 1, 2, 3$, we obtain:

$$\chi = \frac{\bar{a}}{4}(\epsilon_\mu^\mu)^2 + \frac{\bar{b} + \bar{d}}{4}\epsilon^{\mu\nu}\epsilon_{\mu\nu} + \frac{\bar{b} - \bar{d}}{4}F^{\mu\nu}F_{\mu\nu} \quad (\text{A.18})$$

In order to avoid cluttering of constants, let us start by substituting $a = \frac{\bar{a}}{2}$, $b = \frac{\bar{b} + \bar{d}}{2}$ and $d = \frac{\bar{b} - \bar{d}}{2}$. Then our imposter field scalar becomes:

$$\chi = \frac{a}{2}(\epsilon_\mu^\mu)^2 + \frac{b}{2}\epsilon^{\mu\nu}\epsilon_{\mu\nu} + \frac{d}{2}F^{\mu\nu}F_{\mu\nu} \quad (\text{A.19})$$

Now as we must vary the imposter field χ , it is important to know how the strain and stress tensor vary respectively.

Upon varying with respect to u^μ we obtain:

$$\delta\epsilon_{\mu\nu} = \nabla_\mu\delta u_\nu + \nabla_\nu\delta u_\mu \quad , \quad \delta F_{\mu\nu} = \nabla_\mu\delta u_\nu - \nabla_\nu\delta u_\mu \quad (\text{A.20})$$

This allows us to consider how the various components of χ vary with respect to the field u^μ :

$$\delta(\epsilon_\mu^\mu)^2 = 4\epsilon_\lambda^\lambda\nabla^\nu\delta u_\nu = 4\epsilon_\lambda^\lambda g^{\mu\nu}\nabla_\mu\delta u_\nu \quad (\text{A.21})$$

$$\delta(\epsilon_{\mu\nu}\epsilon^{\mu\nu}) = \epsilon_{\mu\nu}(\nabla^\mu\delta u^\nu + \nabla^\nu\delta u^\mu) + (\nabla_\mu\delta u_\nu + \nabla_\nu\delta u_\mu)\epsilon^{\mu\nu} = 4\epsilon^{\mu\nu}\nabla_\mu\delta u_\nu \quad (\text{A.22})$$

$$\delta(F_{\mu\nu}F^{\mu\nu}) = F_{\mu\nu}(\nabla^\mu \delta u^\nu - \nabla^\nu \delta u^\mu) + (\nabla_\mu \delta u_\nu - \nabla_\nu \delta u_\mu)F^{\mu\nu} = 4F^{\mu\nu}\nabla_\mu \delta u_\nu \quad (\text{A.23})$$

We can thus determine how our imposter scalar field χ varies with respect to u^μ if we simply add these three components:

$$\delta\chi = 2B^{\mu\nu}\nabla_\mu \delta u_\nu \quad \text{with} \quad B^{\mu\nu} = a\epsilon_\lambda^\lambda g^{\mu\nu} + b\epsilon^{\mu\nu} + dF^{\mu\nu} \quad (\text{A.24})$$

Here we have introduced another tensor in anticipation of our results. What other components in our action A.3 change when we vary u^μ if we ignore backreactions? Well the interaction term of course. The variation of the interaction term is easily determined as:

$$\delta\mathcal{L}_{\text{int}} = \delta\left(\frac{\beta}{2}\frac{u^\mu u^\nu}{u}T_{\mu\nu}\right) = \frac{\beta}{2}\left[2T^{\mu\nu}\frac{u_\mu}{u} + \frac{T^{\mu\lambda}u_\mu u_\lambda u^\nu}{u^3}\right]\delta u_\nu \quad (\text{A.25})$$

As we now know how to vary the scalar field, we can also determine the perturbation to the source term if we only vary u^μ :

$$\delta\mathcal{L}_{\text{source}} = \delta\left(\frac{\alpha}{16\pi G}\chi^{3/2}\right) = \frac{1}{2}\frac{3\alpha}{16\pi G}\chi^{1/2}\delta\chi = \frac{3\alpha}{16\pi G}\chi^{1/2}B^{\mu\nu}\nabla_\mu \delta u_\nu \quad (\text{A.26})$$

Thus stating that the sum of these perturbations should vary up to first order and using integration by parts to get rid of the covariant derivative yields the imposter field equations:

$$\boxed{\frac{3\alpha}{16\pi G}\nabla_\mu\left(\chi^{1/2}B^{\mu\nu}\right) = \frac{\beta}{2}\left[2T^{\mu\nu}\frac{u_\mu}{u} + \frac{T^{\mu\lambda}u_\mu u_\lambda u^\nu}{u^3}\right]} \quad (\text{A.27})$$

These are the imposter field equations of u_ν , assuming that $\delta u^\nu = 0$ on the boundary of space-time. For comments on these equations, see the section on these equations in the report.

A.3 The modified Einstein field equations

Now that we know how our imposter field scalar χ varies with respect to u^μ , it is time to find out how it varies with respect to the inverse metric $g^{\mu\nu}$ in order to solve for the field equations for $g^{\mu\nu}$. Remember that we are interested in the action:

$$S = \iiint\int \sqrt{-g}\left[\frac{1}{16\pi G}R + \frac{\alpha}{16\pi G}\chi^{3/2} + \frac{\beta}{2}\frac{u_\mu u_\nu}{u}T^{\mu\nu}\right]dx^\gamma + S_m \quad (\text{A.28})$$

Varying the first term in this action with respect to the inverse metric simply yields the left-hand side of the Einstein field equations and varying the mass term S_m yields the right-hand side. Let us therefore mainly focus on how the imposter source term and interaction term vary with respect to the inverse metric. Let us start by examining how the imposter scalar field varies with respect to the inverse metric.

As was the case in varying with respect to the imposter field, let us first see how the strain and stress tensor vary with respect to $g^{\mu\nu}$. This time it is important to keep track of whether an index is a superscript or subscript, which was less important in the case of the imposter field variations. We find that the strain tensor varies as:

$$\delta\epsilon_{\mu\nu} = -(2\delta\Gamma_{\mu\nu}^\alpha u_\alpha) \quad (\text{A.29})$$

$$\delta\epsilon_\nu^\mu = \delta(g^{\mu\lambda}\epsilon_{\lambda\nu}) = g^{\mu\lambda}\delta\epsilon_{\lambda\nu} + \delta g^{\mu\lambda}\epsilon_{\lambda\nu} = \epsilon_{\lambda\nu}\delta g^{\mu\lambda} - g^{\mu\lambda}(2\delta\Gamma_{\lambda\nu}^\alpha u_\alpha) \quad (\text{A.30})$$

$$\delta\epsilon^{\mu\nu} = -(2\delta\Gamma_{\beta\gamma}^\alpha u_\alpha)g^{\beta\mu}g^{\gamma\nu} + \epsilon_\gamma^\nu\delta g^{\gamma\mu} + \epsilon_\gamma^\mu\delta g^{\gamma\nu} \quad (\text{A.31})$$

Applying the same logic to the stress tensor yields:

$$\delta F_{\mu\nu} = 0 \quad (\text{A.32})$$

$$\delta F^{\mu\nu} = F_{\beta\gamma}\delta g^{\beta\mu}g^{\gamma\nu} + F_{\beta\gamma}g^{\beta\mu}\delta g^{\gamma\nu} \quad (\text{A.33})$$

We can now ask ourselves how the individual components of the imposter field scalar χ vary with respect to the inverse metric:

$$\delta(\epsilon_\mu^\mu)^2 = 2\epsilon_\mu^\mu[\epsilon_{\lambda\alpha}\delta g^{\alpha\lambda} - g^{\beta\lambda}(2\delta\Gamma_{\lambda\beta}^\alpha u_\alpha)] \quad (\text{A.34})$$

$$\delta(\epsilon_{\mu\nu}\epsilon^{\mu\nu}) = \delta\epsilon_{\mu\nu}\epsilon^{\mu\nu} + \epsilon_{\mu\nu}\delta\epsilon^{\mu\nu} = (2\delta\Gamma_{\mu\nu}^\alpha u_\alpha)\epsilon^{\mu\nu} + \epsilon^{\beta\gamma}(2\delta\Gamma_{\beta\gamma}^\alpha u_\alpha) + 2\epsilon_{\mu\lambda}\epsilon_\nu^\lambda\delta g^{\mu\nu} \quad (\text{A.35})$$

$$\delta(F^{\mu\nu}F_{\mu\nu}) = F_{\mu\nu}(F_\beta^\nu\delta g^{\beta\mu} + F_\gamma^\mu\delta g^{\gamma\nu}) = 2F_{\mu\lambda}F_\nu^\lambda\delta g^{\mu\nu} \quad (\text{A.36})$$

Notice that these variations also include the variations of the Christoffel symbols. These were left out by Hossenfelder [11] in her variations, which is why she recovered different modified Einstein equations. This was noted by Yen-Kheng Lim & Qing-hai Wang and the author of this paper shares their opinion.

Now, if we sum all the variations of the components of χ containing $\delta g^{\mu\nu}$. We will first ignore the variations in the Christoffel symbols. These variations are added later due to their complexity. The variations due to a variation in the inverse metric are:

$$\frac{a}{2}2\epsilon_\mu^\mu\epsilon_{\lambda\alpha}\delta g^{\alpha\lambda} + \frac{b}{2}2\epsilon_{\mu\lambda}\epsilon_\nu^\lambda\delta g^{\mu\nu} + \frac{d}{2}2F_{\mu\lambda}F_\nu^\lambda\delta g^{\mu\nu} = A_{\mu\nu}\delta g^{\mu\nu} \quad (\text{A.37})$$

In which we have defined a new tensor $A_{\mu\nu}$ to abbreviate the results:

$$A_{\mu\nu} = a\epsilon_\lambda^\lambda\epsilon_{\mu\nu} + b\epsilon_{\mu\lambda}\epsilon_\nu^\lambda + dF_{\mu\lambda}F_\nu^\lambda \quad (\text{A.38})$$

The sum of all the variations of the components of χ containing $\delta\Gamma_{\mu\nu}^\lambda u^\lambda$ yield:

$$-\frac{a}{2}2\epsilon_\alpha^\alpha(2g^{\mu\nu}\delta\Gamma_{\mu\nu}^\lambda u_\lambda) - \frac{b}{2}(4\delta\Gamma_{\mu\nu}^\lambda u_\lambda)\epsilon^{\mu\nu} \quad (\text{A.39})$$

Notice that this time, the anti-symmetric tensors do not contribute and we cannot simply use $A_{\mu\nu}$ or $B_{\mu\nu}$ again. However, we would still like a compact formula, thus we will add $0 = -\frac{d}{2}(4\delta\Gamma_{\mu\nu}^\lambda u_\lambda)F^{\mu\nu}$ to the previous result, in order to recover:

$$-\frac{a}{2}2\epsilon_\alpha^\alpha(2g^{\mu\nu}\delta\Gamma_{\mu\nu}^\lambda u_\lambda) - \frac{b}{2}(4\delta\Gamma_{\mu\nu}^\lambda u_\lambda)\epsilon^{\mu\nu} - \frac{d}{2}(4\delta\Gamma_{\mu\nu}^\lambda u_\lambda)F^{\mu\nu} = -2B^{\mu\nu}u_\lambda\Gamma_{\mu\nu}^\lambda \quad (\text{A.40})$$

Thus upon adding the variation with respect to the inverse metric and the Christoffel symbols of χ , we obtain:

$$\delta\chi = A_{\mu\nu}\delta g^{\mu\nu} - 2B^{\mu\nu}u_\lambda\delta\Gamma_{\mu\nu}^\lambda \quad (\text{A.41})$$

For the definiteness, we also include the variation of χ with respect to all its variables:

$$\delta\chi = A_{\mu\nu}\delta g^{\mu\nu} + 2B^{\mu\nu}(\nabla_\mu\delta u_\nu - u_\lambda\delta\Gamma_{\mu\nu}^\lambda) \quad (\text{A.42})$$

We almost know how are scalar field varies with respect to the inverse metric. All that is left is to calculate variation of the Christoffel symbols with respect to the inverse metric:

$$\delta\Gamma_{\mu\nu}^{\lambda} = \frac{1}{2} \left[\delta g^{\lambda\sigma} (\partial_{\mu} g_{\sigma\nu} + \partial_{\nu} g_{\sigma\mu} - \partial_{\sigma} g_{\mu\nu}) + g^{\lambda\sigma} (\partial_{\mu} \delta g_{\sigma\nu} + \partial_{\nu} \delta g_{\sigma\mu} - \partial_{\sigma} \delta g_{\mu\nu}) \right] \quad (\text{A.43})$$

These results however, can be simplified by evaluating this expression in a flat coordinate system. Since $\delta\Gamma_{\mu\nu}^{\lambda}$ is a tensor, we obtain in a locally flat coordinate system with coordinates indicated by hats:

$$\delta\Gamma_{\hat{\mu}\hat{\nu}}^{\hat{\lambda}} = \frac{1}{2} \left[g^{\hat{\lambda}\hat{\sigma}} (\partial_{\hat{\mu}} \delta g_{\hat{\sigma}\hat{\nu}} + \partial_{\hat{\nu}} \delta g_{\hat{\sigma}\hat{\mu}} - \partial_{\hat{\sigma}} \delta g_{\hat{\mu}\hat{\nu}}) \right] + 0 = \frac{1}{2} \left[g^{\hat{\lambda}\hat{\sigma}} (\nabla_{\hat{\mu}} \delta g_{\hat{\sigma}\hat{\nu}} + \nabla_{\hat{\nu}} \delta g_{\hat{\sigma}\hat{\mu}} - \nabla_{\hat{\sigma}} \delta g_{\hat{\mu}\hat{\nu}}) \right] \quad (\text{A.44})$$

Since $\delta\Gamma_{\mu\nu}^{\lambda}$ is a tensor, we would obtain the same tensorial expression in any coordinate system:

$$\delta\Gamma_{\mu\nu}^{\lambda} = \frac{1}{2} g^{\lambda\sigma} (\nabla_{\mu} \delta g_{\sigma\nu} + \nabla_{\nu} \delta g_{\sigma\mu} - \nabla_{\sigma} \delta g_{\mu\nu}) \quad (\text{A.45})$$

But we want an expression for the inverse metric. Luckily we have the identity:

$$\delta g_{\mu\nu} = -g_{\mu\rho} g_{\nu\lambda} \delta g^{\rho\lambda} \quad (\text{A.46})$$

This allows us to rewrite the variations with respect to the metric into variations with respect to the inverse metric. Our variations in the Christoffel symbols thus become:

$$\delta\Gamma_{\mu\nu}^{\lambda} = \frac{1}{2} g^{\lambda\sigma} (-g_{\sigma\alpha} g_{\nu\rho} \nabla_{\mu} \delta g^{\alpha\rho} - g_{\sigma\alpha} g_{\mu\rho} \nabla_{\nu} \delta g^{\alpha\rho} + g_{\mu\rho} g_{\nu\alpha} \nabla_{\sigma} \delta g^{\rho\alpha}) \quad (\text{A.47})$$

Upon using properties of the metric, we obtain:

$$\delta\Gamma_{\mu\nu}^{\lambda} = \frac{1}{2} \left(-g_{\nu\rho} \nabla_{\mu} \delta g^{\lambda\rho} - g_{\mu\rho} \nabla_{\nu} \delta g^{\lambda\rho} + g_{\mu\rho} g_{\nu\alpha} \nabla^{\lambda} \delta g^{\rho\alpha} \right) \quad (\text{A.48})$$

This is the expression for the variations in the Christoffel symbols we were after. This allows us to finally write the variations with respect to the Christoffel symbols in our scalar field χ in terms of variations with respect to the inverse metric:

$$2B^{\mu\nu} u_{\lambda} \delta\Gamma_{\mu\nu}^{\lambda} = B^{\mu\nu} u_{\lambda} \left(-g_{\nu\rho} \nabla_{\mu} \delta g^{\lambda\rho} - g_{\mu\rho} \nabla_{\nu} \delta g^{\lambda\rho} + g_{\mu\rho} g_{\nu\alpha} \nabla^{\lambda} \delta g^{\rho\alpha} \right) \quad (\text{A.49})$$

Upon permuting indices:

$$2B^{\mu\nu} u_{\lambda} \delta\Gamma_{\mu\nu}^{\lambda} = -u_{\nu} B^{\alpha}_{\mu} \nabla_{\alpha} \delta g^{\mu\nu} - u_{\nu} B_{\mu}^{\alpha} \nabla_{\alpha} \delta g^{\mu\nu} + B_{\mu\nu} u^{\alpha} \nabla_{\alpha} \delta g^{\mu\nu} \quad (\text{A.50})$$

Since the variations $g^{\mu\nu}$ have to be symmetric, we can neglect the anti-symmetric components within this contraction, since for every anti-symmetric tensor $F_{\mu\nu}$, $F_{\mu\nu} \delta g^{\mu\nu} = 0$. Thus we obtain:

$$2B^{\mu\nu} u_{\lambda} \delta\Gamma_{\mu\nu}^{\lambda} = -B^{\alpha}_{(\mu} u_{\nu)} \nabla_{\alpha} \delta g^{\mu\nu} - u_{(\nu} B_{\mu)}^{\alpha} \nabla_{\alpha} \delta g^{\mu\nu} + B_{(\mu\nu)} u^{\alpha} \nabla_{\alpha} \delta g^{\mu\nu} \quad (\text{A.51})$$

The brackets indicate the symmetric part of a tensor, thus:

$$T_{(\mu\nu)} = \frac{1}{2} (T_{\mu\nu} + T_{\nu\mu}) \quad (\text{A.52})$$

This allows us to finally write:

$$\delta\chi = A_{\mu\nu} \delta g^{\mu\nu} + B^{\alpha}_{(\mu} u_{\nu)} \nabla_{\alpha} \delta g^{\mu\nu} + u_{(\nu} B_{\mu)}^{\alpha} \nabla_{\alpha} \delta g^{\mu\nu} - B_{(\mu\nu)} u^{\alpha} \nabla_{\alpha} \delta g^{\mu\nu} \quad (\text{A.53})$$

Since we assume that the variation of the metric at the boundary is zero, we can determine the following variation (using partial integration):

$$\delta \left(\chi^{\frac{3}{2}} \right) = \frac{3}{2} \chi^{\frac{1}{2}} \delta \chi = \frac{3}{2} \chi^{\frac{1}{2}} A_{\mu\nu} \delta g^{\mu\nu} - \frac{3}{2} \nabla_{\alpha} \left[\chi^{\frac{1}{2}} \left(B^{\alpha}_{(\mu} u_{\nu)} + u_{(\nu} B_{\mu)}^{\alpha} - B_{(\mu\nu)} u^{\alpha} \right) \right] \delta g^{\mu\nu} \quad (\text{A.54})$$

Thus we finally figured out how to vary the imposter field scalar with respect to the inverse metric. Accounting for the square root of the metric, the source term has a variations of:

$$\delta L_{\text{source}} = \delta \left(\sqrt{-g} \frac{\alpha}{16\pi G} \chi^{\frac{3}{2}} \right) \quad (\text{A.55})$$

The variation of $\sqrt{-g}$ with respect to the inverse metric is a known quantity, namely:

$$\delta \sqrt{-g} = \frac{-\sqrt{-g}}{2} g_{\mu\nu} \delta g^{\mu\nu} \quad (\text{A.56})$$

Since we know the variation of the imposter field scalar, this yields a variation of the density Lagrangian of the source term using the product rule as:

$$\frac{\delta \mathcal{L}_{\text{source}}}{\delta g^{\mu\nu}} = \frac{\alpha}{16\pi G} \frac{3}{2} \chi^{\frac{1}{2}} A_{\mu\nu} - \frac{\alpha}{16\pi G} \frac{3}{2} \nabla_{\alpha} \left[\chi^{\frac{1}{2}} \left(B^{\alpha}_{(\mu} u_{\nu)} + u_{(\nu} B_{\mu)}^{\alpha} - B_{(\mu\nu)} u^{\alpha} \right) \right] \quad (\text{A.57})$$

We are almost done. All that is left is to vary the other terms in the action with respect to the inverse metric. By definition:

$$\delta S_m = \frac{-\sqrt{-g}}{2} T_{\mu\nu} \delta g^{\mu\nu} \quad (\text{A.58})$$

Furthermore, it is known from general relativity that the Ricci scalar has the following variation:

$$\delta R = R_{\mu\nu} \delta g^{\mu\nu} \quad (\text{A.59})$$

Thus all that is left is to vary the interaction term:

$$\frac{\delta L_{\text{int}}}{\delta g^{\mu\nu}} = \delta \left(\sqrt{-g} \frac{\beta}{2} \frac{u_{\mu} u_{\nu}}{u} T^{\alpha\beta} \right) = \frac{-\sqrt{-g}}{2} g_{\mu\nu} \frac{\beta}{2} \frac{u_{\alpha} u_{\beta}}{u} T^{\alpha\beta} + \sqrt{-g} \frac{\beta}{2} \left[\frac{u_{\alpha} u_{\beta}}{2u^3} u_{\mu} u_{\nu} T^{\alpha\beta} + \frac{2u_{\beta}}{u} u_{(\mu} T_{\nu)}^{\beta} \right] \quad (\text{A.60})$$

Now using that the total variation of the sum of our Lagrangians must be zero, we obtain the modified Einstein field equations:

$$\begin{aligned} R_{\mu\nu} - \frac{1}{2} g_{\mu\nu} R = 8\pi G T_{\mu\nu} - \frac{1}{2} g_{\mu\nu} \left[\alpha \chi^{\frac{3}{2}} + 8\pi G \beta \frac{u_{\alpha} u_{\beta}}{u} T^{\alpha\beta} \right] + \frac{3\alpha}{2} \chi^{\frac{1}{2}} A_{\mu\nu} - \\ \frac{3\alpha}{2} \nabla_{\alpha} \left[\chi^{\frac{1}{2}} \left(B^{\alpha}_{(\mu} u_{\nu)} + u_{(\nu} B_{\mu)}^{\alpha} - B_{(\mu\nu)} u^{\alpha} \right) \right] - \\ 8\pi G \beta \left[\frac{u_{\alpha} u_{\beta}}{2u^3} u_{\mu} u_{\nu} T^{\alpha\beta} + \frac{2u_{\beta}}{u} u_{(\mu} T_{\nu)}^{\beta} \right] \end{aligned} \quad (\text{A.61})$$

The first terms of which are the original Einstein equations as mentioned in the section of the field equations in formula 5.37. For comments on these modified Einstein equations see the relevant sections in the report. As a final exercise in tensor calculations, let us calculate the stress-energy tensor of the field:

A.4 Energy momentum tensor

The stress-energy tensor $\tilde{T}_{\mu\nu}$ of a source Lagrangian density $\mathcal{L}_{\text{source}}$ is found by:

$$\tilde{T}_{\mu\nu} = 2 \frac{\delta \mathcal{L}_{\text{source}}}{\delta g^{\mu\nu}} - g_{\mu\nu} \mathcal{L}_{\text{source}} \quad (\text{A.62})$$

One does not actually have to calculate the stress-energy tensor from this expression as we already know what the stress-energy tensor of the field is from our variations of the source term with respect to the inverse metric $g^{\mu\nu}$. The stress-energy tensor is then exactly the contribution of the source term to the modified Einstein equations. This yields:

$$\tilde{T}_{\mu\nu} = \frac{\alpha}{16\pi G} \left[3\chi^{\frac{1}{2}} A_{\mu\nu} - g_{\mu\nu} \chi^{\frac{3}{2}} - 3\nabla_{\alpha} \left[\chi^{\frac{1}{2}} \left(B^{\alpha}_{(\mu} u_{\nu)} + u_{(\nu} B_{\mu)}^{\alpha} - B_{(\mu\nu)} u^{\alpha} \right) \right] \right] \quad (\text{A.63})$$

This is in general not equal to the Noether stress-energy momentum tensor of the field. In Hossenfelder's paper, she argued that a constant field $u_{\mu} = (u, 0, 0, 0)$ could only have a conserved energy momentum tensor and fulfill the equations of motion if:

$$-3\bar{a} = 4\bar{b} + 4\bar{d} \implies 3a + 4b = 0 \quad (\text{A.64})$$

In the paper by Yen-Kheng Lim & Qing-hai Wang [18], they argue for the constraint:

$$3a + b = 0 \quad (\text{A.65})$$

We will test this assumption as Hossenfelder did in the easiest non-flat background, namely a de-Sitter space with static coordinates in the next section.

Appendix B

Constraints on coefficients imposter field scalar

B.1 Constraints in De Sitter space

In her paper, Hossenfelder [11] claims that if we want to allow for a non-changing static imposter field in a De Sitter space, which is required for Erik Verlinde's theory, the only possible combination for the constants $\bar{a}, \bar{b}, \bar{d}$ is:

$$-3\bar{a} = 4\bar{b} + 4\bar{d} \implies 3a + 4b = 0 \quad (\text{B.1})$$

In the paper by Yen-Kheng Lim & Qing-hai Wang [18], they argue for the constraint:

$$3a + b = 0 \quad (\text{B.2})$$

We will indeed prove the latter by proving that a static imposter field can only occur when this second constraint is satisfied by solving the imposter field equations. First let us solve for the imposter field scalar. The de Sitter universe in Lemaître-Robertson form is:

$$ds^2 = -dt^2 + e^{2Ht} [dx^2 + dy^2 + dz^2] \quad (\text{B.3})$$

For u^0 we obtain:

$$\nabla_{\mu} u_{\nu} = \partial_{\mu} u^{\nu} - \Gamma_{\mu\nu}^{\lambda} u_{\lambda} = 0 - \Gamma_{\mu\nu}^0 u_0 = \Gamma_{\mu\nu}^0 u^0 \quad (\text{B.4})$$

Before introducing the strain and stress tensor, let us define a matrix $\mathcal{J} = \text{diag}(0, 1, 1, 1)$ in order to simplify our results:

$$\mathcal{J} = \begin{bmatrix} 0 & 0 & 0 & 0 \\ 0 & 1 & 0 & 0 \\ 0 & 0 & 1 & 0 \\ 0 & 0 & 0 & 1 \end{bmatrix} \quad (\text{B.5})$$

Since we know the metric, we can solve for the Christoffel symbols and thus the strain and stress tensors. This implies for our strain and stress tensors: For our strain and stress tensor these imply:

$$\epsilon_{\mu\nu} = 2He^{2Ht} u^0 \mathcal{J} \quad , \quad F_{\mu\nu} = 0 \quad (\text{B.6})$$

Using the metric, this allows us to solve for the superscript components as:

$$\epsilon^{\mu\nu} = 2He^{-2Ht} u^0 \mathcal{J} \quad \epsilon_{\nu\lambda} = 2Hu^0 \mathcal{J} \quad (\text{B.7})$$

These results allow us to calculate the imposter field scalar by using that $\epsilon = 6Hu^0$ and $\epsilon_{\mu\nu}\epsilon^{\mu\nu} = 12H^2 (u^0)^2$. Thus our imposter field scalar becomes:

$$\chi = (18aH^2 + 6bH^2 + 0) u^0 \quad (\text{B.8})$$

Furthermore our simplifying tensors become:

$$A_{\mu\nu} = 2(6a + 2b)He^{2Ht}u^0\mathcal{J} \quad B_{\mu\nu} = 2(6a + 2b)He^{-2Ht}u^0\mathcal{J} \quad (\text{B.9})$$

Now since there is no mass present in our space, the equations of motion become:

$$\nabla^\mu \chi^{\frac{1}{2}} B_{\mu\nu} = 0 \quad (\text{B.10})$$

This implies:

$$\frac{1}{2}B^{\mu\nu}\nabla_\mu(\chi) + \chi\nabla_\mu(B^{\mu\nu}) = 0 \quad (\text{B.11})$$

For $\nu = 0$, these equations are trivially satisfied. For $\nu \neq 0$ we notice that the nonzero components of $B_{\mu\nu}$ are simply $\frac{2}{3H}e^{-2Ht}\chi$. This implies that the scalar field should be zero. This can only be true for a nonzero u^μ if:

$$3a + b = 0 \quad (\text{B.12})$$

In the report, we found that in order to obtain the same force as Erik Verlinde, we had to require that $b + d = -4$. We also argued that $d = 0$ as Erik Verlinde's theory is associated with the strain components of the imposter ifield. This yields the following set of constants:

$$a = \frac{4}{3} \quad b = -4 \quad d = 0 \quad (\text{B.13})$$

In terms of Hossenfelder's coefficients, this implies:

$$\bar{a} = \frac{8}{3} \quad \bar{b} = -4 \quad \bar{d} = -4 \quad (\text{B.14})$$

These differ from the set found by Hossenfelder, which were:

$$\bar{a} = \frac{4}{3} \quad \bar{b} = -\frac{1}{2} \quad \bar{d} = -\frac{1}{2} \quad (\text{B.15})$$

There are two reasons for this discrepancy. First, this report uses a different constraint for the coefficients. Secondly, it is the opinion of this author that Hossenfelder made a mistake in calculating equation 8 in her report from equation 4 and her choice for coefficients.

Appendix C

General lensing systems

For general lensing systems, the situation is a bit more complicated. For instance, when a source is lensed by a galaxy, the image will appear both magnified and distorted, just as with a normal non-perfect lens. Two important quantities of such a general lens are its convergence κ and its shear γ . The convergence can be thought of as the power of the lens, thus it describes the focusing of the lens. The shear, is a measure of the distortion of the shape of the source. An often cited example is that circular sources can be distorted into elliptical ones. The convergence κ is clearly related to the mass along the path the light ray takes, whilst the shear is related to how the potential of the current path differs from a nearby light ray's path.

In order to investigate such properties, we define the lensing matrix:

$$A_{ij} := \frac{\partial \beta^i}{\partial \theta^j} = \delta_{ij} - \frac{\partial \alpha^i}{\partial \theta^j} = \delta_{ij} - \frac{D_{ds}}{D_s} \frac{\partial \hat{\alpha}^i}{\partial \theta^j} \quad (\text{C.1})$$

This matrix allows us to convert properties of the lens into properties of the deflection angle. The derivative with respect to θ follows from the following consideration: Since our impact parameter is given by $\mathbf{b} = D_d \theta$, we find that we can equivalently write our potentials as function of the impact parameter and the traveled distance s

$$\phi(\mathbf{b}, s) = \phi(D_d \theta, s) \quad (\text{C.2})$$

In particular, we find that we can write the perpendicular gradient as:

$$\nabla_{\perp} = \frac{1}{D_d} \nabla_{\theta} \quad (\text{C.3})$$

This allows us to re-express the deflection angle in terms of the angle θ :

$$\hat{\alpha}(\theta) = \int [\nabla_{\perp} \phi_D + 2\nabla_{\perp} \phi_B] ds = \frac{1}{D_d} \int [\nabla_{\theta} \phi_D + 2\nabla_{\theta} \phi_B] ds \quad (\text{C.4})$$

We know now split A in an isotropic part $\frac{1}{2}\text{trace}(A)I$ and an an-isotropic part $A - \frac{1}{2}\text{trace}(A)I$. The isotropic part is related to the magnification of the entire object:

$$\frac{1}{2}\text{trace}(A)I = (1 - \kappa) \begin{bmatrix} 1 & 0 \\ 0 & 1 \end{bmatrix} \quad \text{with} \quad \kappa(\theta) = \frac{1}{2} \frac{D_{ds}}{D_d D_s} \int [\nabla_{\theta}^2 \phi_D + 2\nabla_{\theta}^2 \phi_B] ds \quad (\text{C.5})$$

The defined function κ is the convergence of the lens and is related to the mass distribution along the path by Poisson's equation. For convenience, let us define the lensing potential:

$$\psi(\theta) := \frac{D_{ds}}{D_d D_s} \int [\phi_D + 2\phi_B] ds \quad \text{and} \quad \psi_{ij} = \frac{\partial^2 \psi}{\partial \theta^i \partial \theta^j} \quad (\text{C.6})$$

The lensing matrix and convergence then become:

$$A_{ij} = \delta_{ij} - \psi_{ij} \quad \text{and} \quad \kappa = \frac{1}{2} [\psi_{11} + \psi_{22}] = \frac{1}{2} \nabla_{\theta}^2 \psi \quad (\text{C.7})$$

The an-isotropic part can now be written in a convenient form:

$$A_{ij} - \frac{1}{2} (1 - \psi_{11} + 1 - \psi_{22}) = \begin{bmatrix} -\frac{1}{2} (\psi_{11} - \psi_{22}) & -\psi_{12} \\ -\psi_{12} & \frac{1}{2} (\psi_{11} - \psi_{22}) \end{bmatrix}_{ij} \quad (\text{C.8})$$

We define the shear $\gamma_1 := \frac{1}{2} (\psi_{11} - \psi_{22})$ and $\gamma_2 := \psi_{12}$. The matrix then has eigenvalues $\gamma = \pm \sqrt{\gamma_1^2 + \gamma_2^2}$. Thus there is an rotation angle ξ such that:

$$A = (1 - \kappa) \begin{bmatrix} 1 & 0 \\ 0 & 1 \end{bmatrix} - \gamma \begin{bmatrix} \cos \xi & \sin \xi \\ \sin \xi & -\cos \xi \end{bmatrix} \quad (\text{C.9})$$

Thus the convergence κ magnifies the image, whilst the shear γ distorts the image. The magnification M is the determinant of the inverse of A and is, which is:

$$M = \frac{1}{(1 - \kappa)^2 - \gamma^2} \quad (\text{C.10})$$

Appendix D

Fits CEG and MOND

D.0.1 Fits CEG to SPARC

The following table indicate the MCMC fits of CEG to the SPARC galaxies. The fit parameters were the mass-to-light ratio γ_{disk} , the galactic distance D and the inclination i of the galaxy disk. The first column shows the galaxies name and the second its Hubble type. The third column shows the total luminosity of the galaxy. D_0 and i_0 are the distance as denoted in the SPARC database. The fittings were done based on Gaussian priors on the fit parameters and a maximum likelihood based on a χ^2 estimate.

Galaxy name	Type	$\log_{10} L [L_{\odot}]$	$\gamma_{\text{disk}} \left[\frac{M_{\odot}}{L_{\odot}} \right]$	Dist. [Mpc]	D/D_0	Inc. [Deg. °]	i/i_0	R^2
CamB	10	7.88	0 ± 0.05	2.5 ± 0.8	0.75	32.8 ± 14.3	0.5	-0.08
D512-2	10	8.51	0.98 ± 0.15	11.9 ± 2.7	0.78	40.4 ± 7.6	0.72	0.92
D564-8	10	7.52	0 ± 0.1	8.7 ± 0.5	0.98	49.3 ± 7.6	0.78	-0.19
D631-7	10	8.29	0 ± 0.02	7.1 ± 1.3	0.91	47.1 ± 15.6	0.8	-2.12
DDO064	10	8.2	0.44 ± 0.15	6.3 ± 0.9	0.93	55.1 ± 3.9	0.92	0.73
DDO154	10	7.72	0.06 ± 0.05	3 ± 0.3	0.75	75.8 ± 6.1	1.18	0.98
DDO161	10	8.74	0 ± 0.13	5.8 ± 0.6	0.78	55.1 ± 8.4	0.79	0.94
DDO168	10	8.28	0.22 ± 0.17	4.1 ± 0.5	0.95	49.1 ± 11.2	0.78	-1.43
DDO170	10	8.73	1.24 ± 0.13	8.7 ± 1	0.56	59.9 ± 5.8	0.91	0.93
ESO079-G014	4	10.71	0.37 ± 0.11	32.6 ± 3.5	1.14	76.2 ± 4	0.97	0.67
ESO116-G012	7	9.63	0.26 ± 0.07	17.6 ± 1.3	1.35	74.8 ± 2.4	1.01	0.9
ESO444-G084	10	7.85	0.04 ± 0.13	5.2 ± 0.3	1.07	40 ± 1.8	1.25	0.62
ESO563-G021	4	11.49	0.29 ± 0.07	93.5 ± 6.3	1.54	86.3 ± 2.3	1.04	0.74
F563-1	9	9.28	0.72 ± 0.14	59.4 ± 6.7	1.21	23.8 ± 2.3	0.95	0.75
F563-V2	10	9.48	1.18 ± 0.14	52.6 ± 8.4	0.88	32.6 ± 4	1.13	0.73
F565-V2	10	8.75	0.3 ± 0.15	58.7 ± 5.9	1.13	62.9 ± 6.1	1.05	0.49
F568-1	5	9.8	1.08 ± 0.14	85.1 ± 7.1	0.94	28.5 ± 2.2	1.1	0.14
F568-3	7	9.92	0.27 ± 0.13	82.1 ± 6.6	1	40.7 ± 4	1.02	0.38
F568-V1	7	9.58	1.42 ± 0.12	87.5 ± 5.9	1.09	39.8 ± 4.3	0.99	0.89
F571-8	5	10.01	0.07 ± 0.03	123.8 ± 8.1	2.32	90 ± 2.9	1.06	-5.79
F571-V1	7	9.27	0.43 ± 0.14	75.9 ± 6.4	0.95	28 ± 1.9	0.93	0.87
F574-1	7	9.82	0.99 ± 0.11	92.1 ± 6.8	0.95	52.2 ± 6.2	0.8	0.71
F579-V1	5	10.07	1.13 ± 0.13	84.3 ± 7.1	0.94	21.5 ± 2.4	0.83	0.88
F583-1	9	8.99	1.22 ± 0.12	24.4 ± 4	0.69	63.7 ± 3.9	1.01	0.05
F583-4	5	9.23	0.36 ± 0.13	40.9 ± 7.5	0.77	62.5 ± 6.4	1.14	0.82
IC2574	9	9.01	0.06 ± 0.01	3.7 ± 0.2	0.95	63.3 ± 5	0.84	0.98
KK98-251	10	7.93	0 ± 0.15	2.8 ± 0.4	0.41	71 ± 4.1	1.2	0.86
NGC0024	5	9.59	0.88 ± 0.09	7.3 ± 0.3	0.99	64.5 ± 2.2	1.01	1
NGC0055	9	9.67	0 ± 0.02	1.7 ± 0.1	0.82	74.9 ± 2.9	0.97	0.94
NGC0100	6	9.51	0.1 ± 0.11	22.7 ± 2.4	1.68	89.4 ± 0.7	1	0.83

Galaxy name	Type	$\log_{10} L [L_{\odot}]$	$\gamma_{disk} \left[\frac{M_{\odot}}{L_{\odot}} \right]$	Dist. [Mpc]	D/D_0	Inc. [Deg. °]	i/i_0	R^2
NGC0247	7	9.87	2.62 ± 0.09	1.2 ± 0.3	0.33	79.1 ± 3.4	1.07	0.81
NGC0289	4	10.86	0.76 ± 0.1	15.8 ± 2.4	0.76	40 ± 3.7	0.87	1
NGC0300	7	9.47	0.32 ± 0.1	2.1 ± 0.1	1	47 ± 3.1	1.12	0.92
NGC0801	5	11.49	1.48 ± 0.23	24.3 ± 7.1	0.3	85.1 ± 1.1	1.06	1
NGC1003	6	9.83	0.3 ± 0.07	9.6 ± 0.8	0.84	74.4 ± 4.2	1.11	0.97
NGC1090	4	10.86	0.56 ± 0.09	25.1 ± 2.6	0.68	61.4 ± 2.7	0.96	1
NGC2403	6	10	0.41 ± 0.02	2.7 ± 0.2	0.85	84.3 ± 4.7	1.34	1
NGC2903	4	10.91	0.14 ± 0.02	9.8 ± 0.8	1.49	88.7 ± 4.6	1.34	1
NGC2915	11	8.81	0.2 ± 0.12	5.2 ± 0.2	1.27	69 ± 3	1.23	0.62
NGC2976	5	9.53	0.13 ± 0.1	4 ± 0.1	1.13	78 ± 8.1	1.28	0.89
NGC2998	5	11.18	0.75 ± 0.09	42.3 ± 4.8	0.62	58.4 ± 2.3	1.01	1
NGC3109	9	8.29	0.01 ± 0.11	1.5 ± 0.1	1.14	75.5 ± 3.5	1.08	0.85
NGC3198	5	10.58	0.55 ± 0.04	9.7 ± 0.7	0.71	82.1 ± 3	1.12	1
NGC3521	4	10.93	0.3 ± 0.1	9.8 ± 1.3	1.27	71.7 ± 4.2	0.96	1
NGC3726	5	10.85	0.45 ± 0.07	11.4 ± 1.7	0.63	53.8 ± 1.7	1.01	0.94
NGC3741	10	7.45	0.08 ± 0.12	3.4 ± 0.1	1.07	72.2 ± 2.9	1.03	0.91
NGC3769	3	10.27	0.25 ± 0.07	17.3 ± 1.7	0.96	70.4 ± 1.7	1.01	0.99
NGC3877	5	10.86	0.17 ± 0.31	23.4 ± 3.9	1.3	76.1 ± 1.9	1	0.35
NGC3893	5	10.77	0.25 ± 0.07	22.4 ± 1.9	1.25	50.1 ± 1.7	1.02	0.99
NGC3917	6	10.34	0.68 ± 0.12	12.4 ± 2.1	0.69	88.5 ± 1.8	1.12	0.74
NGC3949	4	10.58	0.24 ± 0.06	18.1 ± 1.9	1.01	60.8 ± 1.6	1.1	0.95
NGC3953	4	11.15	1.11 ± 0.09	8.3 ± 2.1	0.46	60.1 ± 1.6	0.97	0.97
NGC3972	4	10.16	0.24 ± 0.12	23.8 ± 2.3	1.32	79.7 ± 1.1	1.04	0.38
NGC3992	4	11.36	1.25 ± 0.07	8.6 ± 1.7	0.36	83.8 ± 1.9	1.5	1
NGC4010	7	10.24	0.13 ± 0.08	25.1 ± 2	1.4	89.4 ± 0.7	1	0.63
NGC4051	4	10.98	0.69 ± 0.07	11 ± 2.1	0.61	42 ± 2.5	0.86	0.95
NGC4068	10	8.37	0.03 ± 0.09	4.3 ± 0.2	0.99	37.2 ± 2.5	0.84	0.96
NGC4085	5	10.34	0.12 ± 0.08	25.9 ± 2.8	1.44	83.1 ± 1.8	1.01	-0.39
NGC4088	4	11.03	0.3 ± 0.05	13 ± 1.9	0.72	67.9 ± 1.8	0.98	0.99
NGC4100	4	10.77	0.73 ± 0.11	12.6 ± 2.1	0.7	72.5 ± 2.1	0.99	0.99
NGC4183	6	10.03	1.97 ± 0.12	7 ± 1.5	0.39	88.4 ± 1.7	1.08	0.99
NGC4214	10	9.06	0.09 ± 0.15	3 ± 0.1	1.04	23.8 ± 1.9	1.59	0.97
NGC4559	6	10.29	0.43 ± 0.11	6.4 ± 0.7	0.71	66.5 ± 0.9	0.99	0.99
NGC5055	4	11.18	0.35 ± 0.04	9.8 ± 2.2	0.98	47.5 ± 3.9	0.86	1
NGC5371	4	11.53	2.25 ± 0.24	5.5 ± 3.9	0.14	71.8 ± 8.1	1.35	1
NGC5585	7	9.47	0.19 ± 0.03	7.7 ± 0.5	1.09	49.9 ± 1.6	0.98	0.9
NGC5907	5	11.24	0.93 ± 0.09	9.8 ± 1.1	0.56	81.8 ± 1.5	0.93	1
NGC6015	6	10.51	0.78 ± 0.09	12.6 ± 1.5	0.74	58.2 ± 2.7	0.97	0.98
NGC6503	6	10.11	0.31 ± 0.03	6.9 ± 0.2	1.1	74.3 ± 2	1	1
NGC6789	11	8	0.3 ± 0.12	3.8 ± 0.1	1.09	66.7 ± 3.7	1.55	0.31
NGC7793	7	9.85	0.48 ± 0.12	3.6 ± 0.1	0.99	40.7 ± 4.6	0.87	0.96
UGC00128	8	10.08	1.69 ± 0.15	54.1 ± 8.2	0.84	44.3 ± 6.4	0.78	0.99
UGC00191	9	9.3	1.17 ± 0.1	15.6 ± 2	0.91	34.7 ± 4.1	0.77	1
UGC00634	9	9.48	0.41 ± 0.07	30.8 ± 5.7	1	36.5 ± 4.2	0.99	0.99
UGC00731	10	8.51	1.8 ± 0.14	7.8 ± 0.7	0.62	66.3 ± 2.4	1.16	0.11
UGC00891	9	8.57	0 ± 0.06	9.2 ± 0.9	0.91	61.8 ± 5.3	1.03	0.2
UGC01230	9	9.88	1.16 ± 0.14	61.1 ± 8.3	1.14	15.1 ± 2	0.69	0.96
UGC01281	8	8.55	1.18 ± 0.11	2.9 ± 0.2	0.54	88.7 ± 0.5	0.99	0.01

Galaxy name	Type	$\log_{10} L [L_{\odot}]$	$\gamma_{disk} \left[\frac{M_{\odot}}{L_{\odot}} \right]$	Dist. [Mpc]	D/D_0	Inc. [Deg. °]	i/i_0	R^2
UGC02023	10	9.12	0.03 ± 0.16	14.4 ± 2.4	1.38	16.7 ± 2.8	0.88	0.68
UGC02259	8	9.24	1.73 ± 0.11	4.3 ± 1.1	0.41	56.9 ± 2.4	1.39	0.96
UGC04278	7	9.12	0.56 ± 0.11	9.1 ± 1.1	0.96	85.6 ± 1.5	0.95	-0.7
UGC04325	9	9.31	1.39 ± 0.12	7.9 ± 1.1	0.82	38.6 ± 2.3	0.94	0.78
UGC04483	10	7.11	0.42 ± 0.13	2.2 ± 0.2	0.66	52.8 ± 2.3	0.91	0.71
UGC04499	8	9.19	0.5 ± 0.11	8.9 ± 1	0.71	49.5 ± 2.4	0.99	0.78
UGC05005	10	9.61	0.26 ± 0.14	48.2 ± 8.1	0.9	36.6 ± 4.1	0.89	0.81
UGC05414	10	9.05	0.15 ± 0.11	7.8 ± 1	0.83	59.3 ± 2.5	1.08	0.94
UGC05716	9	8.77	1.32 ± 0.08	22.4 ± 3.4	1.05	41.1 ± 6.6	0.76	0.97
UGC05721	7	8.73	0.5 ± 0.11	7.6 ± 0.8	1.23	69.2 ± 3.7	1.13	0.97
UGC05750	8	9.52	0.72 ± 0.14	29.5 ± 8.3	0.5	64.4 ± 7.2	1.01	0.67
UGC05764	10	7.93	1.67 ± 0.12	8.1 ± 0.8	1.09	60.2 ± 6.7	1	0.54
UGC05829	10	8.75	1.25 ± 0.14	9.8 ± 1.9	1.13	22.9 ± 4.2	0.67	0.79
UGC05918	10	8.37	1.23 ± 0.14	3.5 ± 1	0.46	53.6 ± 3.7	1.16	0.47
UGC05986	9	9.67	0.19 ± 0.09	15.9 ± 1.3	1.84	88.1 ± 1.3	0.98	0.85
UGC05999	10	9.53	0.4 ± 0.12	57 ± 7.6	1.2	17.3 ± 1.8	0.79	-0.35
UGC06399	9	9.36	0.5 ± 0.11	17.5 ± 1.6	0.97	75.7 ± 1.6	1.01	0.75
UGC06446	7	8.99	1.27 ± 0.13	9.7 ± 1.1	0.81	50.4 ± 2.3	0.99	0.94
UGC06628	9	9.57	1.14 ± 0.15	2.7 ± 3.7	0.18	20 ± 2	1	0.75
UGC06667	6	9.15	3.81 ± 0.14	13.3 ± 1.2	0.74	89.5 ± 0.6	1.01	0.03
UGC06818	9	9.2	0.02 ± 0.05	26.3 ± 2	1.46	78.2 ± 2.4	1.04	0.62
UGC06917	9	9.83	0.49 ± 0.09	17.2 ± 1.5	0.96	55.4 ± 1.6	0.99	0.82
UGC06923	10	9.46	0.14 ± 0.08	19.8 ± 1.7	1.1	67.3 ± 1.6	1.03	0.45
UGC06930	7	9.95	1.19 ± 0.12	14.6 ± 1.9	0.81	24.9 ± 2.2	0.78	0.96
UGC06983	6	9.72	0.98 ± 0.1	9.4 ± 1.3	0.52	65.3 ± 0.8	1.33	0.89
UGC07089	8	9.55	0.14 ± 0.08	17 ± 1.9	0.95	75.5 ± 2.5	0.94	0.44
UGC07125	9	9.43	1.21 ± 0.12	6.2 ± 0.5	0.31	87.7 ± 1.4	0.97	0.92
UGC07151	6	9.36	0.8 ± 0.04	4.2 ± 0.3	0.61	89.7 ± 1.5	1	0.81
UGC07232	10	8.05	0.08 ± 0.07	3.6 ± 0.1	1.28	82.5 ± 3.9	1.4	0.59
UGC07261	8	9.24	0.79 ± 0.13	9.7 ± 2.8	0.74	28.8 ± 3.9	0.96	0.94
UGC07323	8	9.61	0.22 ± 0.12	8.5 ± 1.2	1.07	45 ± 2.4	0.96	0.7
UGC07399	8	9.06	0.42 ± 0.11	15.7 ± 1.1	1.86	57.7 ± 2.3	1.05	0.91
UGC07524	9	9.39	0.88 ± 0.1	4.3 ± 0.2	0.91	36.1 ± 1.9	0.78	0.32
UGC07559	10	8.04	0.17 ± 0.05	3.2 ± 0.2	0.64	56.1 ± 2.3	0.92	0.26
UGC07577	10	7.65	0.03 ± 0.02	0.7 ± 0.2	0.26	81.2 ± 2.8	1.29	0.7
UGC07603	7	8.58	0.15 ± 0.1	7.5 ± 0.6	1.61	75.2 ± 2.4	0.96	0.87
UGC07608	10	8.42	0.24 ± 0.16	12.5 ± 1.7	1.52	23.2 ± 3.6	0.93	0.27
UGC07690	10	8.93	1.02 ± 0.12	7 ± 1.2	0.86	31 ± 3.6	0.76	0.99
UGC07866	10	8.09	0.74 ± 0.14	4.1 ± 0.2	0.9	29.9 ± 2.7	0.68	0.53
UGC08286	6	9.1	1.14 ± 0.07	5.7 ± 0.2	0.88	78.5 ± 1.5	0.87	0.96
UGC08490	9	9.01	0.77 ± 0.11	4.6 ± 0.3	0.99	49.8 ± 2	1	1
UGC08550	7	8.46	0.82 ± 0.11	5.6 ± 0.4	0.83	84.5 ± 1.4	0.94	0.95
UGC08837	10	8.7	0.17 ± 0.03	4.1 ± 0.3	0.56	85.7 ± 4.8	1.07	0.9
UGC09037	6	10.84	0.13 ± 0.03	84.3 ± 5.9	1.01	61.6 ± 3.9	0.95	0.8
UGC09992	10	8.53	1.25 ± 0.15	8.9 ± 2.6	0.84	17.1 ± 3.6	0.57	0.9
UGC10310	9	9.24	1.21 ± 0.13	8.5 ± 2.6	0.56	33 ± 3.6	0.97	0.89
UGC11455	6	11.57	0.22 ± 0.07	100.2 ± 9.2	1.27	89.8 ± 0.5	1	0.97
UGC11557	8	10.08	0.09 ± 0.15	31.6 ± 4.8	1.31	22.5 ± 3.8	0.75	0.15

Galaxy name	Type	$\log_{10} L [L_{\odot}]$	$\gamma_{disk} \left[\frac{M_{\odot}}{L_{\odot}} \right]$	Dist. [Mpc]	D/D_0	Inc. [Deg. °]	i/i_0	R^2
UGC11820	9	8.99	1.14 ± 0.1	23.3 ± 3.6	1.29	28.9 ± 5.8	0.64	1
UGC12506	6	11.14	1.43 ± 0.09	59.7 ± 6.7	0.59	85.1 ± 2.6	0.99	0.99
UGC12632	9	9.11	1.33 ± 0.12	4.6 ± 0.8	0.47	51.7 ± 2.4	1.12	0.88
UGC12732	9	9.22	1.27 ± 0.11	8.4 ± 2.1	0.63	40.5 ± 3.8	1.04	0.99
UGCA442	9	8.15	0 ± 0.15	3.6 ± 0.2	0.83	87.3 ± 3.9	1.36	0.79
UGCA444	10	7.08	0.2 ± 0.16	0.9 ± 0	0.9	62.9 ± 3.4	0.81	-2.33

TABLE D.1: Fits of CEG to 131 SPARC galaxies using a MCMC algorithm and three fit parameters. The fit parameters were the mass-to-light ratio γ_{disk} , the galactic distance D and the inclination i of the galaxy disk. The first column shows the galaxies name and the second its Hubble type. The third column shows the total luminosity of the galaxy. D_0 and i_0 are the original distance and inclination as denoted in the SPARC database. The fittings were done based on Gaussian priors on the fit parameters and a maximum likelihood based on a χ^2 estimate.

D.0.2 Fits MOND to SPARC

The following table indicate the MCMC fits of MOND to the SPARC galaxies. The fit parameters were the mass-to-light ratio γ_{disk} , the galactic distance D and the inclination i of the galaxy disk. The first column shows the galaxies name and the second its Hubble type. The third column shows the total luminosity of the galaxy. D_0 and i_0 are the distance as denoted in the SPARC database. The fittings were done based on Gaussian priors on the fit parameters and a maximum likelihood based on a χ^2 estimate.

Galaxy name	Type	$\log_{10} L [L_{\odot}]$	$\gamma_{disk} \left[\frac{M_{\odot}}{L_{\odot}} \right]$	Dist. [Mpc]	D/D_0	Inc. [Deg. °]	i/i_0	R^2
CamB	10	7.88	0 ± 0.09	1.9 ± 0.7	0.56	32.8 ± 14.3	0.64	-0.06
D512-2	10	8.51	1.12 ± 0.15	13.9 ± 2.6	0.91	40.4 ± 7.6	0.71	0.9
D564-8	10	7.52	0 ± 0.11	9 ± 0.4	1.02	49.3 ± 7.6	0.8	-0.14
D631-7	10	8.29	0 ± 0.05	6.8 ± 0.6	0.88	47.1 ± 15.6	0.93	-1.74
DDO064	10	8.2	0.38 ± 0.14	7.9 ± 1	1.16	55.1 ± 3.9	0.92	0.71
DDO154	10	7.72	0.07 ± 0.06	4.2 ± 0.2	1.05	75.8 ± 6.1	0.95	0.97
DDO161	10	8.74	0.01 ± 0.14	4.7 ± 0.7	0.63	55.1 ± 8.4	1.12	0.97
DDO168	10	8.28	0.76 ± 0.15	4.1 ± 0.2	0.97	49.1 ± 11.2	0.83	-1.05
DDO170	10	8.73	1.33 ± 0.13	8.4 ± 1.1	0.55	59.9 ± 5.8	1.08	0.92
ESO079-G014	4	10.71	0.55 ± 0.11	34.6 ± 3.1	1.2	76.2 ± 4	1.07	0.69
ESO116-G012	7	9.63	0.34 ± 0.1	19.6 ± 1.4	1.51	74.8 ± 2.4	1.05	0.9
ESO444-G084	10	7.85	0.08 ± 0.14	4.4 ± 0.3	0.91	40 ± 1.8	1.54	0.8
ESO563-G021	4	11.49	0.47 ± 0.07	103.5 ± 5.4	1.7	86.3 ± 2.3	1	0.74
F563-1	9	9.28	0.94 ± 0.14	51.9 ± 6.8	1.06	23.8 ± 2.3	1.07	0.75
F563-V2	10	9.48	1.29 ± 0.14	71.9 ± 8.2	1.21	32.6 ± 4	1.11	0.66
F565-V2	10	8.75	0.27 ± 0.15	60.7 ± 5.7	1.17	62.9 ± 6.1	1.18	0.48
F568-1	5	9.8	1.14 ± 0.13	108.6 ± 7	1.2	28.5 ± 2.2	1.1	0.16
F568-3	7	9.92	0.25 ± 0.14	81.5 ± 6.4	0.99	40.7 ± 4	1.14	0.36
F568-V1	7	9.58	1.23 ± 0.13	77.9 ± 5.8	0.97	39.8 ± 4.3	1.31	0.82
F571-8	5	10.01	0.12 ± 0.04	111.6 ± 7	2.09	90 ± 2.9	1	-4.91
F571-V1	7	9.27	0.53 ± 0.15	76.6 ± 6.3	0.96	28 ± 1.9	0.99	0.85
F574-1	7	9.82	1.11 ± 0.11	78.2 ± 6.7	0.81	52.2 ± 6.2	1.1	0.7
F579-V1	5	10.07	1.08 ± 0.14	95.6 ± 6.8	1.07	21.5 ± 2.4	0.93	0.86

Galaxy name	Type	$\log_{10} L [L_{\odot}]$	$\gamma_{disk} \left[\frac{M_{\odot}}{L_{\odot}} \right]$	Dist. [Mpc]	D/D_0	Inc. [Deg.°]	i/i_0	R^2
F583-1	9	8.99	1.19 ± 0.13	30.9 ± 4.1	0.87	63.7 ± 3.9	0.99	0.08
F583-4	5	9.23	0.47 ± 0.14	46.4 ± 7.3	0.87	62.5 ± 6.4	1.06	0.81
IC2574	9	9.01	0.05 ± 0.01	3.5 ± 0.2	0.88	63.3 ± 5	1.06	0.99
KK98-251	10	7.93	0 ± 0.15	3.9 ± 0.5	0.57	71 ± 4.1	1.02	0.83
NGC0024	5	9.59	1.48 ± 0.12	7.1 ± 0.3	0.97	64.5 ± 2.2	1.06	1
NGC0055	9	9.67	0 ± 0.06	2 ± 0.1	0.94	74.9 ± 2.9	1.07	0.95
NGC0100	6	9.51	0.09 ± 0.14	26.2 ± 2	1.94	89.4 ± 0.7	1	0.79
NGC0247	7	9.87	3.13 ± 0.1	1.6 ± 0.2	0.43	79.1 ± 3.4	1.06	0.81
NGC0289	4	10.86	1.19 ± 0.11	7.4 ± 2.4	0.36	40 ± 3.7	1.69	1
NGC0300	7	9.47	0.42 ± 0.12	2.1 ± 0.1	0.99	47 ± 3.1	1.2	0.93
NGC0801	5	11.49	1.33 ± 0.13	38 ± 4.4	0.47	85.1 ± 1.1	1.1	1
NGC1003	6	9.83	0.48 ± 0.1	11.6 ± 0.9	1.02	74.4 ± 4.2	0.95	0.98
NGC1090	4	10.86	1.02 ± 0.12	27.4 ± 2.8	0.74	61.4 ± 2.7	0.9	1
NGC2403	6	10	0.63 ± 0.04	3.5 ± 0.1	1.12	84.3 ± 4.7	1.06	1
NGC2903	4	10.91	0.21 ± 0.02	12.3 ± 0.7	1.87	88.7 ± 4.6	1.07	0.99
NGC2915	11	8.81	0.42 ± 0.13	4.6 ± 0.2	1.13	69 ± 3	1.23	0.55
NGC2976	5	9.53	0.06 ± 0.11	6.6 ± 0.1	1.83	78 ± 8.1	1.41	0.89
NGC2998	5	11.18	1.36 ± 0.13	37.3 ± 6	0.55	58.4 ± 2.3	1.16	1
NGC3109	9	8.29	0.03 ± 0.12	1.5 ± 0.1	1.12	75.5 ± 3.5	1.19	0.79
NGC3198	5	10.58	1.1 ± 0.09	10.2 ± 0.8	0.74	82.1 ± 3	0.97	1
NGC3521	4	10.93	0.37 ± 0.09	12.7 ± 1.3	1.65	71.7 ± 4.2	0.94	1
NGC3726	5	10.85	0.78 ± 0.09	11.7 ± 1.6	0.65	53.8 ± 1.7	1.03	0.95
NGC3741	10	7.45	0.1 ± 0.13	3.7 ± 0.1	1.15	72.2 ± 2.9	1.06	0.91
NGC3769	3	10.27	0.5 ± 0.09	17.2 ± 1.5	0.96	70.4 ± 1.7	0.99	0.99
NGC3877	5	10.86	0.18 ± 0.08	30.1 ± 1.9	1.67	76.1 ± 1.9	1.12	0.37
NGC3893	5	10.77	0.35 ± 0.07	24.9 ± 1.6	1.39	50.1 ± 1.7	1.07	0.99
NGC3917	6	10.34	1.71 ± 0.12	10.5 ± 1.7	0.58	88.5 ± 1.8	1.04	0.73
NGC3949	4	10.58	0.33 ± 0.07	23.3 ± 1.8	1.29	60.8 ± 1.6	1.09	0.95
NGC3953	4	11.15	1.6 ± 0.14	8.7 ± 2.6	0.49	60.1 ± 1.6	1.02	0.99
NGC3972	4	10.16	0.38 ± 0.12	26.1 ± 1.7	1.45	79.7 ± 1.1	0.99	0.42
NGC3992	4	11.36	1.86 ± 0.1	9.8 ± 1.5	0.41	83.8 ± 1.9	1.48	1
NGC4010	7	10.24	0.23 ± 0.11	25.7 ± 1.8	1.43	89.4 ± 0.7	0.98	0.57
NGC4051	4	10.98	1.24 ± 0.1	5.9 ± 1.9	0.33	42 ± 2.5	1.37	0.95
NGC4068	10	8.37	0.01 ± 0.11	4.4 ± 0.2	1	37.2 ± 2.5	0.94	0.97
NGC4085	5	10.34	0.12 ± 0.06	37.8 ± 1.8	2.1	83.1 ± 1.8	1.06	-0.22
NGC4088	4	11.03	0.51 ± 0.08	13.9 ± 1.8	0.77	67.9 ± 1.8	1	0.99
NGC4100	4	10.77	1.18 ± 0.11	13.2 ± 1.6	0.74	72.5 ± 2.1	1.05	0.98
NGC4183	6	10.03	2.64 ± 0.12	8.8 ± 1.3	0.49	88.4 ± 1.7	1.06	0.98
NGC4214	10	9.06	0.33 ± 0.15	2.8 ± 0.1	0.96	23.8 ± 1.9	1.47	0.98
NGC4559	6	10.29	0.71 ± 0.12	6.8 ± 0.8	0.75	66.5 ± 0.9	1	0.99
NGC5055	4	11.18	0.62 ± 0.12	16 ± 4	1.62	47.5 ± 3.9	0.63	1
NGC5371	4	11.53	2.02 ± 0.16	8.4 ± 2.3	0.21	71.8 ± 8.1	1.59	1
NGC5585	7	9.47	0.24 ± 0.04	8.5 ± 0.5	1.21	49.9 ± 1.6	1	0.91
NGC5907	5	11.24	1.65 ± 0.13	9.8 ± 0.9	0.57	81.8 ± 1.5	0.99	1
NGC6015	6	10.51	1.35 ± 0.12	12.8 ± 1.4	0.75	58.2 ± 2.7	0.99	0.99
NGC6503	6	10.11	0.6 ± 0.05	6.5 ± 0.2	1.03	74.3 ± 2	1	1
NGC6789	11	8	0.39 ± 0.12	4.7 ± 0.1	1.33	66.7 ± 3.7	1.66	0.23
NGC7793	7	9.85	0.78 ± 0.12	3.8 ± 0.1	1.04	40.7 ± 4.6	0.9	0.95

Galaxy name	Type	$\log_{10} L [L_{\odot}]$	$\gamma_{disk} \left[\frac{M_{\odot}}{L_{\odot}} \right]$	Dist. [Mpc]	D/D_0	Inc. [Deg.°]	i/i_0	R^2
UGC00128	8	10.08	1.85 ± 0.17	54 ± 8	0.84	44.3 ± 6.4	0.87	0.97
UGC00191	9	9.3	1.44 ± 0.1	11.2 ± 2.3	0.66	34.7 ± 4.1	1.05	1
UGC00634	9	9.48	0.56 ± 0.09	26.5 ± 5	0.86	36.5 ± 4.2	1.17	0.97
UGC00731	10	8.51	1.89 ± 0.14	10.8 ± 0.8	0.86	66.3 ± 2.4	1.02	0.17
UGC00891	9	8.57	0 ± 0.07	9.3 ± 1	0.92	61.8 ± 5.3	1.16	0.45
UGC01230	9	9.88	1.27 ± 0.14	61.3 ± 8.6	1.14	15.1 ± 2	0.74	0.95
UGC01281	8	8.55	1.57 ± 0.13	3.4 ± 0.2	0.65	88.7 ± 0.5	1	0.09
UGC02023	10	9.12	0.02 ± 0.16	8.3 ± 2.4	0.8	16.7 ± 2.8	1.25	0.68
UGC02259	8	9.24	1.67 ± 0.13	6.9 ± 1.3	0.66	56.9 ± 2.4	1.24	0.94
UGC04278	7	9.12	0.52 ± 0.11	11.5 ± 1.2	1.21	85.6 ± 1.5	0.98	-0.45
UGC04325	9	9.31	1.38 ± 0.12	9.1 ± 1.2	0.95	38.6 ± 2.3	1.07	0.74
UGC04483	10	7.11	0.49 ± 0.14	2.8 ± 0.2	0.85	52.8 ± 2.3	0.86	0.66
UGC04499	8	9.19	0.64 ± 0.12	9.5 ± 1	0.76	49.5 ± 2.4	1.05	0.78
UGC05005	10	9.61	0.29 ± 0.14	47.3 ± 7.9	0.88	36.6 ± 4.1	0.96	0.79
UGC05414	10	9.05	0.14 ± 0.13	9.7 ± 1	1.03	59.3 ± 2.5	1.07	0.96
UGC05716	9	8.77	1.59 ± 0.09	21.5 ± 3.1	1.01	41.1 ± 6.6	0.85	0.97
UGC05721	7	8.73	0.84 ± 0.12	8 ± 0.8	1.29	69.2 ± 3.7	1.18	0.97
UGC05750	8	9.52	0.71 ± 0.14	36 ± 7.8	0.61	64.4 ± 7.2	0.98	0.63
UGC05764	10	7.93	1.77 ± 0.12	8.5 ± 0.7	1.13	60.2 ± 6.7	1.15	0.51
UGC05829	10	8.75	1.14 ± 0.14	9.4 ± 1.8	1.08	22.9 ± 4.2	0.78	0.78
UGC05918	10	8.37	1.11 ± 0.14	9.2 ± 1	1.2	53.6 ± 3.7	0.73	0.41
UGC05986	9	9.67	0.27 ± 0.11	17.4 ± 1.1	2.02	88.1 ± 1.3	1	0.82
UGC05999	10	9.53	0.47 ± 0.13	36.5 ± 7.4	0.77	17.3 ± 1.8	1.08	-0.24
UGC06399	9	9.36	0.64 ± 0.12	19.5 ± 1.4	1.08	75.7 ± 1.6	1.03	0.72
UGC06446	7	8.99	1.28 ± 0.13	12.8 ± 1.2	1.07	50.4 ± 2.3	0.97	0.91
UGC06628	9	9.57	1.3 ± 0.15	8.3 ± 3.8	0.55	20 ± 2	0.61	0.73
UGC06667	6	9.15	4.56 ± 0.15	15.1 ± 1.2	0.84	89.5 ± 0.6	1	-0.02
UGC06818	9	9.2	0.02 ± 0.07	29.2 ± 2	1.62	78.2 ± 2.4	0.91	0.36
UGC06917	9	9.83	0.72 ± 0.1	19.6 ± 1.4	1.09	55.4 ± 1.6	0.96	0.85
UGC06923	10	9.46	0.2 ± 0.1	23.3 ± 1.5	1.3	67.3 ± 1.6	1.02	0.46
UGC06930	7	9.95	1.14 ± 0.13	18.7 ± 1.8	1.04	24.9 ± 2.2	0.82	0.94
UGC06983	6	9.72	1.26 ± 0.11	16.1 ± 1.3	0.89	65.3 ± 0.8	1	0.91
UGC07089	8	9.55	0.14 ± 0.1	19 ± 1.8	1.05	75.5 ± 2.5	1.02	0.46
UGC07125	9	9.43	1.25 ± 0.13	7.6 ± 0.5	0.38	87.7 ± 1.4	0.99	0.92
UGC07151	6	9.36	1.16 ± 0.07	5 ± 0.3	0.73	89.7 ± 1.5	0.99	0.8
UGC07232	10	8.05	0.2 ± 0.1	3.5 ± 0.1	1.25	82.5 ± 3.9	1.27	0.03
UGC07261	8	9.24	1.22 ± 0.13	8.7 ± 2.7	0.66	28.8 ± 3.9	1.06	0.94
UGC07323	8	9.61	0.2 ± 0.13	10.1 ± 1.1	1.26	45 ± 2.4	1.01	0.7
UGC07399	8	9.06	0.63 ± 0.11	17.6 ± 1.1	2.09	57.7 ± 2.3	1.03	0.91
UGC07524	9	9.39	0.98 ± 0.11	4.8 ± 0.2	1.01	36.1 ± 1.9	0.83	0.38
UGC07559	10	8.04	0.13 ± 0.08	4.2 ± 0.2	0.84	56.1 ± 2.3	0.86	0.28
UGC07577	10	7.65	0.04 ± 0.02	1.1 ± 0.1	0.41	81.2 ± 2.8	0.95	0.62
UGC07603	7	8.58	0.18 ± 0.12	8.3 ± 0.6	1.77	75.2 ± 2.4	1.04	0.86
UGC07608	10	8.42	0.17 ± 0.15	7.3 ± 1.6	0.89	23.2 ± 3.6	1.38	0.3
UGC07690	10	8.93	1.24 ± 0.13	6.2 ± 1.2	0.77	31 ± 3.6	0.92	0.98
UGC07866	10	8.09	0.81 ± 0.14	4.5 ± 0.2	0.99	29.9 ± 2.7	0.7	0.56
UGC08286	6	9.1	1.62 ± 0.08	6.2 ± 0.2	0.95	78.5 ± 1.5	0.99	0.96
UGC08490	9	9.01	1.29 ± 0.12	4.5 ± 0.3	0.97	49.8 ± 2	1.04	1

Galaxy name	Type	$\log_{10} L [L_{\odot}]$	$\gamma_{disk} \left[\frac{M_{\odot}}{L_{\odot}} \right]$	Dist. [Mpc]	D/D_0	Inc. [Deg.°]	i/i_0	R^2
UGC08550	7	8.46	1.14 ± 0.12	6.1 ± 0.4	0.91	84.5 ± 1.4	0.98	0.97
UGC08837	10	8.7	0.14 ± 0.04	6.4 ± 0.3	0.89	85.7 ± 4.8	0.77	0.9
UGC09037	6	10.84	0.17 ± 0.06	84.5 ± 5.8	1.01	61.6 ± 3.9	1.13	0.81
UGC09992	10	8.53	1.19 ± 0.15	12 ± 2.5	1.12	17.1 ± 3.6	0.56	0.86
UGC10310	9	9.24	1.28 ± 0.14	8.5 ± 2.7	0.56	33 ± 3.6	1.1	0.84
UGC11455	6	11.57	0.43 ± 0.07	94.9 ± 7.6	1.21	89.8 ± 0.5	0.99	0.97
UGC11557	8	10.08	0.09 ± 0.16	22.4 ± 4.7	0.93	22.5 ± 3.8	1	0.14
UGC11820	9	8.99	1.36 ± 0.11	11.6 ± 3.7	0.64	28.9 ± 5.8	1.05	1
UGC12506	6	11.14	1.6 ± 0.11	89.4 ± 6.1	0.89	85.1 ± 2.6	0.95	0.98
UGC12632	9	9.11	1.39 ± 0.13	5.9 ± 0.9	0.61	51.7 ± 2.4	1.09	0.84
UGC12732	9	9.22	1.45 ± 0.12	14.1 ± 2	1.07	40.5 ± 3.8	0.85	0.98
UGCA442	9	8.15	0 ± 0.15	4.2 ± 0.2	0.97	87.3 ± 3.9	1.25	0.89
UGCA444	10	7.08	0.92 ± 0.15	0.9 ± 0	0.89	62.9 ± 3.4	0.83	0

TABLE D.2: Fits of MOND to 131 SPARC galaxies using a MCMC algorithm and three fit parameters. The fit parameters were the mass-to-light ratio γ_{disk} , the galactic distance D and the inclination i of the galaxy disk. The first column shows the galaxies name and the second its Hubble type. The third column shows the total luminosity of the galaxy. D_0 and i_0 are the original distance and inclination as denoted in the SPARC database. The fittings were done based on Gaussian priors on the fit parameters and a maximum likelihood based on a χ^2 estimate.